

Jordan Journal of P H Y S I C S

An International Peer-Reviewed Research Journal

Volume 6, No. 2, 2013, 1435 H

Jordan Journal of Physics (JJP): An International Peer-Reviewed Research Journal issued by the support of the Scientific Research Support Fund, Ministry of Higher Education & Scientific Research, Jordan, and published quarterly by the Deanship of Research & Graduate Studies, Yarmouk University, Irbid, Jordan.

EDITOR-IN-CHIEF:

Nihad A. Yusuf

Department of Physics, Yarmouk University, Irbid, Jordan.

nihadyusuf@yu.edu.jo

EDITORIAL BOARD:

Dia-Eddin M. Arafah

Department of Physics, University of Jordan, Amman, Jordan.

darafah@ju.edu.jo

Nabil Y. Ayoub

Department of Physics, Yarmouk University, Irbid, Jordan.

nayoub@yu.edu.jo

Jamil M. Khalifeh

Department of Physics, University of Jordan, Amman, Jordan.

jkalifa@ju.edu.jo

Sami H. Mahmood

Department of Physics, University of Jordan, Amman, Jordan.

s.mahmood@ju.edu.jo

Marwan S. Mousa

Department of Physics, Mu'tah University, Al-Karak, Jordan.

mmousa@mutah.edu.jo

Ibrahim O. Abu Al-Jarayesh

Department of Physics, Yarmouk University, Irbid, Jordan.

ijaraysh@yu.edu.jo

Akram A. Rousan

Department of Applied Physical Sciences, Jordan University Of Science And Technology, Irbid, Jordan.

akram@just.edu.jo

Saadi M. S. Abdul Jawad

Department of Physics, The Hashemite university, Zarqa, Jordan.

ssadi@hu.edu.jo

EDITORIAL SECRETARY: Majdi Al-Shannaq.

Manuscripts should be submitted to:

Prof. Nihad A. Yusuf
Editor-in-Chief, Jordan Journal of Physics
Deanship of Research and Graduate Studies
Yarmouk University-Irbid-Jordan
Tel. 00 962 2 7211111 Ext. 2075
E-mail: jjp@yu.edu.jo
Website: <http://Journals.yu.edu.jo/jjp>

Jordan Journal of
P H Y S I C S

An International Peer-Reviewed Research Journal

Volume 6, No. 2, 2013, 1435 H

INTERNATIONAL ADVISORY BOARD

Prof. Dr. Ahmad Saleh

Department of Physics, Yarmouk University, Irbid, Jordan.
salema@yu.edu.jo

Prof. Dr. Aurore Savoy-Navarro

LPNHE Université de Paris 6/IN2P3-CNRS, Tour 33, RdC 4,
Place Jussieu, F 75252, Paris Cedex 05, France.
auore@lpnhep.in2p3.fr

Prof. Dr. Bernard Barbara

Laboratoire Louis Neel, Salle/Room: D 108, 25, Avenue des
Martyrs BP 166, 38042-Grenoble Cedex 9, France.
Barbara@grenoble.cnrs.fr

Prof. Dr. Bruno Guiderdoni

Observatoire Astronomique de Lyon, g, avenue Ch. Antre-F-69561,
Saint Genis Laval Cedex, France.
Bruno.guiderdoni@olos.univ-lyon1.fr

Prof. Dr. Buford Price

Physics Department, University of California, Berkeley, CA 94720,
U. S. A.
bprice@berkeley.edu

Prof. Dr. Colin Cough

School of Physics and Astronomy, University of Birmingham, B15
2TT, U. K.
c.gough@bham.ac.uk

Prof. Dr. Desmond Cook

Department of Physics, Condensed Matter and Materials Physics
Research Group, Old Dominion University, Norfolk, Virginia
23529, U. S. A.
Dcook@physics.odu.edu

Prof. Dr. Evgeny Sheshin

MIPT, Institutskij per. 9, Dogoprudnyi 141700, Russia.
sheshin@lafeet.mipt.ru

Prof. Dr. Hans Ott

Laboratorium fuer Festkorperphysik, ETH Honggerberg, CH-
8093 Zurich, Switzerland.
ott@solid.phys.ethz.ch

Prof. Dr. Herwig Schopper

President SESAME Council, Chairman Scientific Board UNESCO
IBSP Programme, CERN, 1211 Geneva, Switzerland.
Herwig.Schopper@cern.ch

Prof. Dr. Humam Ghassib

Department of Physics, Jordan University, Amman, Jordan.
humam@atf.org.jo

Prof. Dr. Ingo Hofmann

GSI Darmstadt, Planckstr. 1, 64291, Darmstadt, Germany.
i.hofmann@gsi.de

Prof. Dr. Jozef Lipka

Department of Nuclear Physics and Technology, Slovak University
of Technology, Bratislava, Ilkovicova 3, 812 19 Bratislava,
Slovakia.
Lipka@elf.stuba.sk

Prof. Dr. Khalid Touqan

Chairman of Jordan Atomic Energy Commission, Amman, Jordan.

Prof. Dr. Mark J. Hagmann

Desert Electronics Research Corporation, 762 Lacey Way, North
Salt Lake 84064, Utah, U. S. A.
MHagmann@NewPathResearch.Com

Prof. Dr. Nasr Zubeidey

President: Al-Zaytoonah University of Jordan, Amman, Jordan.
President@alzaytoonah.edu.jo

Prof. Dr. Patrick Roudeau

Laboratoire de l'Accelérateur, Lineaire (LAL), Université Paris-
Sud 11, Batiment 200, 91898 Orsay Cedex, France.
roudeau@mail.cern.ch

Prof. Dr. Paul Chu

Department of Physics, University of Houston, Houston, Texas
77204-5005, U. S. A.
Ching-Wu.Chu@mail.uh.edu

Prof. Dr. Peter Dowben

Nebraska Center for Materials and Nanoscience, Department of
Physics and Astronomy, 255 Behlen Laboratory (10th and R
Streets), 116 Brace Lab., P. O. Box 880111, Lincoln, NE 68588-
0111, U. S. A.
pdowben@unl.edu

Prof. Dr. Peter Mulser

Institute fuer Physik, T.U. Darmstadt, Hochschulstr. 4a, 64289
Darmstadt, Germany.
Peter.mulser@physik.tu-darmstadt.de

Prof. Dr. Rasheed Azzam

Department of Electrical Engineering, University of New Orleans
New Orleans, Louisiana 70148, U. S. A.
razzam@uno.edu

Dr. Richard G. Forbes

University of Surrey, FEPS (X1), Guildford, Surrey GU2 7XH,
U. K.
R.Forbes@surrey.ac.uk

Prof. Dr. Roy Chantrell

Physics Department, York University, York, YO10 5DD, U. K.
Rc502@york.ac.uk

Prof. Dr. Shawqi Al-Dallal

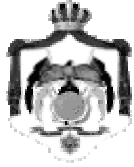
Department of Physics, Faculty of Science, University of Bahrain,
Manamah, Kingdom of Bahrain.

Prof. Dr. Susamu Taketomi

Matsumoto Yushi-Seiyaku Co. Ltd., Shibukawa-Cho, Yao City,
Osaka 581-0075, Japan.
staketomi@hotmail.com

Prof. Dr. Wolfgang Nolting

Institute of Physics / Chair: Solid State Theory, Humboldt-
University at Berlin, Newtonstr. 15 D-12489 Berlin, Germany
Wolfgang.nolting@physik.hu-berlin.de



The Hashemite Kingdom of Jordan



Yarmouk University

Jordan Journal of
PHYSICS

An International Peer-Reviewed Research Journal issued by the
Support of the Scientific Research Support Fund

Volume 6, No. 2, 2013, 1435 H

Instructions to Authors

Instructions to authors concerning manuscript organization and format apply to hardcopy submission by mail, and also to electronic online submission via the Journal homepage website (<http://jjp.yu.edu.jo>).

Manuscript Submission

1- **Hardcopy:** The original and three copies of the manuscript, together with a covering letter from the corresponding author, should be submitted to the Editor-in-Chief:

Professor Nihad A. Yusuf
Editor-in-Chief, Jordan Journal of Physics
Deanship of Scientific Research and Graduate Studies
Yarmouk University, Irbid, Jordan.
Tel: 00962-2-7211111, Ext. 2075
Fax: 00962-2-7211121
E-mail: jjp@yu.edu.jo

2- **Online:** Follow the instructions at the journal homepage website.

Original *Research Articles*, *Communications* and *Technical Notes* are subject to critical review by minimum of two competent referees. Authors are encouraged to suggest names of competent reviewers. *Feature Articles* in active Physics research fields, in which the author's own contribution and its relationship to other work in the field constitute the main body of the article, appear as a result of an invitation from the Editorial Board, and will be so designated. The author of a *Feature Article* will be asked to provide a clear, concise and critical status report of the field as an introduction to the article. *Review Articles* on active and rapidly changing Physics research fields will also be published. Authors of *Review Articles* are encouraged to submit two-page proposals to the Editor-in-Chief for approval. Manuscripts submitted in *Arabic* should be accompanied by an Abstract and Keywords in English.

Organization of the Manuscript

Manuscripts should be typed double spaced on one side of A4 sheets (21.6 x 27.9 cm) with 3.71 cm margins, using Microsoft Word 2000 or a later version thereof. The author should adhere to the following order of presentation: Article Title, Author(s), Full Address and E-mail, Abstract, PACS and Keywords, Main Text, Acknowledgment. Only the first letters of words in the Title, Headings and Subheadings are capitalized. Headings should be in **bold** while subheadings in *italic* fonts.

Title Page: Includes the title of the article, authors' first names, middle initials and surnames and affiliations. The affiliation should comprise the department, institution (university or company), city, zip code and state and should be typed as a footnote to the author's name. The name and complete mailing address, telephone and fax numbers, and e-mail address of the author responsible for correspondence (designated with an asterisk) should also be included for official use. The title should be carefully, concisely and clearly constructed to highlight the emphasis and content of the manuscript, which is very important for information retrieval.

Abstract: A one paragraph abstract not exceeding 200 words is required, which should be arranged to highlight the purpose, methods used, results and major findings.

Keywords: A list of 4-6 keywords, which expresses the precise content of the manuscript for indexing purposes, should follow the abstract.

PACS: Authors should supply one or more relevant PACS-2006 classification codes, (available at <http://www.aip.org/pacs/pacs06/pacs06-toc.html>)

Introduction: Should present the purpose of the submitted work and its relationship to earlier work in the field, but it should not be an extensive review of the literature (e.g., should not exceed 1 ½ typed pages).

Experimental Methods: Should be sufficiently informative to allow competent reproduction of the experimental procedures presented; yet concise enough not to be repetitive of earlier published procedures.

Results: should present the results clearly and concisely.

Discussion: Should be concise and focus on the interpretation of the results.

Conclusion: Should be a brief account of the major findings of the study not exceeding one typed page.

Acknowledgments: Including those for grant and financial support if any, should be typed in one paragraph directly preceding the References.

References: References should be typed double spaced and numbered sequentially in the order in which they are cited in the text. References should be cited in the text by the appropriate Arabic numerals, enclosed in square brackets. Titles of journals are abbreviated according to list of scientific periodicals. The style and punctuation should conform to the following examples:

1. Journal Article:

- a) Heisenberg, W., *Z. Phys.* 49 (1928) 619.
- b) Bednorz, J. G. and Müller, K. A., *Z. Phys.* B64 (1986) 189
- c) Bardeen, J., Cooper, L.N. and Schrieffer, J. R., *Phys. Rev.* 106 (1957) 162.
- d) Asad, J. H., Hijjawi, R. S., Sakaji, A. and Khalifeh, J. M., *Int. J. Theor. Phys.* 44(4) (2005), 3977.

2. Books with Authors, but no Editors:

- a) Kittel, C., "Introduction to Solid State Physics", 8th Ed. (John Wiley and Sons, New York, 2005), chapter 16.
- b) Chikazumi, S., C. D. Graham, JR, "Physics of Ferromagnetism", 2nd Ed. (Oxford University Press, Oxford, 1997).

3. Books with Authors and Editors:

- a) Allen, P. B. "Dynamical Properties of Solids", Ed. (1), G. K. Horton and A. A. Maradudin (North-Holland, Amsterdam, 1980), p137.
- b) Chantrell, R. W. and O'Grady, K., "Magnetic Properties of Fine Particles" Eds. J. L. Dormann and D. Fiorani (North-Holland, Amsterdam, 1992), p103.

4. Technical Report:

Purcell, J. "The Superconducting Magnet System for the 12-Foot Bubble Chamber", report ANL/HEP6813, Argonne Natl. Lab., Argonne, III, (1968).

5. Patent:

Bigham, C. B., Schneider, H. R., US patent 3 925 676 (1975).

6. Thesis:

Mahmood, S. H., Ph.D. Thesis, Michigan State University, (1986), USA (Unpublished).

7. Conference or Symposium Proceedings:

Blandin, A. and Lederer, P. *Proc. Intern. Conf. on Magnetism, Nottingham* (1964), P.71.

8. Internet Source:

Should include authors' names (if any), title, internet website, URL, and date of access.

9. Prepublication online articles (already accepted for publication):

Should include authors' names (if any), title of digital database, database website, URL, and date of access.

For other types of referenced works, provide sufficient information to enable readers to access them.

Tables: Tables should be numbered with Arabic numerals and referred to by number in the Text (e.g., Table 1). Each table should be typed on a separate page with the legend above the table, while explanatory footnotes, which are indicated by superscript lowercase letters, should be typed below the table.

Illustrations: Figures, drawings, diagrams, charts and photographs are to be numbered in a consecutive series of Arabic numerals in the order in which they are cited in the text. Computer-generated illustrations and good-quality digital photographic prints are accepted. They should be black and white originals (not photocopies) provided on separate pages and identified with their corresponding numbers. Actual size graphics should be provided, which need no further manipulation, with lettering (Arial or Helvetica) not smaller than 8 points, lines no thinner than 0.5 point, and each of uniform density. All colors should be removed from graphics except for those graphics to be considered for publication in color. If graphics are to be submitted digitally, they should conform to the following minimum resolution requirements: 1200 dpi for black and white line art, 600 dpi for grayscale art, and 300 dpi for color art. All graphic files must be saved as TIFF images, and all illustrations must be submitted in the actual size at which they should appear in the journal. Note that good quality hardcopy original illustrations are required for both online and mail submissions of manuscripts.

Text Footnotes: The use of text footnotes is to be avoided. When their use is absolutely necessary, they should be typed at the bottom of the page to which they refer, and should be cited in the text by a superscript asterisk or multiples thereof. Place a line above the footnote, so that it is set off from the text.

Supplementary Material: Authors are encouraged to provide all supplementary materials that may facilitate the review process, including any detailed mathematical derivations that may not appear in whole in the manuscript.

Revised Manuscript and Computer Disks

Following the acceptance of a manuscript for publication and the incorporation of all required revisions, authors should submit an original and one more copy of the final disk containing the complete manuscript typed double spaced in Microsoft Word for Windows 2000 or a later version thereof. All graphic files must be saved as PDF, JPG, or TIFF images.

Allen, P.B., “.....”, in: Horton, G.K., and Muradudin, A. A., (eds.), “Dynamical.....”, (North.....), pp....

Reprints

Twenty (20) reprints free of charge are provided to the corresponding author. For orders of more reprints, a reprint order form and prices will be sent with the article proofs, which should be returned directly to the Editor for processing.

Copyright

Submission is an admission by the authors that the manuscript has neither been previously published nor is being considered for publication elsewhere. A statement transferring copyright from the authors to Yarmouk University is required before the manuscript can be accepted for publication. The necessary form for such transfer is supplied by the Editor-in-Chief. Reproduction of any part of the contents of a published work is forbidden without a written permission by the Editor-in-Chief.

Disclaimer

Opinions expressed in this Journal are those of the authors and neither necessarily reflects the opinions of the Editorial Board or the University, nor the policy of the Higher Scientific Research Committee or the Ministry of Higher Education and Scientific Research. The publisher shoulders no responsibility or liability whatsoever for the use or misuse of the information published by JJP.

Indexing

JJP is currently applying for indexing and abstracting to all related International Services.

Table of Contents:

English Articles	Pages
Periodicity of Diurnal Variation of Soil Radon Concentration Levels and Temperature N. M. Ershaidat, R. R. Almomani, B. A. Al-Bataina and W. S. Al-Rayashi	47-54
Canonical Quantization for Fractional Schrödinger Lagrangian Density in Caputo Definition Emad K. Jaradat	55-63
On the Gravitational Properties of Dark Matter B. Al-Khasawneh and M.B. Altaie	65-72
Concerning the Existence of a Discrete Space Ahmed Isam	73-77
Quantization of Nonholonomic Constraints Using the WKB Approximation A. A. Al-Ajaleen and K. I. Nawafleh	79-86
New Design of Objective Lens Geometry for Low Voltage SEM M. A. Al-Khashab and R. Y. Al-Salih	87-94
IBM-1 Calculations of Energy Levels and Electric Transition Probabilities B(E2) in “¹⁵⁸⁻¹⁶⁰Gd Isotopes” K. A. Al-Maqtary	95-102

Periodicity of Diurnal Variation of Soil Radon Concentration Levels and Temperature

N. M. Ershaidat^a , R. R. Almomani^b , B. A. Al-Bataina^a and W. S. Al-Rayashi^a

^a *Department of Physics, Yarmouk University, Irbid 21163, Jordan.*

^b *Department of Mathematics, Yarmouk University, Irbid 21163, Jordan.*

Received on: 2/1/2013; Accepted on: 13/8/2013

Abstract: Concentration levels of soil radon at various depths (25, 50 and 75 cm), over a period of two days, in a phosphatic formation site located in Irbid, Jordan were measured using an active detector, the RAD7[®] from DurrIDGE Company, USA.

Periodicity of diurnal soil radon concentration levels is observed. Data were fitted using a cosine function. This fit produces a pattern similar to that of the variation of temperature of the soil with time obtained by the solution of the heat equation. The angular frequency of the periodicity is consistent with that of the temporal variation of the temperature of the soil for a given depth. Periodicity is clearly marked for the depths 25 cm and 50 cm, which is consistent with previous studies.

Keywords: Soil radon; Heat equation; Diurnal variation, RAD7[®]; Active detector; Phosphatic formation; Irbid.

PACS: 93.85.Np, 29.40.-n, 92.40.Lg

Introduction

Radon gas isotopes, ²¹⁹Rn (actinon), ²²⁰Rn (thoron) and ²²²Rn (radon) occur in the environment, being produced in the natural decay chains of ²³⁵U, ²³²Th and ²³⁸U, respectively, all decaying by alpha emission. Because of its relative high life-time ($t_{1/2} = 3.82$ days), the ²²²Rn isotope is considered important in applied nuclear and environmental studies.

In addition to radon, soil gas measurements will normally also register the presence of thoron, depending on soil composition. It is well known that exposure of population to high concentrations of radon and thoron and their solid daughters for long periods leads to pathological effects like respiratory functional changes and lung cancer [1]. In this work, only soil radon will be considered. At least 80% of the radon emitted into the atmosphere comes from the top few meters of the ground [2]. The radon emanation rate varies from one place to

another due to differences in radium concentration and soil parameters such as moisture content, porosity, permeability and grain size [3, 4]. The exhalation of radon from soil involves two mechanisms: diffusion and convection. These two mechanisms are affected by many factors including the properties of the soil [5].

The health hazards of radon and its decay products have led to study radon transport in soils and into buildings [6]. A thorough understanding of gas transport is required to evaluate these issues.

Diffusion of radon is characterized by the (effective) diffusion coefficient. The diffusion coefficient of ²²²Rn in air is $0.11 \text{ cm}^2 \text{ s}^{-1}$ [7]. The effective diffusion coefficient is about a factor of four smaller than the free air diffusion coefficient in fairly dry soils [6, 8]. Effective diffusivities in saturated systems are about four

orders of magnitude less than those in dry soils [9]. Models explaining the diffusion of soil radon are, in general, based on the solution of the diffusion equation in the quasi-homogenous approximation with boundary conditions assuming a semi-infinite medium [8, 10].

Many studies of diurnal variation of indoor radon [11, 12], radon near the ground [13, 14], soil radon [15, 16] and even in the atmosphere [17 – 20] exist in the literature. The case of soil radon is particularly interesting for the studies of earthquakes [21 - 23].

Neves *et al.* studied the indoor radon periodicities and their physical constraints in the inland Coimbra region in Portugal [11]. They reported a well marked periodicity in radon activity with maximum values occurring more frequently in the morning between 9 and 10 a.m. Their principle conclusion is that daily variations are shown to have no relation with earth tides and their amplitudes exhibit a significant correlation with outdoor temperature; no dependence on barometric pressure was found. Rainfall disturbs the observed daily radon cycles through a strong reduction of their amplitude, but has no effect on the long-term variability of the gas concentration.

Diurnal radon variations in the upper soil layers and at the soil-air interface related to meteorological parameters were studied by Schubert and Schulz [16]. In their work, conducted in the laboratory using a column consisting of a homogenous mixture of dry sand and uranium tailings, measurements of radon concentration levels were performed in order to obtain information on the radon transport under well defined conditions

The dependence of radon concentration has been exclusively studied on the soil/air temperature gradient and on the wind speed. The soil moisture content has been kept constant. Significant diurnal variations of the radon concentration were detected in the uppermost soil layer and at the soil/air interface. Such a behavior was not found deeper than 30 cm in soil layers. It is argued that the diurnal radon variation in the uppermost soil layer is mainly associated with the diurnal inversion of the soil/air temperature gradient giving rise to a convective soil gas migration additional to the common upward diffusion processes, whereas the diurnal variation of the radon concentration at the soil/air interface is caused by the interplay

of the temperature gradient and the wind speed. No impact of atmospheric pressure variation on the radon migration has been observed [16].

Dueñas and Fernandez [22] measured soil radon concentration at different depths at two sampling sites, in the region of Malaga, Spain, to determine if these exhibited significant temporal and quantitative relationships with a number of earthquakes. The magnitudes of the earthquakes ranged from 2 to 4. While both positive and negative precursory perturbations of radon concentrations were observed, in some cases the perturbations were detected after the earthquakes, and several earthquakes occurred without any perturbation of the radon signal being observed, either before or after the events. The study was also aimed at evaluating exhalation of soil radon as an early warning of imminent earthquake activity but meteorological factors were observed to interfere with, or mask the signal so that radon exhalation alone does not appear to be a reliable parameter for predicting earthquakes.

The aim of this work is to study the diurnal variation of soil radon concentration levels, and to correlate it with the variation of temperature with time using a mathematical model based on the heat equation. The influence of atmospheric pressure on soil radon diffusion as well as that of the soil properties: moisture, water saturation and porosity, are not considered in this work. This is justified by the fact that the measurements have been performed over a period of two days where the effects of the variation of these parameters can be neglected.

Methodology and Experimental Procedure

A calibrated active radon device, RAD7[®], (Durrige Company, USA) was used for the measurement of soil radon activity levels. RAD7[®] is a portable radon gas surveyor (PRS) which is suitable for continuous, or grab, sampling measurements of soil radon gas by a solid state detector. RAD7[®] uses a silicon detector that converts alpha radiation directly to an electrical signal. One important advantage of solid state detectors is their ability to electronically determine the energy of alpha particle. Every nucleus of ²²²Rn decays through the sequence ²¹⁸Po, ²¹⁴Pb, ²¹⁴Bi, ²¹⁴Po and ²¹⁰Pb. With each transformation the nuclei emit alpha,

beta or gamma radiation. RAD7[®] is designed to detect alpha radiation only [24].

RAD7[®] can be used in a continuous monitoring mode, which is the most appropriate for this study. A group of commands configure RAD7[®] to perform tests according to the study's requirements. The used probe, a simple

transparent plastic tube, is connected to the device for the measurement of soil radon concentration at different depths (25, 50, 75 cm) below the soil/air interface. The RAD7[®] pack contains a drying unit which is connected to the probe (Fig. 1).

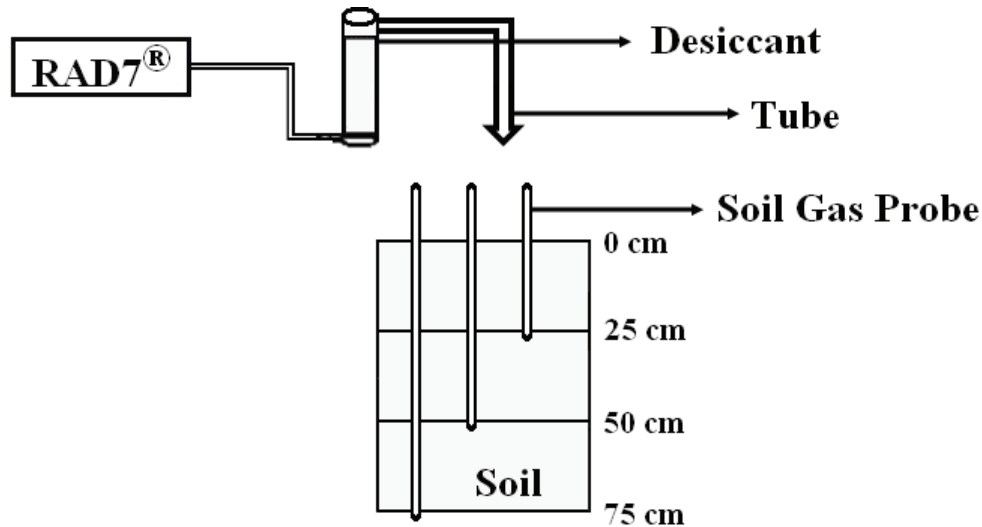


FIG. 1. Field work - Schematic.

It is necessary first to purge the RAD7[®] for one hour or more with dry, fresh air, before connecting the probe. The purging procedure is achieved with the probe disconnected but the drying unit hooked up to RAD7[®]. The used measurement protocol is a 2 hours cycle, 24 recycles, auto mode thoron off and auto pump. The associated printer prints out a header for each measurement. The test is started after checking the header to make sure that the setup is what is required [25].

The total duration of a run was determined by multiplication of cycle time by recycle number; so each depth was automatically measured for 48 hours. In auto pump setting, the pump is switched on for 4 minutes and the air containing radon gas is pumped to the detector through the drying unit. There will be a reading after every two hours cycle, though the first reading will be low because the ^{218}Po decay rate in the detector takes more than 10 minutes to reach equilibrium with the radon concentration in the measurement chamber. Readings are stored in the RAD7[®] memory for later use.

The site chosen is located near the campus of Yarmouk University, Irbid - Jordan. The soil formation is phosphatic [26]. Data were taken in autumn during the period Nov. 15-21, 2011, just

before the beginning of the rainfall season in the region, which means that variation of water saturation can be neglected. A hole was dug and the probe was inserted at depths of 25, 50 and 75 cm (Fig. 1). When measurements were taken at a depth of 25 cm, the external temperature varied between 23.1 °C and 24.4 °C for the first day and between 22.1 °C and 23.7 °C for the second day. For the other depths, the minimum temperature registered was 20.7 °C and the maximum one was 25.8 °C.

RAD7[®] is calibrated by the manufacturer against a master instrument, which, in turn, is calibrated against a standard maintained by the National Radiological Protection Board (NRPB). The overall calibration accuracy is estimated to be about $\pm 5\%$. In most circumstances, the precision of individual RAD7[®] measurements of radon concentration is limited by counting statistics. The error values in Table 1 are those given by the device itself. In the figures, an overall error of $\pm 5\%$ is considered for each individual measurement.

The first remark is the fact that the highest values were obtained in the morning period (between 7 and 10 am). The lowest values were obtained in the late afternoon period (depth 25 cm) or in the evening (depths 50 and 75 cm).

TABLE 1. Highest and lowest soil radon concentration levels (C_{Rn} in Bq/m^3) for all depths.

Depth (cm)	First day		Second day	
	Highest value	Lowest value	Highest value	Lowest value
25	6335 ± 156 at 07:00 am	1855 ± 105 at 5:00 pm	4504 ± 135 at 05:00 am	697 ± 85 at 05:00 pm
50	19088 ± 251 at 08:00 am	12336 ± 332 at 10:00 pm	19394 ± 2 at 12:00 pm	14782 ± 225 at 08:00 pm
75	28823 ± 305 at 10:00 am	19568 ± 374 at 12:00 am	31768 ± 324 at 12:00 pm	21114 ± 267 at 12:00 am

Results and Data Analysis

Table 1 shows the highest and lowest measured values for all depths.

Figures 2, 3 and 4 show the results of measurements, over the two days period, of relative soil radon concentration levels (C/C_{max}) as a function of time, for the depths: 25, 50 and 75 cm, respectively. C_{max} is the maximum concentration value for a given depth over 24 hours. The vertical axis is thus unitless. The very first measurement for each set of data is neglected, thus the number of data points considered is 23 for each depth.

The time scale in Fig. 2, for the depth 25 cm, is such that $t = 0$ h corresponds to the reading taken the first day at 1:00 am. For the depths 50 and 75 cm, $t = 0$ corresponds to the reading taken the first day at midnight and 02:00 am, respectively. The time interval between two

measurements is two hours. The figures will be discussed later in this paper.

A preliminary non-linear least squares fit using a cosine function ($A \cos(\omega t + \delta) + B$) was used in order to smooth the data showing the periodic behavior of soil radon concentration with time. The fit parameters are: A and B are dimensionless offset parameters, ω is the angular frequency and δ is a phase constant. The value of these parameters for data at depths 25, 50 and 75 cm for the two days period are shown in Figures 2 to 4, respectively.

The periodicity of the soil radon levels is clearly observed for the depths 25 and 50 cm which is consistent with previous studies [16].

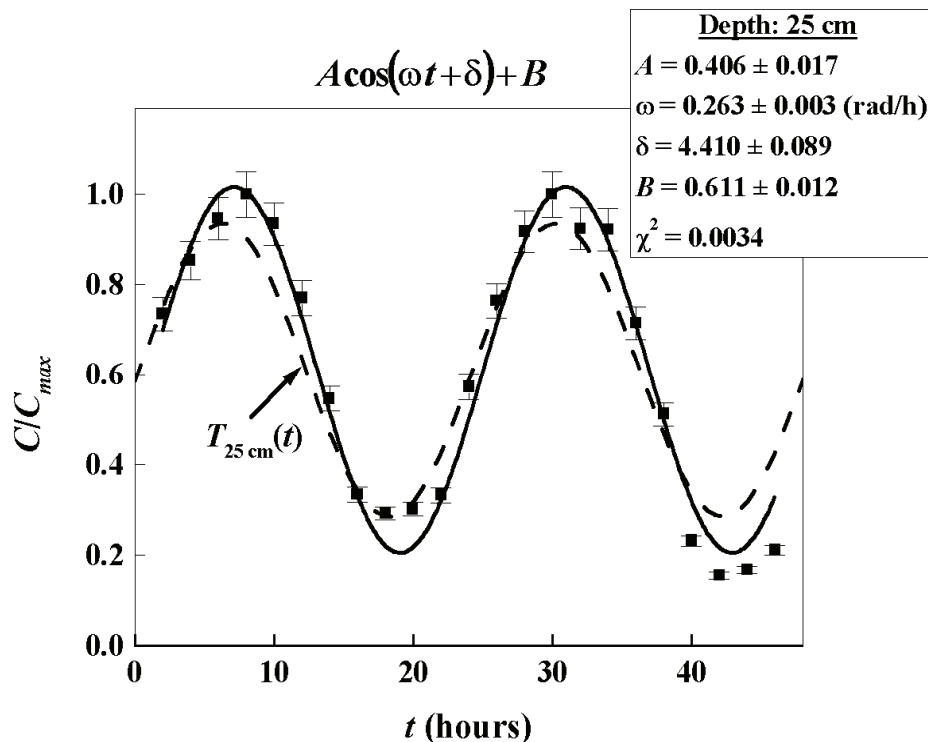


FIG. 2. Diurnal variation of soil radon concentration levels at depth 25 cm over two days (48 h cycle). See text for $T_{25 \text{ cm}}(t)$.

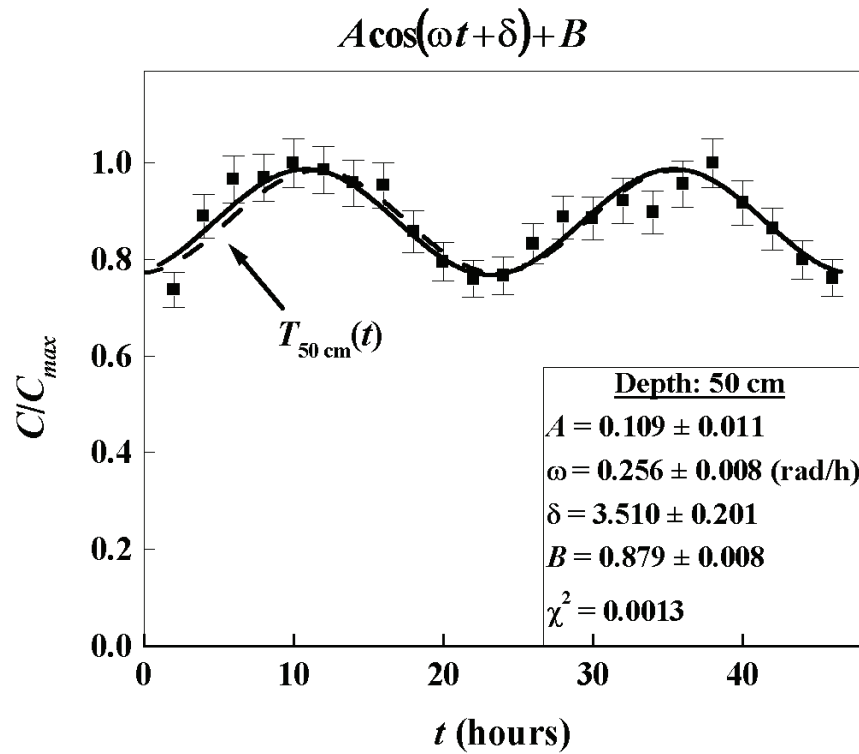


FIG. 3. Diurnal variation of soil radon concentration levels at depth 50 cm over two days (48 h cycle). See text for $T_{50\text{ cm}}(t)$.

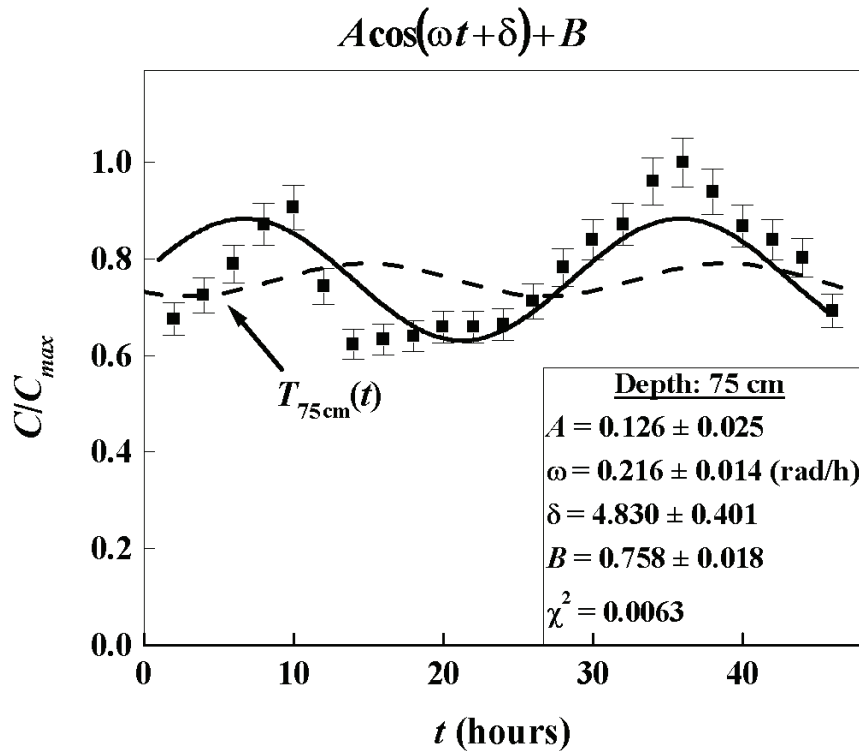


FIG. 4. Diurnal variation of soil radon concentration levels at depth 75 cm over two days (48 h cycle). See text for $T_{75\text{ cm}}(t)$.

Tentative explanation of the choice of a cosine fitting function

The fact that the cosine function fits well the data was thought of being related to the periodic variation of the temperature of the soil. The following assumptions support this idea:

- 1- The soil is considered as a semi-infinite homogenous medium. Porosity of the soil η is considered to be constant ($\eta \approx 0.5$ as confirmed by a separate study). Since measurements in this study were done just before the beginning of the rainfall season in the region, soil moisture variation is neglected.
- 2- Dependence of soil radon diffusion on pressure is also neglected. For relatively short periods of measuring time, atmospheric pressure in the study region does not vary. In addition, various previous studies, in particular that of Schubert and Schulz [16], support this assumption.
- 3- The temperature of the soil can be obtained from the solution of the heat equation:

$$\nabla^2 T = -k \frac{\delta T}{\delta t} \quad (1)$$

with a heat wave, originating from the sun and hitting the soil, given by:

$$T(t) = T_0 \cos(\omega t + \delta) \text{ at } z = 0. \quad (2)$$

k is the thermal diffusivity. k is related to the Fourier coefficient, a , of a medium of density ρ and specific heat capacity at constant pressure c_p , by the relation:

$$k = a \frac{\rho}{c_p} \quad (3)$$

T_0 is the maximum amplitude of the heat source (the sun) generally taken to be 15 °C, i.e. the average temperature of the earth, ω is the angular frequency of the earth ($\omega = 7.27 \cdot 10^{-5}$ rad/s = 0.262 rad/hour) and δ is a phase constant.

- 4- The temperature field, $T(z, t)$, at depth z below the soil/air interface is the solution of the heat equation with the boundary conditions:

$$T(0, t) = T_{av} + T_0 \cos(\omega t) \quad (4)$$

$$T(\infty, t) = T_{av} \quad (5)$$

where T_{av} is the average temperature of the soil-air interface (around 20 °C in this study). This solution has the form:

$$T(z, t) = T_{av} + T_0 e^{-Fz} \cos\left(\omega\left(t - \frac{z}{v}\right)\right) \quad (6)$$

Taking a , the Fourier coefficient for soil ($0.018 \text{ cm}^2 \text{ s}^{-1}$),

$$F = \sqrt{\omega/(2a)} = 0.0449 \text{ cm}^{-1},$$

$$v = \sqrt{2a\omega} = 0.0016 \text{ cm s}^{-1} = 5.827 \text{ cm h}^{-1}$$

The fitted values of ω , δ and B are used in order to plot the dimensionless function:

$$\left. \begin{aligned} T_z(t) &= \frac{T(z, t) - T_{av}}{T_0} \\ &= B + e^{-Fz} \cos\left(\omega\left(t - \frac{z}{v}\right)\right) \end{aligned} \right\} \quad (7)$$

for the depth $z = 25$ cm. The offset parameter B obtained by the fit is used here to scale the function with the data. The origin for $T_z(t)$ is shifted by two hours. The dimensionless functions $T_{25\text{cm}}(t)$, $T_{50\text{cm}}(t)$ and $T_{75\text{cm}}(t)$ are, respectively, shown in Figures 2, 3 and 4 (dashed line) – no units needed.

For clarity we give below these functions,

$$T_{25\text{cm}}(t) = 0.611 + 0.325 \cos(0.262((t-2) - 4.290)) \quad (8a)$$

$$T_{50\text{cm}}(t) = 0.879 + 0.105 \cos(0.262((t-2) - 8.580)) \quad (8b)$$

$$T_{75\text{cm}}(t) = 0.758 + 0.034 \cos(0.262((t-2) - 12.870)) \quad (8c)$$

The diurnal variation of soil radon concentration levels follows a pattern similar to that of the temperature variation with time for the depths 25 and 50 cm.

The cosine behavior is less marked for the depth 75 cm, and as can be seen in Fig. 4 the diurnal variation of temperature shows no correlation with the variation of C/C_{max} . The incoming solar radiation energy is utilized as heat as it travels down the soil profile. Thus, available energy decreases with depth. An

amplitude damping is observed. This damping is due, as expected, to the factor

e^{-Fz} in Eq. (7). This damping causes a distortion which is visible in Fig. 4. In addition, there is a delay in the time at which any specific location on the temperature cycle reaches a given point in the soil. This time lag becomes more pronounced with increasing depth [27].

Conclusion

The present study shows that the measured periodicity of soil radon concentration levels can be fitted using a cosine function. This fit produces a pattern similar to that of the variation of temperature with time at the depths 25 cm and 50 cm. The variation of temperature is obtained by resolving the heat equation for a heat wave,

originating from the sun, hitting the soil which is approximated as a semi-infinite homogenous medium. Besides its theoretical importance, this work may help in the study of earthquakes. An application of this work would be the following: permanent monitoring of the soil radon concentration levels in real time and their pattern similar to the diurnal variation of the temperature of the soil, could indicate, in the case of sensitive perturbations in the cosine pattern, changes of the structure of the soil due to tremors following an earthquake.

Acknowledgement

The authors wish to thank the Abdul Hameed Shoman Fund for Supporting Scientific Research.

References

- [1] BEIR, VI, "Health effects of exposure to radon/Committee on Health Risks of Exposure to Radon", (Board on Radiation Effects Research, Commission on Life Sciences, National Research Council, USA, 1999).
- [2] NCRP Report No. 78. Evaluation of occupational and environmental exposures to radon and radon daughters in the United States (1984).
- [3] Khayrat, A.H., Oliver, M.A. and Durrani, S.A., *Radiat. Meas.*, 34 (2001) 365.
- [4] Shweikani, R., Giaddui, T.G. and Durrani, S.A., *Radiat. Meas.*, 25 (1995) 581.
- [5] Tanner, A.B., "Radon migration in the ground: A supplementary review". In: Gessell, T.F. and Lowder, W.M. (eds.), *Natural radiation environment III*. (US Department of Energy Report CONF-780422, Washington, vol. 1, 1980), p 5.
- [6] Nazaroff, W.W., *Rev. Geophys.*, 30 (1992) 137.
- [7] Hirst, W. and Harrison, G.E., *Proc. R. Soc. London, Ser. A* 169 (1939) 573.
- [8] Ershaidat, N.M., Al-Bataina, B.A. and Al-Shereideh, S.A., *Environ. Geol.*, 55 (2008) 29.
- [9] Tanner, A.B., "Radon migration in the ground: A review", In: Adams, J.A.S. and Lowder, W.M. (eds.), *Natural Radiation Environment*, (Chicago University Press, Chicago, 1964), p. 161.
- [10] Yakovleva, V., *Annals of Geophys.*, 48 (2005) 195.
- [11] Neves, L.J.P.F., Barbosa, S.M. and Pereira, A.J.S.C, *Journal of Environmental Radioactivity*, 100 (2009) 896. doi: 10.1016/j.jenvrad.2009.06.017
- [12] Sheets, R.W., *J. Air Waste Manage. Assoc.*, 42 (1992) 457.
- [13] Nagaraja, K., Prasada, B.S.N., Madhavaa, M.S., Chandrashekaraa, M.S. and Paramesha, L., *Radiat. Meas.*, 36 (2003) 413.
- [14] Seftelis, I., Nicolaou, G., Trassanidis, S. and Tsagas, F.N., *Journal of Environmental Radioactivity*, 97 (2007) 116.
- [15] Kovach, E.M., *Terr. Magn. Atmos. Electr.*, 51 (1946) 45.
doi:10.1029/TE051i001p 00045.
- [16] Schubert, M. and Schulz, H., *Health Physics*, 83 (2002) 91.
- [17] El-Hussein, A., Mohamemed, A., Abd El-Hady, M., Ahmed, A.A, Ali, A.E. and Barakat, A., *Atmospheric Environment*, 35 (2001) 4305.

- [18] Malakhov, S.G., Bakulin, V.N., Dmitrieva, G.V., Kirichenko, L.V., Ssissigina, T.I. and Starikov, B.G., *Tellus XVIII*, 2 (1966) 643.
- [19] Pearson, J.E. and Moses, H., *Journal of Applied Meteorology*, 5 (1966) 175.
- [20] Porstendörfer, J., Butterweck, G. and Reineking, A., *Atmos. Environ.*, 25 (1991) 709.
- [21] Chyi, L.L., Quick, T.J., Yang, T.F. and Chen, C-H., *TAO*, 16 (2005) 763.
- [22] Dueñas, C., Fernandez, M.C., Carretero, J., Liger, E. and Perez, M., *Ann. Geophys.*, 15 (1997) 124.
- [23] Singh, S., Kumar, A., Singh Bajwa¹, B., Mahajan¹, S., Kumar, V. and Dhar, S., *Terr. Atmos. Ocean. Sci.*, 21 (2009) 685.
- [24] Durrige Company, Inc., Reference Manual version 6.0.1, RAD7 Electronic Radon Detector (2000).
- [25] Durrige Company, Inc., Soil gas probe instructions, measurements, continuous monitoring. <http://www.durrige.com>, (2003). Accessed 7 June 2012.
- [26] Al-Rayashi, W.S., M. Sc. Thesis, Yarmouk University, (2011), Irbid - Jordan (Unpublished).
- [27] Hillel, D., *Introduction to soil physics*. Academic Press, San Diego, CA.

Jordan Journal of Physics

ARTICLE

Canonical Quantization for Fractional Schrödinger Lagrangian Density in Caputo Definition

Emad K. Jaradat

Department of Physics, Mu'tah University, Al-Karak, Jordan.

Received on: 21/2/2013; Accepted on: 29/9/2013

Abstract: The fractional form of the Schrödinger Lagrangian density is presented using the Caputo's fractional derivative. Agrawal procedure is employed to obtain time dependent and time independent Schrödinger equations in Caputo's fractional form. The Hamiltonian density resulting from the Schrödinger Lagrangian density is obtained in fractional form. Then, we used Dirac algebraic method to quantize the Schrödinger Lagrangian density by determining the fractional creation and annihilation operators and constructing the fractional Canonical Commutation Relations (CCRs).

Keywords: Fractional Schrödinger Lagrangian density; Fractional Canonical Quantization; Fractional time dependent Schrödinger equation; Fractional Caputo's Definition.

Introduction

The concept of fractional calculus goes back to Leibniz, Liouville, Riemann, Grunwald and Letnikov [1-3]. Derivatives and integrals of fractional order have found many applications in recent studies in mechanics and physics. In a fairly short period of time, the list of such applications becomes long. For example, mechanics of fractal media, quantum mechanics, physical kinetics, plasma physics, mechanics of non-Hamiltonian systems, theory of long-range interaction and many other physical topics [4-20]. In mathematics and theoretical physics, the variational (functional) derivative is a generalization of the usual derivative that arises in the calculus of variations. In this paper, we consider the fractional generalization of Schrödinger Lagrangian density and obtain the Fractional dependent Schrödinger equation from it by using Agrawal approach in Caputo's formula.

Schrödinger equation represents a fundamental equation in quantum field theory. This equation can be derived from classical physics by using Nelson's stochastic theory [21]. However, only during the last decade have scientific papers concerning fractional quantum

mechanics appeared. Muslih *et al.* [6] presented a fractional Schrödinger equation and its solution. They extended the variational principle formulations for fractional discrete system to fractional field system defined in terms of Caputo derivatives to obtain the fractional Euler Lagrange equations of motion.

Laskin [21-25] has shown that the path integral approach over Levy paths leads to fractional quantum mechanics. Next, he considered the fractional Schrödinger equation for some particular cases like fractional Bohr atom and 1-dimensional fractional oscillator. Naber [26] showed a time Caputo fractional Schrödinger equation. Wang and Xu [27] generalized the fractional Schrödinger equation to construct a space-time fractional Schrödinger equation. Hall and Reginatta [28] showed that the fractional Schrödinger equation can be derived exactly from Uncertainty principle.

In this paper, we would like to derive the time - dependent and independent fractional Schrödinger equation from fractional Schrödinger Lagrangian density using the fractional variational principle, and also to quantize this Lagrangian density by writing the

creation and annihilation operators in fractional formula.

The plan of this paper is as follows:

In the next section, we present the fractional Caputo definition in left right term. Then, we define fractional Schrödinger Lagrangian density and use the theory developed to derive the Euler Lagrange equations which represent the Schrödinger equations. Thereafter, the fractional Schrödinger Lagrangian density is canonically quantized in terms of Caputo's definition by writing the fractional canonical commutation relations. Finally some concluding remarks are given.

Caputo Fractional Derivative

Several definitions of fractional derivatives and integrals have been proposed. These definitions include Caputo, Riemann-Liouville, Grunwald-Letnikov, Marchaud and Riesz fractional derivative [1-2]. Here, we reformulate the Schrödinger Lagrangian density and Euler-Lagrange equations in terms of left-right Caputo fractional derivatives, which are defined in [1].

We begin with the left and the right Riemann–Liouville fractional derivatives of order $\alpha > 0$ of a function $x(t)$ which are defined as:

$${}_a D_t^\alpha x(t) = \frac{1}{\Gamma(n-\alpha)} \left(\frac{d}{dt}\right)^n \int_a^t (t-\tau)^{n-\alpha-1} x(\tau) d\tau \tag{1}$$

and

$${}_t D_b^\alpha x(t) = \left. \frac{1}{\Gamma(n-\alpha)} \left(-\frac{d}{dt}\right)^n \int_t^b (\tau-t)^{n-\alpha-1} x(\tau) d\tau \right\} \tag{2}$$

The left Caputo Fractional Derivative LCFD:

$${}_a^c D_t^\alpha f(t) = \left. \frac{1}{\Gamma(n-\alpha)} \int_a^t (t-\tau)^{n-\alpha-1} \left(\frac{d}{d\tau}\right)^n f(\tau) d\tau \right\} \tag{3}$$

and the right Caputo Fractional Derivative RCFD:

$${}_t^c D_b^\alpha f(t) = \left. \frac{1}{\Gamma(n-\alpha)} \int_t^b (\tau-t)^{n-\alpha-1} \left(-\frac{d}{d\tau}\right)^n f(\tau) d\tau \right\} \tag{4}$$

Here, Γ represents the Euler's gamma function and α is the order of derivative such that $n-1 < \alpha \leq n$. If α is an integer, these derivatives are defined in the usual sense, i.e.:

$${}_a D_t^\alpha f(t) = \left(\frac{df(t)}{dt}\right)^\alpha \tag{5-a}$$

$${}_t D_b^\alpha f(t) = \left(-\frac{df(t)}{dt}\right)^\alpha \tag{5-b}$$

$${}_a^c D_t^\alpha f(t) = \left(\frac{df(t)}{dt}\right)^\alpha \tag{5-c}$$

$${}_t^c D_b^\alpha f(t) = \left(-\frac{df(t)}{dt}\right)^\alpha \tag{5-d}$$

Our fractional Hamiltonian formulation presented here is based on the following theorem [15]. This theorem is stated here (without proof) for completeness.

Theorem. Let $J[q]$ be a functional of the form

$$J[q] = \int_a^b L(t, q, {}_a^c D_{x_\mu}^\alpha q, {}_x_\mu^c D_b^\beta q) dx_\mu$$

where $0 < \alpha, \beta < 1$ and defined on the set of functions $y(x)$ which have continuous LCFD of order α and RCFD of order β in $[a, b]$. Then, a necessary condition for $J[q]$ to have an extremum for a given function $q(t)$ is that $q(t)$ satisfy the generalized Euler–Lagrange equation given by:

$$\frac{\partial L}{\partial q} + {}_t^c D_b^\alpha \frac{\partial L}{\partial {}_a^c D_t^\alpha q} + {}_a^c D_t^\beta \frac{\partial L}{\partial {}_t^c D_b^\beta q} = 0 \tag{6}$$

$$t \in [a, b].$$

The Euler-Lagrange equation has been extended to classical field systems [14-15]. The action of the classical field containing fractional partial derivatives takes the form:

$$J(q) = \int L(\psi, {}_a^c D_t^\alpha \psi, {}_t^c D_b^\beta \psi, {}_a^c D_x^\alpha \psi, {}_x^c D_b^\beta \psi, t) d^4 x$$

The extremization of this action leads to the fractional Euler-Lagrange equation of the form:

$$\frac{\partial L}{\partial q} + {}_{x_\mu} D_b^\alpha \frac{\partial L}{\partial {}^c D_a^\alpha q} + {}_a D_{x_\mu}^\beta \frac{\partial L}{\partial {}^c D_{x_\mu}^\beta q} = 0$$

$$x_\mu \in [a, b], \quad (7)$$

$$\left. \begin{aligned} & \frac{\partial L}{\partial \psi} + {}^c D_b^\alpha \frac{\partial L}{\partial {}^c D_t^\alpha \psi} + {}_a D_t^\beta \frac{\partial L}{\partial {}^c D_b^\beta \psi} + \\ & {}^c D_{x_i}^\alpha \frac{\partial L}{\partial {}^c D_{x_i}^\alpha \psi} + {}_{x_i} D_b^\beta \frac{\partial L}{\partial {}^c D_{x_i}^\beta \psi} = 0 \end{aligned} \right\} \quad (8)$$

Note that for $\alpha = \beta = 1$, the last equation can be reduced to the standard Euler-Lagrange equation for classical fields [29].

Schrödinger Lagrangian Density in Caputo Fractional Definition

The concept of Lagrangian density is defined as the kinetic energy per unit volume minus the potential energy per unit volume. The usual Lagrangian of the system will be then equal to the Lagrangian density integrated over the whole volume of the system. Many applications of fractional calculus amount to replacing the time derivative in an evolution with a derivative of fractional order. A given classical Lagrangian is not unique because there are several possibilities to replace the time derivative by fractional case. One of the requirements is to obtain the same Lagrangian expression if the order α becomes 1.

The main purpose here is to write the fractional formula for the Schrödinger Lagrangian density using the above definitions:

$$\left. \begin{aligned} \mathcal{L} &= i\hbar \psi^* \left[{}^c D_t^\alpha \psi + {}_t D_b^\beta \psi \right] \\ &- \frac{\hbar^2}{2m} \left[{}^c D_{x_i}^\alpha \psi^* + {}_{x_i} D_b^\beta \psi^* \right] \left[{}^c D_{x_i}^\alpha \psi + {}_{x_i} D_b^\beta \psi \right] \\ &- V(r) \psi^* \psi \end{aligned} \right\} \quad (9)$$

Apply generalized Euler-Lagrange Eq. (7) on the fields ψ^*, ψ respectively to get equations of motion from the Schrödinger Lagrangian density in Caputo Form.

First for ψ^*

$$\frac{\partial L}{\partial \psi^*} = i\hbar \left[{}^c D_t^\alpha \psi + {}_t D_b^\beta \psi \right] - V(r) \psi$$

and

$$\left. \begin{aligned} & {}_{x_\mu} D_b^\alpha \frac{\partial L}{\partial {}^c D_a^\alpha \psi^*} + {}_a D_{x_\mu}^\beta \frac{\partial L}{\partial {}^c D_{x_\mu}^\beta \psi^*} = \\ & \left. \begin{aligned} & {}_i D_b^\alpha \frac{\partial L}{\partial {}^c D_t^\alpha \psi^*} + {}_{x_i} D_b^\alpha \frac{\partial L}{\partial {}^c D_{x_i}^\alpha \psi^*} \\ & + {}_a D_t^\beta \frac{\partial L}{\partial {}^c D_b^\beta \psi^*} + {}_a D_{x_i}^\beta \frac{\partial L}{\partial {}^c D_{x_i}^\beta \psi^*} \end{aligned} \right\}$$

Then

$$\left. \begin{aligned} & {}_{x_\mu} D_b^\alpha \frac{\partial L}{\partial {}^c D_a^\alpha \psi^*} + {}_a D_{x_\mu}^\beta \frac{\partial L}{\partial {}^c D_{x_\mu}^\beta \psi^*} = \\ & \left. \begin{aligned} & -\frac{\hbar^2}{2m} \left({}_{x_i} D_b^\alpha \left[{}^c D_{x_i}^\alpha \psi + {}_{x_i} D_b^\beta \psi \right] \right) \\ & + {}_a D_{x_i}^\beta \left[{}^c D_{x_i}^\alpha \psi + {}_{x_i} D_b^\beta \psi \right] \end{aligned} \right\}$$

Adding these results and putting them equal to zero, we get:

$$\left. \begin{aligned} & i\hbar \left[{}^c D_t^\alpha \psi + {}_t D_b^\beta \psi \right] - V(r) \psi \\ & + \frac{-\hbar^2}{2m} \left({}_{x_i} D_b^\alpha \left[{}^c D_{x_i}^\alpha \psi + {}_{x_i} D_b^\beta \psi \right] \right) \\ & + {}_a D_{x_i}^\beta \left[{}^c D_{x_i}^\alpha \psi + {}_{x_i} D_b^\beta \psi \right] \end{aligned} \right\} \quad (10)$$

$$= 0$$

This represents fractional time-dependent Schrödinger equation in terms of Caputo definition. As $\alpha, \beta \rightarrow 1$, we obtain the classical time dependent Schrödinger equations [30].

For second field ψ , we get:

$$\frac{\partial L}{\partial \psi} = -V(r) \psi^*$$

and

$$\left. \begin{aligned} & {}_{x_\mu} D_b^\alpha \frac{\partial L}{\partial {}^c D_a^\alpha \psi} + {}_a D_{x_\mu}^\beta \frac{\partial L}{\partial {}^c D_{x_\mu}^\beta \psi} = \\ & \left. \begin{aligned} & {}_i D_b^\alpha \frac{\partial L}{\partial {}^c D_t^\alpha \psi} + {}_{x_i} D_b^\alpha \frac{\partial L}{\partial {}^c D_{x_i}^\alpha \psi} \\ & + {}_a D_t^\beta \frac{\partial L}{\partial {}^c D_b^\beta \psi} + {}_a D_{x_i}^\beta \frac{\partial L}{\partial {}^c D_{x_i}^\beta \psi} \end{aligned} \right\}$$

then

$$\left. \begin{aligned} & {}^c D_b^\alpha \frac{\partial L}{\partial {}^c D_{x_\mu}^\alpha \psi} + {}^c D_{x_\mu}^\beta \frac{\partial L}{\partial {}^c D_b^\beta \psi} = \\ & -\frac{\hbar^2}{2m} \left[{}^c D_{x_i}^\beta + {}^c D_b^\alpha \right] \left[{}^c D_{x_i}^\alpha \psi^* + {}^c D_b^\beta \psi^* \right] \end{aligned} \right\}$$

Similarly, adding these results and putting them equal to zero, we obtain:

$$\left. \begin{aligned} & -V(r)\psi^* + \\ & -\frac{\hbar^2}{2m} \left[{}^c D_{x_i}^\beta + {}^c D_b^\alpha \right] \left[{}^c D_{x_i}^\alpha \psi^* + {}^c D_b^\beta \psi^* \right] \\ & = 0 \end{aligned} \right\} \quad (11)$$

This equation represents the fractional time independent Schrödinger equation in fractional Caputo definition. As $\alpha, \beta \rightarrow 1$, we obtain the classical time independent Schrödinger equations [30].

Canonical Quantization of Schrödinger Lagrangian Density

In order to quantize the Schrödinger equation, we will treat it as an ordinary field equation for which we will first develop the Hamiltonian density formalism:

$$\left. \begin{aligned} & \mathcal{H} = \pi \left({}^c D_t^\alpha \psi + {}^c D_b^\beta \psi \right) \\ & + \pi^* \left({}^c D_t^\alpha \psi^* + {}^c D_b^\beta \psi^* \right) - \mathcal{L} \end{aligned} \right\} \quad (12)$$

$$\mathcal{H} = \left[\begin{aligned} & \left(\sqrt{\frac{\hbar^2}{2m}} \left\{ \left({}^c D_{x_i}^\alpha + {}^c D_b^\beta \right) \psi^* \left({}^c D_{x_i}^\alpha + {}^c D_b^\beta \right) \psi \right\}^{\frac{1}{2}} + i \{ V(r) \psi^* \psi \}^{\frac{1}{2}} \right) \times \\ & \left(\sqrt{\frac{\hbar^2}{2m}} \left\{ \left({}^c D_{x_i}^\alpha + {}^c D_b^\beta \right) \psi^* \left({}^c D_{x_i}^\alpha + {}^c D_b^\beta \right) \psi \right\}^{\frac{1}{2}} - i \{ V(r) \psi^* \psi \}^{\frac{1}{2}} \right) \end{aligned} \right] \quad (14)$$

Generalize this formula using fractional definition in terms of μ, ν as:

$$\mathcal{H}_{\mu\nu} = \left[\begin{aligned} & \left(\sqrt{\frac{\hbar^2}{2m}} \left\{ \left({}^c D_{x_i}^\alpha + {}^c D_b^\beta \right) \psi^* \left({}^c D_{x_i}^\alpha + {}^c D_b^\beta \right) \psi \right\}^{\frac{\mu}{2}} + i \{ V(r) \psi^* \psi \}^{\frac{\nu}{2}} \right) \times \\ & \left(\sqrt{\frac{\hbar^2}{2m}} \left\{ \left({}^c D_{x_i}^\alpha + {}^c D_b^\beta \right) \psi^* \left({}^c D_{x_i}^\alpha + {}^c D_b^\beta \right) \psi \right\}^{\frac{\mu}{2}} - i \{ V(r) \psi^* \psi \}^{\frac{\nu}{2}} \right) \end{aligned} \right] \quad (15)$$

where μ, ν are noninteger numbers.

where π, π^* canonical conjugate momentum for fields ψ, ψ^* respectively, which are defined as:

$$\pi = \frac{\partial \mathcal{L}}{\partial \left({}^c D_t^\alpha \psi + {}^c D_b^\beta \psi \right)}, \quad \pi = i\hbar \psi^*$$

$$\pi^* = \frac{\partial \mathcal{L}}{\partial \left({}^c D_t^\alpha \psi^* + {}^c D_b^\beta \psi^* \right)}, \quad \pi^* = 0.$$

Substituting these values in the Hamiltonian density formula, we get:

$$\left. \begin{aligned} & \mathcal{H} = i\hbar \psi^* \left({}^c D_t^\alpha \psi + {}^c D_b^\beta \psi \right) \\ & - i\hbar \psi^* \left[{}^c D_t^\alpha \psi + {}^c D_b^\beta \psi \right] \\ & + \frac{\hbar^2}{2m} \left[{}^c D_{x_i}^\alpha \psi^* + {}^c D_b^\beta \psi^* \right] \left[{}^c D_{x_i}^\alpha \psi + {}^c D_b^\beta \psi \right] \\ & + V(r) \psi^* \psi \end{aligned} \right\}$$

After some algebraic operations, we obtain:

$$\left. \begin{aligned} & \mathcal{H} = \\ & \frac{\hbar^2}{2m} \left[{}^c D_{x_i}^\alpha \psi^* + {}^c D_b^\beta \psi^* \right] \left[{}^c D_{x_i}^\alpha \psi + {}^c D_b^\beta \psi \right] \\ & + V(r) \psi^* \psi \end{aligned} \right\} \quad (13)$$

Using Derac algebraic method to rewrite this quantity [27] gives:

We can define a^+, a as:

$$a^+ = \sqrt{\frac{\hbar^2}{2m}} \left\{ \left({}^c D_{x_i}^\alpha + {}^c D_{x_i}^\beta \right) \psi^* \left({}^c D_{x_i}^\alpha + {}^c D_{x_i}^\beta \right) \psi \right\}^{\frac{\mu}{2}} + i \left\{ V(r) \psi^* \psi \right\}^{\frac{\nu}{2}} \quad (16)$$

$$a = \sqrt{\frac{\hbar^2}{2m}} \left\{ \left({}^c D_{x_i}^\alpha + {}^c D_{x_i}^\beta \right) \psi^* \left({}^c D_{x_i}^\alpha + {}^c D_{x_i}^\beta \right) \psi \right\}^{\frac{\mu}{2}} - i \left\{ V(r) \psi^* \psi \right\}^{\frac{\nu}{2}} \quad (17)$$

where a^+, a are the fractional creation and annihilation operators.

Now, we want to write the canonical commutation relations CCRs as:

$$[a^+, a] = \left[\begin{array}{l} \sqrt{\frac{\hbar^2}{2m}} \left\{ \left({}^c D_{x_i}^\alpha + {}^c D_{x_i}^\beta \right) \psi^* \left({}^c D_{x_i}^\alpha + {}^c D_{x_i}^\beta \right) \psi \right\}^{\frac{\mu}{2}} + i \left\{ V(r) \psi^* \psi \right\}^{\frac{\nu}{2}}, \\ \sqrt{\frac{\hbar^2}{2m}} \left\{ \left({}^c D_{x_i}^\alpha + {}^c D_{x_i}^\beta \right) \psi^* \left({}^c D_{x_i}^\alpha + {}^c D_{x_i}^\beta \right) \psi \right\}^{\frac{\mu}{2}} - i \left\{ V(r) \psi^* \psi \right\}^{\frac{\nu}{2}} \end{array} \right]$$

This is equal to:

$$[a^+, a] = a^+ a - a a^+ \quad (18)$$

Expanding these values, we get:

$$[a^+, a] = \left[\begin{array}{l} \left(\sqrt{\frac{\hbar^2}{2m}} \left\{ \left({}^c D_{x_i}^\alpha + {}^c D_{x_i}^\beta \right) \psi^* \left({}^c D_{x_i}^\alpha + {}^c D_{x_i}^\beta \right) \psi \right\}^{\frac{\mu}{2}} + i \left\{ V(r) \psi^* \psi \right\}^{\frac{\nu}{2}} \right)^* \\ \left(\sqrt{\frac{\hbar^2}{2m}} \left\{ \left({}^c D_{x_i}^\alpha + {}^c D_{x_i}^\beta \right) \psi^* \left({}^c D_{x_i}^\alpha + {}^c D_{x_i}^\beta \right) \psi \right\}^{\frac{\mu}{2}} - i \left\{ V(r) \psi^* \psi \right\}^{\frac{\nu}{2}} \right) \\ - \left(\sqrt{\frac{\hbar^2}{2m}} \left\{ \left({}^c D_{x_i}^\alpha + {}^c D_{x_i}^\beta \right) \psi^* \left({}^c D_{x_i}^\alpha + {}^c D_{x_i}^\beta \right) \psi \right\}^{\frac{\mu}{2}} - i \left\{ V(r) \psi^* \psi \right\}^{\frac{\nu}{2}} \right)^* \\ \left(\sqrt{\frac{\hbar^2}{2m}} \left\{ \left({}^c D_{x_i}^\alpha + {}^c D_{x_i}^\beta \right) \psi^* \left({}^c D_{x_i}^\alpha + {}^c D_{x_i}^\beta \right) \psi \right\}^{\frac{\mu}{2}} + i \left\{ V(r) \psi^* \psi \right\}^{\frac{\nu}{2}} \right) \end{array} \right]$$

The first term can be written as:

$$a^+ a = \left(\sqrt{\frac{\hbar^2}{2m}} \left\{ \left({}^c D_{x_i}^\alpha + {}^c D_{x_i}^\beta \right) \psi^* \left({}^c D_{x_i}^\alpha + {}^c D_{x_i}^\beta \right) \psi \right\}^{\frac{\mu}{2}} + i \left\{ V(r) \psi^* \psi \right\}^{\frac{\nu}{2}} \right) \left(\sqrt{\frac{\hbar^2}{2m}} \left\{ \left({}^c D_{x_i}^\alpha + {}^c D_{x_i}^\beta \right) \psi^* \left({}^c D_{x_i}^\alpha + {}^c D_{x_i}^\beta \right) \psi \right\}^{\frac{\mu}{2}} - i \left\{ V(r) \psi^* \psi \right\}^{\frac{\nu}{2}} \right)$$

Using the Hamiltonian density definition, then:

$$a^+ a = \mathcal{H}_{\mu\nu} + i \sqrt{\frac{\hbar^2}{2m}} \left[\left\{ V(r) \psi^* \psi \right\}^{\frac{\nu}{2}}, \left\{ \left({}^c D_{x_i}^\alpha + {}^c D_{x_i}^\beta \right) \psi^* \left({}^c D_{x_i}^\alpha + {}^c D_{x_i}^\beta \right) \psi \right\}^{\frac{\mu}{2}} \right] \quad (19)$$

The second term equals:

$$aa^+ = \left(\sqrt{\frac{\hbar^2}{2m}} \left\{ \left({}^C D_{x_i}^\alpha + {}^C D_{x_i}^\beta \right) \psi^* \left({}^C D_{x_i}^\alpha + {}^C D_{x_i}^\beta \right) \psi \right\}^{\frac{\mu}{2}} - i \left\{ V(r) \psi^* \psi \right\}^{\frac{\nu}{2}} \right) \\ * \left(\sqrt{\frac{\hbar^2}{2m}} \left\{ \left({}^C D_{x_i}^\alpha + {}^C D_{x_i}^\beta \right) \psi^* \left({}^C D_{x_i}^\alpha + {}^C D_{x_i}^\beta \right) \psi \right\}^{\frac{\mu}{2}} + i \left\{ V(r) \psi^* \psi \right\}^{\frac{\nu}{2}} \right)$$

Similarly, using the Hamiltonian density definition gives:

$$aa^+ = \mathcal{H}_{\mu\nu} + i \sqrt{\frac{\hbar^2}{2m}} \left[\left\{ \left({}^C D_{x_i}^\alpha + {}^C D_{x_i}^\beta \right) \psi^* \left({}^C D_{x_i}^\alpha + {}^C D_{x_i}^\beta \right) \psi \right\}^{\frac{\mu}{2}}, \left\{ V(r) \psi^* \psi \right\}^{\frac{\nu}{2}} \right] \quad (20)$$

Rearranging this term, we get:

$$aa^+ = \mathcal{H}_{\mu\nu} - i \sqrt{\frac{\hbar^2}{2m}} \left[\left\{ V(r) \psi^* \psi \right\}^{\frac{\nu}{2}}, \left\{ \left({}^C D_{x_i}^\alpha + {}^C D_{x_i}^\beta \right) \psi^* \left({}^C D_{x_i}^\alpha + {}^C D_{x_i}^\beta \right) \psi \right\}^{\frac{\mu}{2}} \right] \quad (21)$$

Substituting these results in Eq. (18), we get:

$$a^+a - aa^+ = 2i \sqrt{\frac{\hbar^2}{2m}} \left[\left\{ V(r) \psi^* \psi \right\}^{\frac{\nu}{2}}, \left\{ \left({}^C D_{x_i}^\alpha + {}^C D_{x_i}^\beta \right) \psi^* \left({}^C D_{x_i}^\alpha + {}^C D_{x_i}^\beta \right) \psi \right\}^{\frac{\mu}{2}} \right] \quad (22)$$

Expanding the square brackets, we get:

$$a^+a - aa^+ = 2i \sqrt{\frac{\hbar^2}{2m}} \left\{ \left\{ V(r) \psi^* \psi \right\}^{\frac{\nu}{2}} \left\{ \left({}^C D_{x_i}^\alpha + {}^C D_{x_i}^\beta \right) \psi^* \left({}^C D_{x_i}^\alpha + {}^C D_{x_i}^\beta \right) \psi \right\}^{\frac{\mu}{2}} \right. \\ \left. - \left\{ \left({}^C D_{x_i}^\alpha + {}^C D_{x_i}^\beta \right) \psi^* \left({}^C D_{x_i}^\alpha + {}^C D_{x_i}^\beta \right) \psi \right\}^{\frac{\mu}{2}} \left\{ V(r) \psi^* \psi \right\}^{\frac{\nu}{2}} \right\} \quad (23)$$

Rearranging the terms in the square brackets, we obtain:

$$a^+a - aa^+ = 2i \sqrt{\frac{\hbar^2}{2m}} \left\{ \left\{ V(r) \psi^* \psi \right\}^{\frac{\nu}{2}} \left\{ \left({}^C D_{x_i}^\alpha + {}^C D_{x_i}^\beta \right) \psi^* \left({}^C D_{x_i}^\alpha + {}^C D_{x_i}^\beta \right) \psi \right\}^{\frac{\mu}{2}} \right. \\ \left. - \left\{ V(r) \right\}^{\frac{\nu}{2}} \left\{ \left({}^C D_{x_i}^\alpha + {}^C D_{x_i}^\beta \right) \psi^* \right\}^{\frac{\mu}{2}} \left\{ \psi^* \right\}^{\frac{\nu}{2}} \right. \\ \left. \times \left\{ \left({}^C D_{x_i}^\alpha + {}^C D_{x_i}^\beta \right) \psi \right\}^{\frac{\mu}{2}} \left\{ \psi \right\}^{\frac{\nu}{2}} \right\} \quad (24)$$

Using fractional Leibniz rule to rewrite the second term in the square brackets, we obtain [31]:

$$a^+a - aa^+ = 2i \sqrt{\frac{\hbar^2}{2m}} \left\{ \left\{ V(r) \psi^* \psi \right\}^{\frac{\nu}{2}} \left\{ \left({}^C D_{x_i}^\alpha + {}^C D_{x_i}^\beta \right) \psi^* \left({}^C D_{x_i}^\alpha + {}^C D_{x_i}^\beta \right) \psi \right\}^{\frac{\mu}{2}} \right. \\ \left. - \left\{ V(r) \right\}^{\frac{\nu}{2}} \sum_{j=0}^{\frac{\mu}{2}} \frac{\Gamma\left(\frac{\mu}{2}+1\right)}{j! \Gamma\left(\frac{\mu}{2}-j+1\right)} \frac{\partial^{\frac{\mu}{2}-j}}{\partial x^{\frac{\mu}{2}-j}} \psi^* \frac{\partial^j f}{\partial x^j} \sum_{j=0}^{\frac{\mu}{2}} \frac{\Gamma\left(\frac{\mu}{2}+1\right)}{j! \Gamma\left(\frac{\mu}{2}-j+1\right)} \frac{\partial^{\frac{\mu}{2}-j}}{\partial x^{\frac{\mu}{2}-j}} \psi^2 \frac{\partial^j f}{\partial x^j} \right\} \quad (25)$$

As a special case, taking $\mu, \nu = 2$, the Canonical Commutation Relations CCRs reduce to the original relations like:

$$[a^+, a] = 2i\sqrt{\frac{\hbar^2}{2m}} [V(r)\psi^*\psi, \nabla\psi^*\nabla\psi] \quad (26)$$

$$[a^+, a] = 2iV(r)\sqrt{\frac{\hbar^2}{2m}} \left\{ \begin{aligned} &\psi^* [\psi, \nabla\psi^*] \nabla\psi + \psi^* \nabla\psi^* [\psi, \nabla\psi] + \\ &[\psi^*, \nabla\psi^*] \nabla\psi\psi + \nabla\psi^* [\psi^*, \nabla\psi] \psi \end{aligned} \right\}$$

$$[a^+, a] = 2iV(r)\sqrt{\frac{\hbar^2}{2m}} \left\{ \psi^* \nabla\psi^* [\psi, \nabla\psi] + [\psi^*, \nabla\psi^*] \nabla\psi\psi \right\}$$

Similarly, we can define other canonical commutation relations as:

$$[a^+, \mathcal{H}] = \left[\begin{aligned} &\sqrt{\frac{\hbar^2}{2m}} \left\{ ({}^c D_{x_i}^\alpha + {}^c D_{x_i}^\beta) \psi^* ({}^c D_{x_i}^\alpha + {}^c D_{x_i}^\beta) \psi \right\}^{\frac{\mu}{2}} + i \{V(r)\psi^*\psi\}^{\frac{\nu}{2}} \\ &\left(\sqrt{\frac{\hbar^2}{2m}} \left\{ ({}^c D_{x_i}^\alpha + {}^c D_{x_i}^\beta) \psi^* ({}^c D_{x_i}^\alpha + {}^c D_{x_i}^\beta) \psi \right\}^{\frac{\mu}{2}} + i \{V(r)\psi^*\psi\}^{\frac{\nu}{2}} \right) \times \\ &\left(\sqrt{\frac{\hbar^2}{2m}} \left\{ ({}^c D_{x_i}^\alpha + {}^c D_{x_i}^\beta) \psi^* ({}^c D_{x_i}^\alpha + {}^c D_{x_i}^\beta) \psi \right\}^{\frac{\mu}{2}} - i \{V(r)\psi^*\psi\}^{\frac{\nu}{2}} \right) \end{aligned} \right] \quad (27)$$

$$[a^+, a^+a] = a^+ [a^+, a]$$

Substituting the values of creation and annihilation operators gives:

$$[a^+, a^+a] = \left\{ \begin{aligned} &\sqrt{\frac{\hbar^2}{2m}} \left\{ ({}^c D_{x_i}^\alpha + {}^c D_{x_i}^\beta) \psi^* ({}^c D_{x_i}^\alpha + {}^c D_{x_i}^\beta) \psi \right\}^{\frac{\mu}{2}} + i \{V(r)\psi^*\psi\}^{\frac{\nu}{2}} \\ &\times \left[\begin{aligned} &\sqrt{\frac{\hbar^2}{2m}} \left\{ ({}^c D_{x_i}^\alpha + {}^c D_{x_i}^\beta) \psi^* ({}^c D_{x_i}^\alpha + {}^c D_{x_i}^\beta) \psi \right\}^{\frac{\mu}{2}} + i \{V(r)\psi^*\psi\}^{\frac{\nu}{2}} \\ &\left(\sqrt{\frac{\hbar^2}{2m}} \left\{ ({}^c D_{x_i}^\alpha + {}^c D_{x_i}^\beta) \psi^* ({}^c D_{x_i}^\alpha + {}^c D_{x_i}^\beta) \psi \right\}^{\frac{\mu}{2}} - i \{V(r)\psi^*\psi\}^{\frac{\nu}{2}} \right) \end{aligned} \right] \end{aligned} \right\}$$

Similarly, we can write other commutation relations as:

$$[a, \mathcal{H}] = \left[\begin{aligned} &\sqrt{\frac{\hbar^2}{2m}} \left\{ ({}^c D_{x_i}^\alpha + {}^c D_{x_i}^\beta) \psi^* ({}^c D_{x_i}^\alpha + {}^c D_{x_i}^\beta) \psi \right\}^{\frac{\mu}{2}} - i \{V(r)\psi^*\psi\}^{\frac{\nu}{2}} \\ &\left(\sqrt{\frac{\hbar^2}{2m}} \left\{ ({}^c D_{x_i}^\alpha + {}^c D_{x_i}^\beta) \psi^* ({}^c D_{x_i}^\alpha + {}^c D_{x_i}^\beta) \psi \right\}^{\frac{\mu}{2}} + i \{V(r)\psi^*\psi\}^{\frac{\nu}{2}} \right) \times \\ &\left(\sqrt{\frac{\hbar^2}{2m}} \left\{ ({}^c D_{x_i}^\alpha + {}^c D_{x_i}^\beta) \psi^* ({}^c D_{x_i}^\alpha + {}^c D_{x_i}^\beta) \psi \right\}^{\frac{\mu}{2}} - i \{V(r)\psi^*\psi\}^{\frac{\nu}{2}} \right) \end{aligned} \right] \quad (28)$$

$$[a, a^+a] = [a, a^+]a$$

This is equal to:

$$[a, a^+ a] = \left[\begin{aligned} & \sqrt{\frac{\hbar^2}{2m}} \left\{ \left({}^C D_{x_i}^\alpha + {}^C D_{x_i}^\beta \right) \psi^* \left({}^C D_{x_i}^\alpha + {}^C D_{x_i}^\beta \right) \psi \right\}^{\frac{\mu}{2}} - i \{V(r) \psi^* \psi\}^{\frac{\nu}{2}} \\ & , \sqrt{\frac{\hbar^2}{2m}} \left\{ \left({}^C D_{x_i}^\alpha + {}^C D_{x_i}^\beta \right) \psi^* \left({}^C D_{x_i}^\alpha + {}^C D_{x_i}^\beta \right) \psi \right\}^{\frac{\mu}{2}} + i \{V(r) \psi^* \psi\}^{\frac{\nu}{2}} \\ & \times \sqrt{\frac{\hbar^2}{2m}} \left\{ \left({}^C D_{x_i}^\alpha + {}^C D_{x_i}^\beta \right) \psi^* \left({}^C D_{x_i}^\alpha + {}^C D_{x_i}^\beta \right) \psi \right\}^{\frac{\mu}{2}} - i \{V(r) \psi^* \psi\}^{\frac{\nu}{2}} \end{aligned} \right]$$

and

$$[\pi, \mathcal{H}] = \left[\begin{aligned} & i\hbar \psi^* \left(\sqrt{\frac{\hbar^2}{2m}} \left\{ \left({}^C D_{x_i}^\alpha + {}^C D_{x_i}^\beta \right) \psi^* \left({}^C D_{x_i}^\alpha + {}^C D_{x_i}^\beta \right) \psi \right\}^{\frac{\mu}{2}} + i \{V(r) \psi^* \psi\}^{\frac{\nu}{2}} \right) \\ & \times \left(\sqrt{\frac{\hbar^2}{2m}} \left\{ \left({}^C D_{x_i}^\alpha + {}^C D_{x_i}^\beta \right) \psi^* \left({}^C D_{x_i}^\alpha + {}^C D_{x_i}^\beta \right) \psi \right\}^{\frac{\mu}{2}} - i \{V(r) \psi^* \psi\}^{\frac{\nu}{2}} \right) \end{aligned} \right] \tag{29}$$

and

$$[a^+, a^+] = [a, a] = [\mathcal{H}, \mathcal{H}] = 0. \tag{30}$$

Using equation [30], we find the Heisenberg equation [30] for the a, a^+

$$\frac{da}{dt} = \frac{i}{\hbar} [\mathcal{H}, a] = -\frac{i}{\hbar} [a, \mathcal{H}] \tag{31}$$

$$\frac{da^+}{dt} = -\frac{i}{\hbar} [\mathcal{H}, a^+] = \frac{i}{\hbar} [a^+, \mathcal{H}]. \tag{32}$$

Conclusion

Schrödinger time - dependent and independent equations in Caputo's fractional form are derived using Agrawal procedure for a given fractional Schrödinger Lagrangian density. The classical time - dependent and independent Schrödinger equations are obtained as a particular case of the fractional formulation. In the second part of this paper, we write the

general formula for creation and annihilation operators and construct the fractional Canonical Commutation Relations (CCRs) using Dirac algebraic method. We have shown that the Canonical Commutation Relations (CCRs) in classical form are a special case of the fractional form of these equations.

References

- [1] Podlubny, I., "Fractional Differential Equations", (San Diego: Academic, 1999).
- [2] Oldham, K.B. and Spanier, J., "The Fractional Calculus", (New York: Academic, 1974).
- [3] Hilfer, R. (ed.), "Applications of Fractional Calculus in Physics", (Singapore: World Scientific, 2000).
- [4] Agrawal, O.P., J. Math. Anal. Appl., 272 (2002) 368.
- [5] Agrawal, O.P., Journal of Vibration and Control, 13 (2007) 1217.
- [6] Muslih, S.I., Agrawal, O.P. and Baleanu, D., Int. J. Theor. Phys., 49 (2010) 1746.

- [7] Tenreiro-Machado, J.A. (ed.), “Special Issue of Fractional Order Calculus and Its Applications, Nonlinear Dynamics”, (Berlin: Springer, 2002).
- [8] Tarasov, V.E. and Zaslavsky, G.M., *J. Phys. A: Stat. Mech. Appl.*, 354 (2005) 249.
- [9] Tarasov, V.E. and Zaslavsky, G.M., *J. Phys. A: Math. Gen.*, 39 (2006) 9797.
- [10] Jaradat, E.K., Hijjawi, R.S. and Khalifeh, J.M., *J. Math. Phys.*, 53 (2012) 033505.
- [11] Jaradat, E.K., Hijjawi, R.S. and Khalifeh, J.M., *JJP*, 3(2) (2010) 47.
- [12] Jaradat, E.K., Mu'tah Lil-Buhoth wad-Dirasat, 26(2) (2011).
- [13] Muslih, S.I. and Baleanu, D., *J. Math. Anal. Appl.*, 304 (2005) 599.
- [14] Nawafleh, K.I. and Hijjawi, R.S., *JJP*, 4 (2011) 87.
- [15] Baleanu, D. and Agrawal, O.P., *Czechoslovak. J. Phys.*, 56 (2006) 1087.
- [16] Muslih, S.I., Baleanu, D. and Rabei, E., *Phys. Scr.*, 73 (2006) 436.
- [17] Dong, J.P. and Xu, M.Y., *J. Math. Phys.*, 48 (2007) 072105.
- [18] Rozmej, P. and Bandrowski, B., *Computational Methods in Science and Technology*, 16(2) (2010) 191.
- [19] Agrawal, O.P., *J. Phys. A: Math. Theor.*, 40 (2007) 6287.
- [20] Baleanu, D. and Muslih, S.I., *Physica Scripta*, 72 (2-3) (2005) 119.
- [21] Nelson, E., *Phys. Rev.*, 150 (1966) 1079.
- [22] Laskin, N., *Phys. Rev. E*, 66 (2002) 056108.
- [23] Laskin, N., *Chaos*, 10 (2000) 780.
- [24] Laskin, N., *Phys. Rev. E*, 62 (2000) 3135.
- [25] Laskin, N., *Phys. Lett. A*, 268 (2000) 298.
- [26] Naber, M., *J. Math. Phys.*, 45 (2004) 3339.
- [27] Wang, S.W. and Xu, M.Y., *J. Math. Phys.*, 48 (2007) 043502.
- [28] Hall, M.J.W. and Reginatto, M., *J. Phys. A*, 35 (2002) 3289.
- [29] Goldstein, H. "Classical Mechanics". 2nd Edition, (Addison Wesley, 1980).
- [30] Griffiths, D.J., “Introduction to Quantum Mechanics” (2nd Edition).
- [31] Jaradat, E.K., Thesis, Unpublished, (2009).

Jordan Journal of Physics

ARTICLE

On the Gravitational Properties of Dark Matter

B. Al-Khasawneh^a and M.B. Altaie^b

^a *Department of Physics, Jordanian University of Science and Technology, Jordan.*

^b *Department of Physics, Yarmouk University, 21163 Irbid, Jordan.*

Received on: 23/5/2013; Accepted on: 14/11/2013

Abstract: Analyzing ten known galactic clusters, we were able to identify a serious mass discrepancy when comparing masses calculated from the velocity dispersions of galaxies through virial method and the masses estimated through gravitational lensing. The masses obtained through virial theorem are more than twice those obtained from weak gravitational lensing observations. This might indicate that the equivalence of inertial and gravitational mass is violated in the case of dark matter.

Keywords: Dark matter; Gravitational mass; Inertial mass; Virial theorem.

Introduction

Dark matter (DM) is a concept that was invented in order to explain the mass discrepancy which was calculated in studying the rotation of galaxies and their motion in clusters. The mass needed to explain the motion of stars in galaxies and the galaxies in galactic clusters is much larger than the observed mass [1]. The difference between the calculated and the observed mass was called *Dark Matter*, and it is named as such since it does not emit any form of known radiation.

Physicists can measure the mass of dark matter indirectly by observing its gravitational effects in a variety of ways: rotation of galaxies and their motions within the galactic clusters [2] and [3], gravitational lensing [4], and the Cosmic Microwave Background (CMB) analysis [5]. All these observations have confirmed the need for dark matter as an extra component for the total mass of the universe.

The nature of dark matter is far from being explained let alone be carefully understood. For example, some observations indicate that DM is collisionless [6, 7]. On the other hand, the application of known laws of gravitational physics, using the assumption of the equivalence of the inertial mass and the gravitational mass,

requires DM to get concentrated in centers of galaxies and galactic clusters, not in the halos as is usually indicated by observations, which is counter intuitive. Moreover, being non-emissive of any sort of radiation, DM must be either a dynamical effect or a new sort of mass that is composed of a weird sort of constituents.

Several proposals were put forward in order to explain DM. Among them was the dynamical effect proposal of Milogrim [8] to explain the rotation curves of the galaxies by assuming that Newton's second law of motion should be modified for systems experiencing extremely low accelerations. Other proposals include the expectations to find some massive objects in the galactic halos called MACHO, but particle physicists suggested that DM might be some sorts of exotic particles like Weakly-Interacting Massive Particles (WIMPs) or the super-symmetric components generated by the development of the standard model.

The other problem we face with DM is the estimations of the mass obtained through different observations and analyses. Here, we have different sorts of discrepancies in these estimations, some are attributed to inaccuracies in the measurement techniques and some others

are attributed to the physical conditions of the systems under measurement. Whereas the CMB analysis suggests that the DM component of the universe is about 6 times the baryonic mass [5], the analysis of mass estimates by gravitational lensing of several clusters indicates that the total mass of these clusters is about 2.4 times the baryonic mass [9]. This has motivated us to calculate the inertial masses of some galactic clusters and compare them with masses obtained from gravitational lensing. The inertial masses are obtained from the observations of the velocity dispersions in clusters using virial method for those clusters which satisfy the necessary stability condition required by the virial method. Our results show that the mass calculated via the virial method is more than two times larger than that obtained through estimates based on weak gravitational lensing observations for the same object. This will open prospects to discuss the nature of DM, and may answer several other questions; for example: Is DM a real mass or an effective mass?

We will start by presenting the basic formulation for the mass function derived from the virial theorem and then calculate the virial mass of some clusters and compare the results with the estimated mass from gravitational lensing. Then, we discuss the problem of DM distribution in galaxies and comment on the implications of having the gravitational potential of the DM being different from that of ordinary baryonic matter. Here, we try to give an explanation for the results obtained by Bidin and his collaborators [10] which suggest a polate distribution for DM in galaxies. Finally, we discuss the implications and possibilities of having DM enjoying different gravitational properties.

The Virial Theorem

The first application of the virial theorem for the determination of the mass of a cluster was conducted by Zwicky who applied the method to the Coma cluster and predicted the existence of DM [3]. We can use the virial theorem to estimate the total mass of an object such as a galaxy or a cluster of galaxies from the movement of its individual members. Suppose you have a finite collection of point particles interacting gravitationally via classical mechanics, and suppose that:

- 1) The time averages of the total kinetic energy and the total potential energy are well defined.
- 2) The positions and velocities of the particles are bounded for all time.

Then, the average gravitational potential energy of the constituents is twice their average kinetic energy $\langle T \rangle = -\frac{1}{2} \langle V \rangle$ [11].

The virial theorem applies to systems of stars that have reached a steady equilibrium state. It can be used for many galaxies, but can also be used for other systems such as some star clusters. The virial theorem cannot be used for clusters of galaxies that are still forming.

Now, assume that the system is stationary, then we can apply the virial theorem. Suppose that the radius vector from a fixed point in the cluster to the mass m_i is \vec{r}_i , then we have:

$$m_i \frac{d^2 \vec{r}_i}{dt^2} = \vec{F}_i,$$

Multiplying by \vec{r}_i gives:

$$\frac{1}{2} \frac{d^2 (m_i r_i^2)}{dt^2} = \vec{r}_i \cdot \vec{F}_i + m_i \left(\frac{d \vec{r}_i}{dt} \right)^2, \quad (1)$$

Assume that the cluster -on the average- is uniformly distributed inside a sphere of radius R , and we have $G = -2 \langle T \rangle$,

$\rho = \frac{3}{4} \frac{M}{\pi R^3}$, In this case:

$$\left. \begin{aligned} G = r_i \cdot F_i &= \frac{-GMm_i r_i^2}{R^3} \\ &= -2 \langle T \rangle = -m_i \langle v_i^2 \rangle \\ \langle v_i^2 \rangle &= \frac{GM \langle r_i^2 \rangle}{R^3}, \end{aligned} \right\} \quad (2)$$

where v_i is the velocity vector. To find the average of r^2 , we use the standard statistical procedure:

$$\left. \begin{aligned} \langle r^2 \rangle &= \frac{\int_V r^4 dr d\Omega}{\int_V r^2 dr d\Omega} = \frac{3}{4\pi R^3} \int_0^R r^4 dr \\ &= \frac{3}{5} R^2, \end{aligned} \right\} \quad (3)$$

Then, the total average mass of the cluster can be written as:

$$M = \langle v_i^2 \rangle R^3 \frac{1}{G \langle I_i^2 \rangle},$$

This means that:

$$M = \frac{5}{3} \frac{R}{G} \langle v_i^2 \rangle. \quad (4)$$

Clearly, the total mass of the cluster depends on the radius of the cluster and on the average velocity. This velocity is a measurable value which can be determined from red-shift phenomena, because only the velocity components (v_s) along the line sight from the observer are known from the observed spectra. Then, we have for a velocity distribution of spherical symmetry:

$$\langle \langle v^2 \rangle \rangle = 3 \langle \langle v_s^2 \rangle \rangle, \quad (5)$$

where double brackets mean double average with respect to time and mass.

The velocity dispersion comes from the fact that the rotation is random, with as many galaxies orbiting in one direction as others orbiting in another (approximately equal numbers of galaxies orbiting in all directions). The line of sight velocity distribution of the galaxies in cluster (the broadening function) is Gaussian.

Average velocity is the speed of the center of mass. The standard deviation from the mean is called (velocity dispersion), then:

$$\langle \langle v^2 \rangle \rangle = 3 \langle \langle v_s^2 \rangle \rangle = 3\sigma^2,$$

where σ is the velocity dispersion for isotropic motion (nothing special about the directions), then we have:

$$M = 5 \frac{R}{G} \sigma^2. \quad (6)$$

This is the basic formula that will be used to calculate the inertial mass, because the measurable value is the velocity dispersion (which is a kinematical property), and since

astrophysical objects move with very low accelerations, then we can take the mass obtained by the virial theorem as representing the inertial mass.

Comparison of Mass Estimates from Gravitational Lensing and Virial Theorem

There are two known methods for calculating masses of galaxies in clusters. These are:

- 1) The mass estimated via weak lensing. The experimental methods to calculate the mass are discussed in several papers and reviews (see [12-15]). Here, we have enough data gathered from observations, and therefore can be taken to be a reliable reference.
- 2) The mass calculated according to the virial theorem, the formula for this mass is shown in Eq. (6).

The mass obtained from lensing is taken to represent the gravitational mass, but the mass obtained from the virial theorem is considered to be representing the inertial mass. Accordingly, the comparison between these two masses is expected to show whether dark matter has different gravitational properties or not. A compilation of the observational data for masses via weak lensing, velocity dispersion and the radius of each cluster under study is done, then we calculate the virial mass from Eq. (6). Table (1) shows the results of these calculations and shows the difference between masses calculated from gravitational lensing and the virial method. The data have been selected in light of the agreement of clusters radii, the radius of equilibrium which is necessary for the application of the virial theorem, and the radius of the measurement of weak lensing. The observational errors have been marked in the table wherever was available in the original sources.

TABLE 1.

Cluster	z_d	R (Mpc)	σ (km/s)	$M_L(10^{14} M_\odot)$	$M_V(10^{14} M_\odot)$	$\frac{M_V}{M_L}$
A1689[15]	0.17	3	1989	89	138	1.55
A2163[16]	0.201	0.9	1680	13 ± 7	29.54	$2.27^{+2.6}_{-0.77}$
A2218[17]	0.175	0.8	1370^{+160}_{-210}	7.8 ± 1.4	$17.46^{+4.3}_{-4.9}$	$2.24^{+0.6}_{-0.6}$
A209[18]	0.206	0.39	898^{+92}_{-102}	1.25	$3.66^{+0.78}_{-0.79}$	$2.93^{+0.6}_{-0.6}$
C10024[19]	0.391	3	1300	40	58.96	1.5
MS1224[20]	0.327	0.96	802	7	7.18	1.03
MS1008[21]	0.306	0.741	1024 ± 110	3.72	$9^{+1.88}_{-1.80}$	$2.42^{+0.5}_{-0.5}$
MS1455[22]	0.2568	1.617	964^{+87}_{-95}	$4.521^{+3.085}_{-2.507}$	$17.47^{+3.3}_{-3.3}$	$3.865^{+2}_{+0.13}$
RXJ1347[21]	0.451	1.408	1400 ± 130	23.94	$32.09^{+6.2}_{-5.7}$	$1.34^{+0.26}_{-0.24}$
1ES065[23]	0.269	0.25	1400 ± 100	2.8 ± 0.2	$5.7^{+0.84}_{-0.79}$	$2.04^{+0.03}_{-0.3}$

In the above table, R is the radius of the cluster, z_d is the red shift, σ is the velocity dispersion, M_L is the lensing mass (obtained from weak lensing), M_V is the virial mass, and last column is the ratio of virial mass to lensing mass.

Clearly, all virial (inertial) masses are larger than lensing (gravitational) masses. The last column has the mean:

$$\mu = \frac{\sum_i \xi_i}{n} = 2.12, \quad (7)$$

where

$$\xi_i = \left(\frac{M_V}{M_L} \right),$$

and the standard deviation is

$$s = \sqrt{\frac{\sum_i (\xi_i - \mu)^2}{n-1}} = 0.84. \quad (8)$$

We can see that the ratios of masses have a mean value in the middle of mass ratio values, with small standard deviation. We have five values larger than the mean and four values smaller than it, and 0.8 of data is situated on one standard deviation ($1s$) from the mean, and *all values* are situated on two standard deviations ($2s$) from the mean.

These results show that the inertial contribution of the DM is higher than gravitational effects, the inertial mass is about twice the gravitational mass. This interesting result may indicate that DM has gravitational properties which are different from those of ordinary matter. Table (2) shows the ratio of difference between the two masses to lensing mass.

TABLE (2)

Cluster	$M_L(10^{14} M_\odot)$	$M_V(10^{14} M_\odot)$	$\frac{M_V - M_L}{M_L}$
A1689[16]	89	138	0.55
A2163[17]	13 ± 7	29.54	$1.27^{+2}_{-0.8}$
A2218[18]	7.8 ± 1.4	$17.46^{+4.3}_{-4.9}$	$1.238^{+0.5}_{-0.3}$
A209[19]	1.25	$3.66^{+0.78}_{-0.79}$	1.928
C10024[20]	40	58.96	0.474
MS1224[21]	7	7.18	0.0257
MS1008[22]	3.72	$9^{+1.88}_{-1.80}$	1.42
MS1455[23]	$4.521^{+3.085}_{-2.507}$	$17.47^{+3.3}_{-3.3}$	$2.866^{+4.2}_{-1.2}$
RXJ1347[22]	23.94	$32.09^{+6.2}_{-5.7}$	0.34
1ES065[24]	2.8 ± 0.2	$5.7^{+0.84}_{-0.79}$	$1.036^{+0.15}_{\pm 0.14}$

The mean of these values is

$$\left\langle \frac{\Delta M}{M} \right\rangle = 1.12, \quad (9)$$

and the standard deviation is

$$s = 0.84. \quad (10)$$

The difference between the two masses is partially attributed to the gravitational properties of the DM. According to this understanding, this result reflects one important aspect of the DM behavior.

The Galactic Disc and DM Discrepancy

The first indication for the possible presence of dark matter came from the dynamical study of our Galaxy. In 1922, the British astronomer James Jeans [25] re-analyzed vertical motions of stars near the plane of the Galaxy that were studied earlier by the Dutch astronomer Jacobus Kapteyn [26]. Both astronomers calculated from these data the density of matter near the Sun. They also estimated the density due to all stars near the galactic plane. Kapteyn found that the spatial density of known stars is sufficient to explain the vertical motions. In contrast, Jeans indicated the presence of two *dark stars* to each bright star.

More modern attempts were carried out in the 1980s by Bahcall and by Kuijken and Gilmore [27] which conclude that there is no evidence for a significant amount of DM in the disk. There has been considerable debate about the interpretation of the results. Early studies claimed evidence of dark matter in the Galactic disc, but more recently some consensus has developed that there is little DM in the disc itself [10]. This indicates that DM distribution does not follow baryonic matter distribution closely on a small scale. A very recent analysis by Moni Bidin et al. [10] suggests that the DM distribution takes the shape of a polate halo. This will be analyzed below and we will try to give our interpretation to these results in the light of our findings in this paper. Earlier, Shaw et al. [28] have shown that cluster halos have polate morphology becoming more so with increasing mass.

The Surface Mass Density of Galactic Disc

The Jeans Equations can be applied to our Galaxy to measure the surface mass density of the galactic disc at the solar distance from the center using observations of the velocities of stars along the line of sight lying some distance above or below the galactic plane. This analysis is important because it allows the quantity of DM in the disc to be estimated. Determining whether there is DM in the galactic disc or not is a very important constraint on its nature.

The second Jeans equation in a cylindrical coordinate system centered on the Galaxy, with $z=0$ in the plane, and $R=0$ at the galactic center for the Z -direction, is given by [30]:

$$\left. \begin{aligned} & \frac{\partial}{\partial t}(n\langle v_r \rangle) + \frac{\partial}{\partial r}(n\langle v_r^2 \rangle) \\ & + \frac{\partial}{\partial z}(n\langle v_r v_z \rangle) + \frac{n}{r}(\langle v_r^2 \rangle - \langle v_\phi^2 \rangle) \\ & = -n \frac{\partial \Phi}{\partial r}, \end{aligned} \right\}$$

where n is the star number density, v_r and v_z are the velocity components in the r and Z -directions, $\Phi(R, z, t)$ is the galactic gravitational potential, and t is time. The galaxy is in a steady state, so n does not change with time. Therefore, the first term is $\frac{\partial}{\partial t}(n\langle v_z \rangle) = 0$.

As it is to be expected, observations show that [27]:

$$\frac{\partial}{\partial r}(n\langle v_r v_z \rangle) = \frac{n}{r} \langle v_r v_z \rangle \approx 0, \quad (11)$$

this is because of the cancelling of positive and negative terms of the Z -components of the velocity. Therefore,

$$\frac{\partial}{\partial z}(n\langle v_z^2 \rangle) = -n \frac{\partial \Phi}{\partial z}, \quad (12)$$

where $\langle v_z^2 \rangle$ is the mean square velocity in the direction perpendicular to the Galactic plane. The Poisson equation in cylindrical coordinates for this system is given by:

$$\frac{\partial^2 \Phi}{\partial z^2} = 4\pi G\rho, \quad (13)$$

(If we observe stars directly above and below the galactic plane, all at the same radius r , we can neglect the $\frac{\partial\Phi}{\partial r}$ and $\frac{\partial^2\Phi}{\partial\phi^2}$ terms).

Then, substituting in Eq. (12), we get:

$$\frac{\partial}{\partial Z} \left[\frac{-1}{n} \frac{\partial}{\partial Z} (n \langle v_z^2 \rangle) \right] = 4\pi G \rho.$$

Integrating on the axis perpendicular to the galactic plane from $-z$ to z , the surface mass density within a distance z of the plane at a galactocentric radius r is:

$$\left. \begin{aligned} \Sigma(r, z) &= \int_{-z}^z \rho dz \\ &= \frac{1}{4\pi G} \int_{-z}^z \frac{\partial}{\partial Z} \left(\frac{-1}{n} \frac{\partial}{\partial Z} (n \langle v_z^2 \rangle) \right) dz \\ &= \frac{-1}{2\pi G n} \frac{\partial}{\partial Z} (n \langle v_z^2 \rangle) \Big|_z, \end{aligned} \right\} \quad (14)$$

where we are assuming symmetry about $z=0$. Therefore, the surface mass density within a distance z of the plane at the solar galactocentric radius R is:

$$\frac{\partial\Phi}{\partial Z} = \Sigma(R, z) = \frac{-1}{2\pi G n} \frac{\partial}{\partial Z} (n \langle v_z^2 \rangle) \Big|_z. \quad (15)$$

If the star number density n can be measured as a function of height z from the plane, and if the z -component of the velocities v_z can be measured as spectroscopic radial velocities, then we can solve for $\Sigma(R; z)$ as a function of z . This gives, after modeling the contribution from the dark matter halo, the mass density of the galactic disc. The recent work by Moni Bidin and collaborators [10] shows that there is little dark matter in the Milky Way disk. This was interpreted to mean that the dark matter forms a highly polate halo for the galaxy. But this interpretation is not consistent with the gravitational behavior of the massive halo if the gravitational properties of DM are the same as those of baryonic matter.

The Gravity of Dark Matter

The previous interpretation assumes that DM behaves gravitationally like ordinary matter, and has explained the discrepancy by assuming that the DM distribution is very extended in the r -direction, not in the z -direction. This interpretation is based on the common idea that the distribution of mass in a cluster (including

both the visible and dark matter) determines the gravitational potential.

Normally, the potential is a function of space and time $\Phi(\vec{r}, t)$, where \vec{r} is the position vector of a point at time t . If the cluster has reached a steady-state, then $\Phi = \Phi(\vec{r})$ only. Accordingly, the potential at any point is related to the local density by Poisson's equation, $\nabla^2\Phi = 4\pi G\rho$. The gravitational potential can be taken at any point as the sum of the potential of the dark and visible matter, $\Phi = \Phi_{DM} + \Phi_{VIS}$. It is easy to see that the dynamical density can therefore be expressed as the sum of two contribution, $\rho = \rho_{DM} + \rho_{VIS}$. Splitting the gravitational potential in this way safeguards the possibility that the gravitational coupling between the dark and ordinary baryonic matter is not the same as that of the standard gravitational coupling of matter. Basically, there is no strong reason for assuming that Φ_{DM} has same gravitational effects as those of Φ_{VIS} . However, the test of this assumption will follow through the subsequent analysis of the kinematics of the systems under consideration.

The gravitational field-Observationally-depends on velocity component in the same direction of field, namely Eq. (30). So, if $\Phi = \Phi_{DM} + \Phi_{VIS}$, then we have:

$$\left. \begin{aligned} &-\frac{\partial}{\partial Z} (\Phi_{DM} + \Phi_{VIS}) \Big|_z \\ &= \Sigma(R, z) \\ &= \frac{1}{2\pi G n} \frac{\partial}{\partial Z} (n \langle v_z^2 \rangle) \Big|_z \end{aligned} \right\}. \quad (16)$$

Now, according to the separation assumption, there are two possibilities:

1. If Φ_{VIS} is effectively dominant, then we can assume that the potential of visible matter is driving the stars to move with velocities that we can measure, and then the surface mass density can be calculated from this motion. On the other hand, having DM with weaker gravitational coupling than ordinary matter will result in resisting the motion since the inertia is large.
2. If the two gravitational coupling constants are different, then the total gravitational potential is inhomogeneous. This leads to distortion in the distribution of matter, and we expect that

the matter will not be distributed spherically. This second possibility may explain the Bidin result and is in agreement with his interpretation about the DM distribution. Therefore, we consider the results obtained by Bidin as an observational evidence for the claimed difference between the gravitational coupling of DM and ordinary matter.

Discussion and Conclusions

The original assumption of DM first appeared when the motion of galaxies within the Coma cluster was observed to be inconsistent with the estimated mass of the cluster obtained from direct observations. Motion of galaxies within the cluster suggested that more mass existed within it and the missing mass was called dark matter. On the other hand, galactic rotation curves show that the outer parts of the galaxies are moving faster than expected by Kepler's law. This again suggested that galaxies contain more mass than observed and that the hidden mass is distributed within the galactic halo. Besides, the investigations of the CMB suggested that the average matter density in the universe is larger than the observed matter density by about 5-6 times. All these three evidences assured cosmologists and astrophysicists that DM exists. However, no one could figure out much of the properties of DM. According to the observations from the rotation curves of the galaxies, DM is thought to reside in the galactic halo, which is counter-intuitive by all means since the large amount of mass should reside at the center of the galaxy and not in the galactic halo.

In this paper, we have investigated the gravitational and the inertial properties of the DM by comparing the masses of several clusters calculated via the virial theorem with the masses

calculated from observations obtained by weak gravitational lensing. We infer that the mass obtained from the virial calculations is the inertial mass and the mass obtained from gravitational lensing is the gravitational mass. Our study shows that the average inertial mass of the clusters is about 2.4 times the average gravitational mass. This suggests that the gravitational coupling of DM is weaker than that of the ordinary baryonic matter.

We believe that this result of our study provides some basis to explain the recent results published on the distribution of DM in the galaxy [10] which show that the distribution of DM is not spherically symmetric and that it takes a polate shape. This was interpreted according to the results of our work here as being due to the two-component potential and the dominance of DM in the galaxy. If DM has a weaker gravitational coupling than ordinary matter then this will cause some asymmetric distribution of matter within the galaxy. However, this is only a qualitative suggestion, the full fledged calculations of the morphology of the galaxy need more accurate specification of the coupling strength and the amounts of both components. This question is beyond the scope of this work.

There remain several other questions on this topic. The one is: how would a gravitationally weak DM contribute to the expansion of the universe? The CMB observations suggest a flat universe with critical density on the other hand observations of the super nova type Ia suggested that the universe is accelerating [31]. The question then arises as: how would a gravitationally weakly coupled DM affect the acceleration of the universe?

References

- [1] Einasto, J., AIP Conf. Proc., 1205:72-81 (2010).
- [2] Oort, J.H., Bull. Astron. Inst., Netherlands, 6 (1932) 249.
- [3] Zwicky, F., Helvicta Phys. Acta, 6 (1934) 11; ApJ. 86 (1937) 217.
- [4] Narayn, R., "Lectures on Gravitational Lensing", Jerusalem Winter School, (1995).
- [5] Hinshaw, G. *et al.*, "Nine-Years WMAP Observations: Cosmological Parameters Results", arXiv: 1212.5226 [astro-ph.CO], (2012).
- [6] Clowe, D. *et al.*, ApJ., 648 (2006) L109.
- [7] Brada, M. *et al.*, ApJ., 687 (2008) 959.
- [8] Milgrom, M., ApJ., 270 (1983) 365.
- [9] Mustafa, M.A., M.Sc. Thesis, Yarmouk University, Jordan (2010).

- [10] Moni Bidin, C., *ApJ.*, 751 (2012) 30.
- [11] Goldstein, H., “Classical Mechanics”, Third Edition, (Addison Wesley, 2001).
- [12] Bartelmann, M. and Schneider, P., *Phys. Rept.*, 340 (2001) 291.
- [13] Van Waerbeke, L., “Weak Lensing As a Probe of Dark Matter”, arXiv: astro-ph/9606100 v1, 17 Jun (1996).
- [14] Slivia & Esteban, “Gravitational Lensing and Microlensing”, (World Scientific).
- [15] Kaiser, N., *ApJ.*, 439 (1995) L1.
- [16] Tyson, J.A. and Fischer, P., *ApJ.*, 446 (1995) 55.
- [17] Squires, G., Kaiser, N. and Babul, A., *ApJ.*, 461 (1996) 572.
- [18] Kneib, J. and Ellis, R.S., *ApJ.*, 471 (1996) 643.
- [19] Horesh, A. *et al.*, *ApJ.*, 633 (2005) 768.
- [20] Bonnt, H., Mellier, Y. and Fort, B., *ApJ.*, 427 (1994) L83.
- [21] Falman, G. and Kaiser, N., *ApJ.*, 437 (1994) 56.
- [22] Zhang, Y. *et al.*, *A&A.*, 429 (2005) 85.
- [23] Pederson, K. and Dahle, H., *ApJ.*, 667 (2007) 26.
- [24] Bardac, M. *et al.*, *ApJ.*, 652 (2006) 932.
- [25] Jeans, J., *MNRAS*, 82 (1922) 122.
- [26] Kapteyn, C., *ApJ.*, 55 (1922) 302.
- [27] Kuijken, K. and Gilmore, G., *MNRAS*, 239 (1989) 605.
- [28] Shaw, L.D. *et al.*, *ApJ.*, 646 (2006) 815-833.
- [29] Tremain, S. and Binny, J., “Galactic Dynamics”, Second Edition, (Princeton University Press, 2008).
- [30] MOLNAR, S.M., *ApJ. Letters*, 724 (2010) L1-L4.
- [31] Perlmutter, S. *et al.*, *ApJ.*, 517(2) (1999) 565–86.

Concerning the Existence of a Discrete Space

Ahmed Isam

Faculty of Medicine, University of Khartoum, P.O. Box 102, Khartoum 111 11, Sudan.

Received on: 29/5/2013; Accepted on: 20/8/2013

Abstract: Loop quantum gravity is considered to be one of the two major candidates for a theory of quantum gravity. The most appealing aspect about this theory is that it predicts that space is not infinitely divisible, but that it has a granular structure. This paper illustrates a missed proof which validates the previous prediction of the theory. It does not prove or validate the model of quantized geometry of the spacetime which is predicted by the theory itself, but instead, it proves the necessity of space discreteness, and the existence of space quanta due to a simple fact or observation which is the existence of the origin position in a coordinates system. This is done in this paper by defining one of the major concepts in physics, which is the quantization concept, in a simple way, and applied directly to the observation. Although the area of quantum gravity – in general – requires a sophisticated level of mathematics, this paper was built on a simple mathematical level to make it accessible to any reader.

Keywords: Quantum gravity; Quantization concept; Discrete space.

Introduction

The problem of quantum gravity represents one of the major problems in physics today. Mainly, the problem does not arise from lack of working theories in this field, but arises –till now– from the absence of any direct experiment or observation to confirm any theory in this field. Loop quantum gravity is considered to be one of the two major candidates for a theory of quantum gravity. The most appealing aspect about loop quantum gravity is that it predicts that space is not infinitely divisible, but that it has a granular structure [1]. This paper illustrates a missed proof, which validates the previous prediction of the theory. It does not prove or validate the model of the quantized geometry of the spacetime which is predicted by the theory, but instead, it proves the necessity of space discreteness, and the existence of space quanta, due to a simple fact which is the existence of the origin position in a coordinates system, but before considering this fact, it is essentially important to consider the concept of quantization.

The Quantization Concept

Quantized quantities have a discrete spectrum and only certain values are allowed, take for example the energy of a one - dimensional quantum harmonic oscillator which is a quantized quantity, from Eq. 1:

$$E_n = \left(n + \frac{1}{2}\right) h\nu \text{ where } n = 0, 1, 2, 3, \dots \dots (1)$$

the spectrum is:

$$\frac{1}{2} h\nu, 1\frac{1}{2} h\nu, 2\frac{1}{2} h\nu, 3\frac{1}{2} h\nu, \dots \dots$$

where E is the oscillator's energy, h is Planck's constant and ν is the oscillator's frequency.

Absence of any possible value in the spectrum between $(\frac{1}{2} h\nu)$ and $(1\frac{1}{2} h\nu)$ results in the existence of a **gap** in the spectrum between them, because values like $(h\nu)$ or $(1\frac{1}{4} h\nu)$ are not allowed, and therefore absent from the spectrum.

Also, the absence of any possible value in the spectrum between $(1\frac{1}{2} h\nu)$ and $(2\frac{1}{2} h\nu)$ results

in the existence of a gap between them, because values like $(2h\nu)$ or $(2\frac{1}{4} h\nu)$ are absent, and therefore are not allowed in the spectrum. The situation is the same between any other two successive values in the spectrum. Therefore, there will be a gap between any two successive values in the spectrum. As a result of this, the spectrum will be discrete.

The quantization of any physical variables arises from the boundary condition used in solving the equation of motion of the system, so any system has its own quantization, but a simple concept which is concluded from the example above is that gaps in the spectrum of a physical quantity in a specific physical system –as in the example above– result from the **absence** of any possible value between the successive values in the spectrum of that system, and the existence of these gaps makes the spectrum discrete and not continuous, which is the characteristic feature of quantized quantities regarding the system which is considered. This represents the quantization concept.

Existence of the Origin Position in a Coordinates System

The physical spacetime represents a geometrical model or a “system” that combines space and time into a single continuum. Mathematically, it is a manifold consisting of “events” which are described by some type of coordinates system. Typically, three spatial dimensions (length, width, height) and one temporal dimension (time) are required. The poof in this paper can only prove the discreteness of space without proving the discreteness of time. For this reason, the spacetime will be treated at specific moment for an observer located in a frame of reference, because at this situation, spacetime intervals can only refer to the spatial measurements, which represent what is required here. For illustration, if event one had occurred at (x_1, y_1, z_1, t_1) , and event two had occurred at (x_2, y_2, z_2, t_1) , for an observer located in the same frame of reference, the spacetime interval (Δs) that separates event one from event two will be:

$$\Delta s^2 = \Delta x^2 + \Delta y^2 + \Delta z^2$$

which is only a spatial interval, since $\Delta t = 0$.

Initially, by considering one spatial dimension for simplicity, the space will be a line, therefore positions in this line are represented with one axis (x) and position spectrum is illustrated on the axis by labeling the axis with position units, as shown in Fig. 1.

Now, let us consider the following facts about this spectrum:

1-From Fig. 1, the positive part of the spectrum represents a continuum of positions directed in the positive direction with respect to the origin, and the negative part of the spectrum represents a continuum of positions directed in the opposite direction with respect to the origin.

2-The existence of the origin position in the spectrum which represents a position that is located outside the positive and the negative parts of the spectrum. Therefore, it is a neutral position (null vector).

In the spectrum above, the number of possible values (positions) between the positive part and the negative part of the spectrum is one, which is the origin position itself, but the number of possible values (positions) between the positive part of the spectrum and the origin is zero.

3- By recalling the quantization concept and by looking at the spectrum in Fig. 1, the **absence** of any possible value (position) between the origin and the positive part of the spectrum results in the existence of a gap between them. This happens because there is no any possible value allowed in the spectrum between them.

4- The gap that exists between the origin and the positive part of the spectrum will represent a gap between the origin and a first positive position, since the positive part of the spectrum is merely a continuum of positive positions. Therefore, the gap between the origin and the positive part of the spectrum represents a gap between the origin and a positive position. Call this position (x_1).

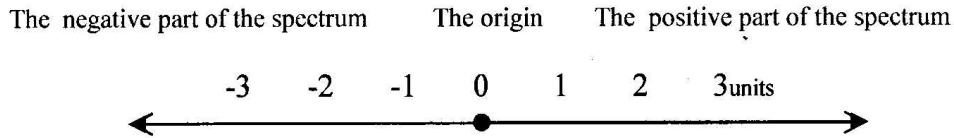


FIG. 1. Position spectrum is illustrated on the (x) axis.

Therefore, there will be a gap between the origin and the **following** position in the spectrum, since the origin position is a relative position and not an absolute one (Fig. 2). Position (x_1) can also be considered as an origin position, then there will be a gap between (x_1) and the following position in the spectrum. Call this position (x_2). Position (x_2) can also be considered as an origin position, since the origin is relative, therefore there will be a gap between (x_2) and the following position in the spectrum. Call this position (x_3), ... and so on.

Therefore, the position spectrum in the positive direction will take the form:

0, $x_1, x_2, x_3, x_4, \dots$

which is discrete and not continuous, and the number of possible positions in the axis interval (Δx) is **limited** and not infinite, but what does this mean?

Before answering the question above, it is important to note that the argument above cannot answer whether the successive positions are equally spaced or not, but it only shows that they are spaced.



FIG.2. The origin is a relative position. Take this example for illustration. For an observer located in position (1), the value of position (2), for example is 4 units to the right (+4 units), and for another observer located in position (2), the value of position (1) is 4 units to the left (-4 units). Both observers are right, since each one uses his own position as origin.

5- The “classical” definition of a line is that it represents a one - dimensional continuum of infinite numbers of points. This definition makes any given value of a line infinitely divisible. By considering this definition, since every point in the line refers to –or represents– a position in the space, the existence of an infinite number of points between two positions, take for example the

interval (Δx) which is bounded by position A and position B as shown in Fig. 3.

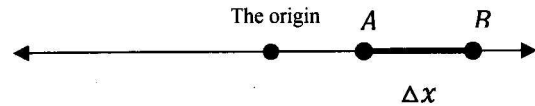


FIG. 3. (Δx) interval bounded by position (A) and position (B).

The existence of an infinite number of points between A and B results in the existence of an infinite number of positions between them, or in the interval (Δx), since every point refers to a position. This makes a contradiction with the conclusion in paragraph (4). By redefining a line as a continuum of quanta, one - dimensional quanta, instead of points, the spatial quantum represents an elementary value of length, hence it is not divisible, and therefore the observation of space below the quantum level or length value is not possible, because it results in the divisibility of the quantum itself. As a result of this, the quantum can only contain –or refer to– one possible position in space, which is at the level of the quantum itself. Therefore, the first quantum in the positive direction will refer to position (x_1), and the second quantum will refer to position (x_2), ... and so on. Since the quantum has a non-zero value of length, the number of quanta between position A and position B in (Δx) interval is limited and not infinite. Therefore, the number of positions between A and B is also limited, and this is consistent with the conclusion in paragraph (4).

From the previous discussion, the existence of the origin position illustrates a discreteness in space structure, but it does not illustrate a specific or certain shape of microscopic geometry at the quantization length scale. This will represent a problem when trying to extend the previous conclusion in (4) to include two and three spatial dimensions. The problem is solved by using a large length scale relative to the scale of quantization, because at this large scale the microscopic quantized geometry is reduced to

the classical macroscopic geometry as an approximation (just as the classical mechanics is used as an approximation of quantum mechanics at the macroscopic length scale).

Therefore, by choosing the large macroscopic length scale, the classical Cartesian coordinates system is used as an approximation, **but** it is important to bear in mind that the axes (x), (y) and (z) are quantized and not continuous, since they contain an origin position.

By considering areas, an additional spatial dimension (y) is required, and it is quantized just like (x), since it contains an origin position. The “classical” definition of area is that it represents a two - dimensional continuum of an infinite number of points, and this definition makes any given value of area infinitely divisible. This definition will make a contradiction with the conclusion in paragraph (4) as will be illustrated below.

Now, take a circle, for example, from the classical definition of area, it represents a continuum of an infinite number of points spreading in two dimensions. Since every point in the circle refers to –or represents– a position in space, the existence of an infinite number of points in the circle results in the existence of an infinite number of positions inside it. This results in the existence of an infinite number of positions in (Δx) and (Δy) intervals which bound this circle as illustrated in Fig. 4-A below.

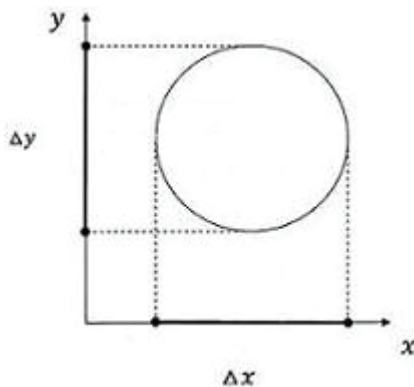


FIG. 4-A. A circle which is bounded by (Δx) and (Δy) intervals.

This happens because every position in the circle refers to a position in (x) and (y) axes, for example, position or point number (1) in the circle refers to position (x_1, y_1) in the axes, position or point number (2) in the circle refers to position (x_2, y_2), and point or position number (3) will refer to position (x_3, y_3) in the circle ...

and so on. Since the number of points inside the circle is infinite, this results in an infinite number of positions in (Δy) and (Δx) intervals, as illustrated in Fig. 4-B below.

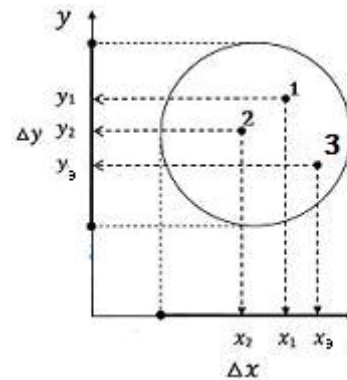


FIG.4-B.

The previous result makes a contradiction with the conclusion in paragraph (4), because the number of positions in (Δx) and (Δy) intervals will be infinite, and not limited as shown from the conclusion in paragraph (4).

By redefining area as a continuum of quanta instead of points, the spatial quantum represents an elementary value of area, therefore it is not divisible, and hence it cannot refer to more than one position in space, just as the case with the previous length quantum. Therefore, every quantum will refer to a single position inside the circle. Since the quantum has a non-zero value of area, the number of quanta, and therefore positions inside the circle, will be limited. Now, since the Cartesian coordinates are used as an approximation, every position in the circle is approximated to a position in (x) and (y) axes. Position number (1) in the circle is approximated to position (x_1, y_1) in the axes, position number (2) in the circle is approximated to position (x_2, y_2) ... and so on, just like the idea from Fig. 4-B, because the number of positions inside the circle is limited. This results in a limited number of positions in (Δx) and (Δy) intervals which bound the circle’s area, which is consistent with the conclusion in paragraph (4).

By considering volume, the same concept used in dealing with area holds here, but with an additional dimension (z) because volume is a three - dimensional quantity. This will lead to redefining volume as a continuum of three - dimensional quanta, instead of points, as illustrated below.

Take the cube in Fig. 5 as example. Classically, the volume inside the cube is

defined as a continuum of an infinite number of points spreading in three dimensions. This definition makes any given value of volume infinitely divisible. The number of positions inside the cube will be infinite, since every point refers to a position, and the number of points is infinite. This results in an infinite number of positions in (Δx) , (Δy) and (Δz) intervals, which bound the cube (the cube's edges), since every position in the cube refers to a position (x, y, z) in the axes. For illustration, just as the case with the circle in Fig. (4-B), but here with an additional dimension (z) , point number (1) in the cube will refer to positions (x_1, y_1, z_1) in the axes intervals, and point number (2) will refer to positions (x_2, y_2, z_2) in the axes intervals, ... and so on. Therefore, the existence of an infinite number of points inside the cube results in the existence of an infinite number of positions in (Δx) , (Δy) and (Δz) intervals (the cube's edges). This makes a contradiction with the previous conclusion about quantized axes, with a limited number of positions inside the intervals (Δx) , (Δy) and (Δz) .

This contradiction is solved by redefining the volume as a continuum of quanta instead of points. The quantum has a volume of a non-zero value, and since it is elementary and not divisible, it will refer to a single position in space, just as the case dealing with area. Therefore, the number of the quanta inside the cube, and hence positions, will be limited. This results in a limited number of positions in (Δx) , (Δy) and (Δz) intervals, since every position in the cube is approximated to a position in (x) , (y) and (z) axes, in agreement with the conclusion in paragraph (4).

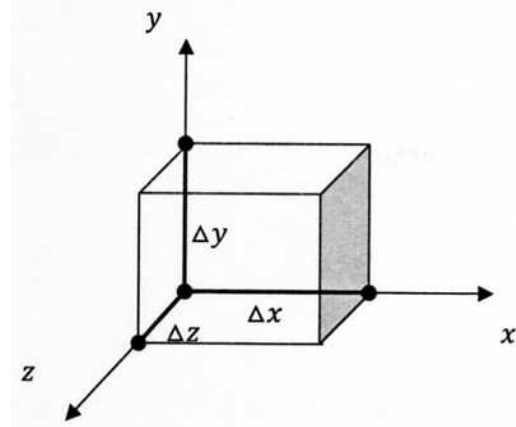


FIG.5.

Reference

- [1] Rovelli, C., "*Quantum Gravity*", (Cambridge University Press, 2004).

Jordan Journal of Physics

ARTICLE

Quantization of Nonholonomic Constraints Using the WKB Approximation

A. A. Al-Ajaleen and K. I. Nawafleh

Department of Physics, Mu'tah University, Al-Karak, Jordan.

Received on: 13/6/2013; Accepted on: 7/10/2013

Abstract: The Hamilton-Jacobi theory is used to obtain the Hamilton function for nonholonomic constraints in addition to the equations of motion. The technique of separation of variables and canonical transformation is applied here to solve the Hamilton-Jacobi partial differential equation for nonholonomic systems. The Hamilton-Jacobi function is then used to construct the wave function and to quantize these systems using the WKB approximation.

Keywords: Nonholonomic constraints; Quantization; WKB approximation.

Introduction

Nonholonomic systems are [1] mechanical systems with constraints on their velocity that are not derivable from position constraints. The construction of Hamilton-Jacobi partial differential equations (HJPDEs) for nonholonomic constrained system is of prime importance. The Hamilton-Jacobi theory provides a bridge between classical and quantum mechanics; it implies that quantum mechanics should reduce to classical mechanics in the limit $\hbar \rightarrow 0$. The principal interest in this theory is based on the hope that it might provide some guidance concerning the form of a Schrödinger-type quantum theory for constrained fields. The fact that [2-4] solving the Hamilton-Jacobi equation gives a generating function for the family of canonical transformation of the dynamics is the theoretical basis for the powerful technique of exact integration of Hamilton's equations that are often employed with the technique of separation of variables. In addition [5, 6], calculating the Hamilton-Jacobi function enables us to construct the wave function of constrained systems, for which the constraints become conditions on it in the semiclassical limit. This limit also is known as the WKB approximation and it is named after physicists

Wentzel, Kramers and Brillouin who all developed it in 1962. The WKB method is a powerful tool to obtain solutions for many physical problems and it is generally applicable to problems of wave propagation in which the frequency of the wave is very high or equivalently, the wave length of the wave is very short, so that the motivation of this work is furnished by the desire to understand the quantization of nonholonomic constrained systems within the framework of the WKB approximation.

Generalized Lagrange and Hamilton Equation for Nonholonomic System

Nonholonomic system [7] originated in the Lagrange-d'Alembert principles. Ferrers by adding constraints in the form of Euler-Lagrange equations derived nonholonomic system of equations of motion. We assume that the Lagrange function for nonholonomic system has the following form:

$$L \equiv L(q, \dot{q}), \quad (1)$$

and the nonholonomic constraints are time independent and linear in the velocities:

$$f_j \equiv f_j(q_i, \dot{q}_i) = 0 \quad (2)$$

The Hamiltonian equations of motion are derived below [8]; we start from the correct equation of state:

$$\frac{d}{dt} \left(\frac{\partial L}{\partial \dot{q}_j} \right) - \frac{\partial L}{\partial q_j} = \lambda \frac{\partial f}{\partial \dot{q}_j} \quad (3)$$

This equation is called the constrained Euler-Lagrange equation.

With

$$p_j = \frac{\partial L}{\partial \dot{q}_j}, \quad (4)$$

the Hamiltonian is defined in the usual way as:

$$H_0(q, \dot{q}, t) = p_i \dot{q}_i - L(q, \dot{q}, t). \quad (5)$$

Theory for Determining Hamilton-Jacobi Function for Nonholonomic Constraints

In classical mechanics [2, 9], the Hamilton-Jacobi equation is first introduced as a partial differential equation that the action integral satisfies:

$$S = \int_0^t (p\dot{q} - H_0) dt. \quad (6)$$

By taking variation of the endpoints, one obtains a partial differential equation satisfied by:

$$\frac{\partial S}{\partial t} + H_0 = 0. \quad (7)$$

This is the Hamilton-Jacobi equation (HJE). If $S(q, t)$ is a solution of the Hamilton-Jacobi equation, then $S(q, t)$ is the generating function for the family of canonical transformations that describe the dynamic defined by Hamilton's equations.

When the Hamiltonian does not depend on time explicitly, the time t can be separated. In this case, the time derivative $\frac{\partial S}{\partial t}$ in the HJE must be a constant, usually denoted by $-E$ giving the separated solution:

$$S(q, E, t) = W(q, E) - Et. \quad (8)$$

Eq. 7 can then be written as:

$$H_0 \left(q_i, p_i = \frac{\partial W}{\partial q_i} \right) = E. \quad (9)$$

For our purposes, we write the solution of Hamilton-Jacobi (H-J) as:

$$S = S(q_1, \dots, q_n, \alpha_1, \dots, \alpha_n, t). \quad (10)$$

The transformation equations for S give:

$$p_i = \frac{\partial S}{\partial q_i} \quad (11)$$

$$\beta_i = \frac{\partial S}{\partial \alpha_i}. \quad (12)$$

β_i can be thus found from the initial conditions.

Following [10-13], the corresponding set of the HJPDEs for constrained systems can be written as:

$$H'_\alpha \left[q_\beta, q_\alpha, p_\mu = \frac{\partial S}{\partial q_\mu}, p_\alpha = \frac{\partial S}{\partial q_\alpha} \right] = 0 \quad (13)$$

$$\alpha, \beta = 0, N - R + 1, \dots, N.$$

For nonholonomic systems, this reduces to:

$$H'_0 = p_0 + H_0 = \frac{\partial S}{\partial t} + H_0 \left(q_\beta, q_\alpha, p_\alpha = \frac{\partial S}{\partial q_\alpha} \right) = 0. \quad (14)$$

Quantization of Nonholonomic Constraints Using the WKB Approximation

The WKB method is a formal \hbar expansion for the wave function that expresses its rapid oscillations in the semi-classical limit. Using this expansion, combined with an approximate quantization condition, we start from the Schrödinger equation for a single particle in a potential $V(q)$:

$$i\hbar \frac{\partial}{\partial t} \psi(q, t) = \left[\frac{-\hbar^2}{2m} \frac{\partial^2}{\partial q^2} + V(q) \right] \psi(q, t). \quad (15)$$

We can rewrite this equation by using [14]:

$$\psi(q, t) = \exp \left[\frac{iS(q, t)}{\hbar} \right] \quad (16)$$

as

$$\frac{-\partial S}{\partial t} \psi = \left[\frac{1}{2m} \left(\frac{\partial S}{\partial q} \right)^2 - \frac{i\hbar}{2m} \left(\frac{\partial}{\partial q} \right)^2 S + V \right] \psi \quad (17)$$

Assuming $\psi \neq 0$, this leads to an equation:

$$\frac{-\partial S}{\partial t} = \left[\frac{1}{2m} \left(\frac{\partial S}{\partial q} \right)^2 - \frac{i\hbar}{2m} \left(\frac{\partial}{\partial q} \right)^2 S + V \right]. \quad (18)$$

Now, taking the formal limit $\hbar \rightarrow 0$, we obtain the classical Hamilton-Jacobi equation:

$$\frac{-\partial S}{\partial t} = \left[\frac{1}{2m} \left(\frac{\partial S}{\partial q} \right)^2 + V \right]. \quad (19)$$

One can use this equation and consider an expansion:

$$S(q, t) = S_0 + \hbar S_1 + \hbar^2 S_2 + \dots \quad (20)$$

This is an expansion in \hbar . Plugging in the expansion into Eq. 18 and collecting the powers of \hbar , we find:

$$\frac{-\partial S_0}{\partial t} = \frac{1}{2m} \left(\frac{\partial S_0}{\partial q} \right)^2 + V, \quad (21)$$

$$\frac{-\partial S_1}{\partial t} = \frac{1}{2m} \left[-i \left(\frac{\partial}{\partial q} \right)^2 S_0 + 2 \left(\frac{\partial S_0}{\partial q} \right) \left(\frac{\partial S_1}{\partial q} \right) \right], \quad (22)$$

and similarly for the higher in \hbar . The leading equation has only S_0 , and it is exactly the same as Hamilton-Jacobi equation. Once you solve these equations starting from S_0, S_1, \dots etc. you have solved the wave function ψ in a systematic expansion in \hbar .

The WKB approximation is used mostly for the time-independent case. Then, the wave function has the ordinary time dependence $\exp\left(\frac{-iEt}{\hbar}\right)$. For one-dimensional problem, the Hamilton-Jacobi function S takes the form:

$$S(q, t) = S(q) - Et. \quad (23)$$

Therefore, only S_0 has the time dependence $S_0(q, t) = S_0(q) - Et$, while higher-order terms do not depend on time. The lowest term S_0 in Eq. 21 satisfies the Hamilton-Jacobi equation

$$E = \frac{1}{2} \left(\frac{\partial S_0}{\partial q} \right)^2 + V. \quad (24)$$

This differential equation can be solved immediately to yield:

$$S_0(q) = \pm \int \sqrt{2m[E - V(q')]} dq' = \int p(q') dq'. \quad (25)$$

Once we have known S_0 , we can solve for S_1 starting from Eqs. 21 and 22, and using

$$\frac{\partial S_1}{\partial t} = 0 \quad (26)$$

we find:

$$2 \left(\frac{\partial S_0}{\partial q} \right) \left(\frac{\partial S_1}{\partial q} \right) = i \left(\frac{\partial^2 S_0}{\partial q^2} \right), \quad (27)$$

which has the solution

$$S_1(q) = \frac{i}{2} \int \left[\frac{\left(\frac{\partial^2 S_0}{\partial q^2} \right)}{\left(\frac{\partial S_0}{\partial q} \right)} \right] dq = \frac{i}{2} \ln p(q) + \text{Constant} \quad (28)$$

Now, the general solution of Schrödinger equation becomes:

$$\psi(q, t) = \exp\left[i \frac{S_0(q)}{\hbar} + i S_1(q) \right] \exp\left(\frac{-iEt}{\hbar}\right) \quad (29)$$

$$= C \frac{1}{\sqrt{P(q)}} \exp\left[\pm \frac{i}{\hbar} \int \sqrt{2(E - V(q'))} dq' \right] \exp\left(\frac{-iEt}{\hbar}\right)$$

where C is constant. The present approximation breaks down when $p(q)$ goes to zero.

However, the semi-classical expansion (WKB approximation) of the Hamilton-Jacobi function of unconstrained systems has been studied [15]. This expansion leads to the following wave function:

$$\psi(q_i, t) = \left[\prod_{i=1}^N \psi_{0i}(q_i) \right] \exp\left[\frac{iS(q_i, t)}{\hbar} \right] \quad (30)$$

where $\psi_{0i}(q_i) = \frac{1}{\sqrt{p(q_i)}}$. The above wave function satisfies the condition:

$$H'_0 \psi = 0 \quad (31)$$

in the semi - classical limit $\hbar \rightarrow 0$.

This condition is obtained when the dynamical coordinates and momenta are turned into their corresponding operators:

$$q_i \rightarrow \hat{q}_i;$$

$$p_i \rightarrow \hat{p}_i = \frac{\hbar}{i} \frac{\partial}{\partial q_i};$$

$$p_0 \rightarrow \hat{p}_0 = \frac{\hbar}{i} \frac{\partial}{\partial t}.$$

Illustrative Examples

1. The Sliding of a Balanced Skate

Let us consider as an illustrating example the problem of a balanced skate on horizontal ice. One can choose units of length, time and mass so that the Lagrangian would take the following form:

$$L = \frac{1}{2} (\dot{x}^2 + \dot{y}^2 + \dot{z}^2). \quad (32)$$

Here, x and y are the coordinates of the point of contact, z is the angle of rotation of the skate. The constraint equation is:

$$f = \dot{x} \sin z - \dot{y} \cos z = 0. \quad (33)$$

Eq. 33 can be rewritten as:

$$\dot{y} = \dot{x} \tan z. \quad (34)$$

According to Eq. 3, we obtain:

$$\ddot{x} = \lambda \sin z \quad (35)$$

$$\ddot{y} = -\lambda \cos z \quad (36)$$

$$\ddot{z} = 0. \quad (37)$$

From Eqs. 34 and 35, we find:

$$\ddot{y} = \frac{-\ddot{x}}{\tan z}. \quad (38)$$

Differentiating constraint Eq. 34 with respect to time to eliminate λ , we find:

$$\dot{y} = \ddot{x} \tan z + \dot{x} \sec^2 z. \quad (39)$$

Inserting Eq. 38 into Eq. 39 and multiplying the result by $(-\tan z)$ lead to:

$$\ddot{x} = -\ddot{x} \tan^2 z - \dot{x} \sec^2 z \tan z. \quad (40)$$

By using the identity:

$$1 + \tan^2 z = \sec^2 z,$$

Eq. 40 becomes:

$$\ddot{x} = -\dot{x} \tan z. \quad (41)$$

From Eq. 37, we can solve $z(t)$ as follows:

$$z(t) = \alpha_1 t + \beta_1. \quad (42)$$

Differentiating Eq. 42 with respect to time, we obtain:

$$\dot{z} = \alpha_1. \quad (43)$$

Integrating Eq. 41, we get:

$$\int \frac{\ddot{x}}{\dot{x}} dt = \int -\tan z dz, \quad \dot{z} = \frac{dz}{dt}. \quad (44)$$

This gives:

$$\ln \dot{x} = \ln \cos z \quad (45)$$

or

$$\dot{x} = \cos z. \quad (46)$$

Substituting Eq. 42 into Eq. 46 and integrating the resulting equation:

$$\int \dot{x} dt = \int \cos(\alpha_1 t + \beta_1) dt, \quad (47)$$

lead to:

$$x(t) = \alpha_2 \sin z + \beta_2. \quad (48)$$

Substituting Eq. 46 into Eq. 34, we obtain:

$$\dot{y} = \sin z. \quad (49)$$

Now, inserting Eq. 42 into Eq. 49 and integrating the resulting equation:

$$\int \dot{y} dt = \int \sin(\alpha_1 t + \beta_1) dt, \quad (50)$$

we find:

$$y(t) = \alpha_3 \cos z + \beta_3, \quad (51)$$

where $\alpha_2 = \frac{1}{\alpha_1}$, $\alpha_3 = -\frac{1}{\alpha_1}$.

Here, β_1, β_2 and β_3 are constants of integration related to the initial values of z, x, y ; while α_1, α_2 and α_3 are the initial values of velocities.

We rewrite Eqs. 42, 48 and 51, respectively as:

$$\beta_1 = z - \alpha_1 t = \frac{\partial S_1}{\partial \alpha_1}, \quad (52)$$

$$\beta_2 = x - \alpha_2 \sin z = \frac{\partial S_2}{\partial \alpha_2}, \quad (53)$$

$$\beta_3 = y - \alpha_3 \cos z = \frac{\partial S_3}{\partial \alpha_3}. \quad (54)$$

Solving Eqs. 52, 53 and 54, we obtain:

$$S_1(z, \alpha_1) = z\alpha_1 - \frac{1}{2}\alpha_1^2 t, \quad (55)$$

$$S_2(x, \alpha_2) = x\alpha_2 - \frac{1}{2}\alpha_2^2 \sin z, \quad (56)$$

$$S_3(y, \alpha_3) = y\alpha_3 - \frac{1}{2}\alpha_3^2 \cos z. \quad (57)$$

Now, we collect Eqs. 55, 56 and 57, which give the Hamilton-Jacobi function $S(z, x, y, \alpha_1, \alpha_2, \alpha_3, t)$.

$$S = \left. \begin{aligned} & z\alpha_1 + x\alpha_2 + y\alpha_3 \\ & - \frac{1}{2}\alpha_1^2 t - \frac{1}{2}\alpha_2^2 \sin z \\ & - \frac{1}{2}\alpha_3^2 \cos z \end{aligned} \right\} \quad (58)$$

The generalized momenta can be derived as:

$$p_z = \frac{\partial S}{\partial z} = \alpha_1 - \frac{1}{2}\alpha_2^2 \cos z - \frac{1}{2}\alpha_3^2 \sin z \quad (59)$$

$$p_x = \frac{\partial S}{\partial x} = \alpha_2 \quad (60)$$

$$p_y = \frac{\partial S}{\partial y} = \alpha_3. \quad (61)$$

From these equations, we can obtain $\alpha_1, \alpha_2, \alpha_3$ as functions of p_i and q_i :

$$\alpha_1 = p_z + \frac{1}{2}\alpha_2^2 \cos z - \frac{1}{2}\alpha_3^2 \sin z, \quad (62)$$

$$\alpha_2 = p_x, \quad (63)$$

$$\alpha_3 = p_y. \quad (64)$$

The Hamiltonian is defined as:

$$H_0 = \frac{-\partial S}{\partial t} = \frac{1}{2}\alpha_1^2. \quad (65)$$

Inserting Eq. 62 into Eq. 65, we get the following expression for the Hamiltonian:

$$H_0 = \frac{1}{2} \left[p_z + \frac{1}{2} (p_x^2 \cos z - p_y^2 \sin z) \right]^2. \quad (66)$$

Now, we will quantize our example; first let us apply the HJPDEs to the wave function:

$$\check{H}'_0 \psi = \left[\check{P}_0 + H_0 \right] \psi \quad (67)$$

We can rewrite Eq. 67 as:

$$\check{H}'_0 \psi = \left[\frac{\hbar}{i} \frac{\partial}{\partial t} + \frac{1}{2} \left(\frac{\hbar}{i} \frac{\partial}{\partial z} - \frac{\hbar^2}{2} \frac{\partial^2}{\partial x^2} \cos z + \frac{\hbar^2}{2} \frac{\partial^2}{\partial y^2} \sin z \right) \right] \psi \quad (68)$$

where

$$\hat{p}_0 = \frac{\hbar}{i} \frac{\partial}{\partial t}, \quad \hat{p}_x = \frac{\hbar}{i} \frac{\partial}{\partial x}, \quad \hat{p}_y = \frac{\hbar}{i} \frac{\partial}{\partial y}, \quad \hat{p}_z = \frac{\hbar}{i} \frac{\partial}{\partial z}.$$

$$\hat{H}_0 = \frac{1}{2} \left[\frac{\hbar}{i} \frac{\partial}{\partial z} + \frac{1}{2} \left(-\hbar^2 \frac{\partial^2}{\partial x^2} \cos z + \hbar^2 \frac{\partial^2}{\partial x^2} \sin z \right) \right]^2$$

and again we can rewrite Eq. 68 as:

$$\check{H}'_0 \psi = \left[\frac{\hbar}{i} \frac{\partial}{\partial t} - \frac{\hbar^2}{2} \frac{\partial^2}{\partial z^2} + \frac{\hbar^4}{8} \frac{\partial^4}{\partial x^4} \cos^2 z + \frac{\hbar^4}{8} \frac{\partial^4}{\partial y^4} \sin^2 z - \frac{\hbar^3}{2i} \frac{\partial}{\partial z} \frac{\partial^2}{\partial x^2} \cos z + \frac{\hbar^3}{2i} \frac{\partial}{\partial z} \frac{\partial^2}{\partial y^2} \sin z - \frac{\hbar^4}{4} \frac{\partial^2}{\partial x^2} \cos z \frac{\partial^2}{\partial y^2} \sin z \right] \psi \quad (69)$$

where

$$\psi(x, y, z, t) =$$

$$\exp \left[\frac{i(z\alpha_1 + x\alpha_2 + y\alpha_3 - \frac{1}{2}\alpha_1^2 t - \frac{1}{2}\alpha_2^2 \sin z - \frac{1}{2}\alpha_3^2 \cos z)}{\hbar} \right]$$

After a simplification, we get:

$$\hat{H}'_0 \psi = \left[-\frac{\hbar}{4} \alpha_2^2 \sin z - \frac{\hbar}{4} \alpha_3^2 \sin z - \frac{\hbar}{2i} \alpha_2^2 \sin z \right] \psi \quad (70)$$

Taking the limit $\hbar \rightarrow 0$, we have:

$$\hat{H}'_0 \psi = 0. \quad (71)$$

2. The Snakeboard

The snakeboard is a modified version [16, 17] of a skate board in which the front and back pairs of wheels are independently actuated.

Let m be the total mass of the board, J the inertia of the board, J_0 the inertia of the rotor, J_1 the inertia of each wheel, and assume the relation $J + J_0 + J_1 = mr^2$.

The Lagrangian is given by:

$$L = \frac{1}{2} \left[m(\dot{x}^2 + \dot{y}^2 + r^2 \dot{\theta}^2) + 2J_0 \dot{\theta} \dot{\Psi} + 2J_1 \dot{\phi}^2 + J_0 \dot{\Psi}^2 \right]. \quad (72)$$

The system has two nonholonomic constraints:

$$f_1 = \dot{x} + r \dot{\theta} \cos \theta \cot \phi \quad (73)$$

$$f_2 = \dot{y} + r \dot{\theta} \sin \theta \cot \phi. \quad (74)$$

The equations of motion can be obtained from Eq. 3 as:

$$m\ddot{x} = \lambda_1 \quad (75)$$

$$m\ddot{y} = \lambda_2 \quad (76)$$

$$mr^2 \ddot{\theta} + 2J_0 \ddot{\Psi} = \lambda_1 r \cot \phi \cos \theta + \lambda_2 r \cot \phi \sin \theta \quad (77)$$

$$p_\phi = \text{Constant} = \mu \quad (78)$$

$$p_\Psi = \text{Constant} = \kappa \quad (79)$$

The Hamiltonian H is calculated by using Eq. 5 as:

$$H_0 = \frac{1}{2m} (p_x^2 + p_y^2) + \frac{1}{2(mr^2 - J_0)} (p_\theta - p_\Psi)^2 + \frac{1}{4J_1} p_\phi^2 + \frac{1}{2J_0} p_\Psi^2 \quad (80)$$

According to Eq. 78 and Eq. 79, we can rewrite this equation as:

$$H_0 = \frac{1}{2m} (p_x^2 + p_y^2) + \frac{1}{2(mr^2 - J_0)} (p_\theta - \kappa)^2 + \frac{\mu^2}{4J_1} + \frac{\kappa^2}{2J_0} \quad (81)$$

Following Eq. 11, the generalized momenta are:

$$p_x = \frac{\partial S}{\partial x}, \quad p_y = \frac{\partial S}{\partial y}. \quad (82)$$

According to Eq. 7, the Hamilton-Jacobi equation becomes:

$$\left[\frac{\partial S}{\partial t} + \frac{1}{2m} \left(\frac{\partial S}{\partial x} \right)^2 + \frac{1}{2m} \left(\frac{\partial S}{\partial y} \right)^2 + \frac{1}{2(mr^2 - J_0)} \left(\frac{\partial S}{\partial \theta} - \kappa \right)^2 + \frac{\mu^2}{4J_1} + \frac{\kappa^2}{2J_0} \right] = 0 \quad (83)$$

Using Eq. 8, we get:

$$\left. \begin{aligned} \mathcal{A}(x, y, \theta, E_x, E_y, E_\theta) = \\ \mathcal{W}(x, y, \theta, E_x, E_y, E_\theta) + f(t) \end{aligned} \right\} \quad (84)$$

where $f(t)$ in this example can be written as:

$$f(t) = -E_x t - E_y t - E_\theta t. \quad (85)$$

Here, we consider:

$$E = E_x + E_y + E_\theta. \quad (86)$$

We can rewrite Eq. 83 as:

$$\left[\frac{\partial S}{\partial t} + \frac{1}{2m} \left(\frac{\partial W_x}{\partial x} \right)^2 + \frac{1}{2m} \left(\frac{\partial W_y}{\partial y} \right)^2 + \frac{1}{2(mr^2 - J_0)} \left(\frac{\partial W_\theta}{\partial \theta} - \kappa \right)^2 + \frac{\mu^2}{4J_1} + \frac{\kappa^2}{2J_0} \right] = 0. \quad (87)$$

Let

$$\frac{\mu^2}{4J_1} + \frac{\kappa^2}{2J_0} = C_1 + C_2 + C_3 \quad (88)$$

Again we can rewrite Eq. 87 as:

$$\left[\begin{aligned} & \frac{\partial S}{\partial t} + \frac{1}{2m} \left(\frac{\partial W_x}{\partial x} \right)^2 + \frac{1}{2m} \left(\frac{\partial W_y}{\partial y} \right)^2 \\ & + \frac{1}{2(mr^2 - J_0)} \left(\frac{\partial W_\theta}{\partial \theta} - \kappa \right)^2 \\ & + C_1 + C_2 + C_3 \end{aligned} \right] = 0. \quad (89)$$

We will separate the variables as follows:

$$\left. \begin{aligned} \mathcal{W}(x, y, \theta, E_x, E_y, E_\theta) = \\ \mathcal{W}(x, E_x) + \mathcal{W}(y, E_y) + \mathcal{W}(\theta, E_\theta) \end{aligned} \right\} \quad (90)$$

Then we obtain:

$$\frac{1}{2m} \left(\frac{\partial W_x}{\partial x} \right)^2 + C_1 = E_x \quad (91)$$

$$\frac{1}{2m} \left(\frac{\partial W_y}{\partial y} \right)^2 + C_2 = E_y \quad (92)$$

$$\frac{1}{2(mr^2 - J_0)} \left(\frac{\partial W_\theta}{\partial \theta} - \kappa \right)^2 + C_3 = E_\theta \quad (93)$$

Integrating Eqs. 91, 92 and 93, we get:

$$W_x = \sqrt{2m(E_x - C_1)}x \quad (94)$$

$$W_y = \sqrt{2m(E_y - C_2)}y \quad (95)$$

$$W_\theta = \sqrt{2(mr^2 - J_0)(E_\theta - C_3)}\theta + \kappa\theta. \quad (96)$$

Now, the Hamilton-Jacobi function takes the form:

$$S = \left[\begin{aligned} & -E_x t - E_y t - E_\theta t + \sqrt{2m(E_x - C_1)}x \\ & + \sqrt{2m(E_y - C_2)}y \\ & + \sqrt{2(mr^2 - J_0)(E_\theta - C_3)}\theta + \kappa\theta \end{aligned} \right] \quad (97)$$

$$\text{Let } mr^2 - J_0 = C_4. \quad (98)$$

Then, applying the HJDEs to the wave function using Eq. 14, we obtain:

$$\check{H}'_0 \psi = \left[\begin{aligned} & \frac{\hbar}{i} \frac{\partial}{\partial t} + \frac{1}{2m} \left(-\hbar^2 \frac{\partial^2}{\partial x^2} - \hbar^2 \frac{\partial^2}{\partial y^2} \right) \\ & + \frac{1}{2C_4} \left(\frac{\hbar}{i} \frac{\partial}{\partial \theta} - \kappa \right)^2 + C_1 + C_2 + C_3 \end{aligned} \right] \psi \quad (99)$$

where

$$\psi(x, y, \theta, t) = \exp \left[\frac{i(-E_x t - E_y t - E_\theta t + \sqrt{2m(E_x - C_1)}x + \sqrt{2m(E_y - C_2)}y + \sqrt{2(E_\theta - C_3)C_4}\theta + \kappa\theta)}{\hbar} \right].$$

After some simplification, we get:

$$\hat{H}'_0 \psi = 0. \quad (100)$$

It is worth mentioning that there exist other examples for a continuous constrained systems such as the mobile robot which is a classical example of a continuous nonholonomic system that has smellier Lagrangian and constraint equation for the first example [18]. If we apply the process applied in the first example to this suggested example, we will get the same results. Although examples of constraints that are non-linear in velocities are frequent in mechanics and engineering, the solution is usually not available and the mechanical behavior of systems is often surprising or even unpredictable. Therefore, in the future one hopes to investigate this type of nonholonomic constraints for example the Appell-Hamel.

Conclusion

The nonholonomic constrained systems are investigated using the Hamilton-Jacobi quantization scheme to yield the complete equations of motion of the system. The principal function S is determined using the method of separation of variables in the same manner as for regular systems. Further, this function enables us to formulate the wave function. We illustrate through two examples how the Hamilton-Jacobi equation can be used to exactly integrate the equations of motion: The sliding of a balanced skate and the snakeboard. It is found that the nonholonomic constraints become new condition on the wave function to be satisfied in the semi-classical limit.

References

- [1] Bloch, A.M., Marsden, J.E. and Zenkov, D.V., American Mathematical Society, 52 (2005) 324.
- [2] Arnold, V.I., "Mathematical Methods of Classical Mechanics", (Springer-Verlag, 1989).
- [3] Goldstein, H., Poole, C.P. and Safko, J.L., "Classical Mechanics", 3rd Edition, (Addison Wesley, 2001).
- [4] Lanzos, C., "The Variational Principles of Mechanics", 4th Edition, (Dover, 1986).
- [5] Nawafleh, K.I., Rabei, E.M. and Ghassib, H.B., International Journal of Modern Physics, A19(3) (2004) 347.
- [6] Nawafleh, K.I., Dirasat, Pure Sciences, 34(1) (2007) 119.
- [7] Van der Schaft, A.J. and Maschke, B.M., Reports on Mathematical Physics, 34(2) (1994) 225.
- [8] Koon, W.S. and Marsden, J.E., Reports on Mathematical Physics, 42(1-2) (1998) 101.
- [9] Bloch, A.M., Krishnaprasad, P.S., Marsden, J.E. and Murray, R.M., Archive for Rational Mechanics and Analysis, 136(1) (1996) 21.
- [10] Rabei, E.M. and Guler, Y., Physical Review A, 46 (1992) 3513.
- [11] Rabei, E.M., Hadronic Journal, 19 (1996) 597.
- [12] Rabei, E.M., Nawafleh, K.I. and Ghassib, H.B., Hadronic Journal, 22 (1999) 241.
- [13] Rabei, E.M., IL Nuovo Cimento, 115 B(10) (2000) 1159.
- [14] Griffiths, D.J., "Introduction to Quantum Mechanics", (Prentice Hall Englewood Cliffs, New Jersey, 1995).
- [15] Rabei, E.M., Nawafleh, K.I. and Ghassib, H.B., Physical Review A, 66 (2002) 024101.
- [16] Ostrowski, J., Lewis, A., Murray, R.M. and Burdick, J., IEEE International Conference, 3 (1994) 2391.
- [17] Koon, W.S. and Marsden, J.E., Reports on Mathematical Physics, 40(1) (1997) 21.
- [18] Laurent, O.J., Conference on Scientific Computing in Honor of Ernst Hairer's 60th Birthday, Geneva, Switzerland (2009).

New Design of Objective Lens Geometry for Low Voltage SEM

M. A. Al-Khashab^a and R. Y. Al-Salih^b

^a *Department of Physics, College of Science, University of Mosul, Mosul, Iraq.*

^b *Department of Physics, College of Science, University of Tikrit, Tikrit, Iraq.*

Received on: 5/8/2013; Accepted on: 6/11/2013

Abstract: Five new models of magnetic objective lens geometry have been designed and studied in this work. Different excitation coil shapes and their positions inside the lenses at a constant excitation ($NI = 10 \text{ kA.t}$) were included. Spacious comparison between these models was realized using the finite element method (FEM) to analyze the magnetic field distribution, magnetic flux density and optical properties for each model at low relativistic corrected accelerating voltage ($V_r = 10 \text{ kV}$). The effect of the lens geometrical shape on the electron beam voltage passing throughout the optical axis of the lenses at zero image plane ($Z_i = 0 \text{ mm}$) has been inspected as well. The optimized one of the deliberated lenses has been selected as an objective lens for low voltage scanning electron microscope (SEM) preparatory for next research.

Keywords: Objective lens geometry design; Electron magnetic properties; Electron optical properties; Relativistic corrected accelerating voltage; Low voltage SEM.

Introduction

In recent years, there is a high demand for high- resolution scanning electron microscope (SEM) in all areas of development and fabrication of micro-electronic and opto-electronic components in order to visually evaluate sub - micrometer structures, as well as to be able to identify the deviations from standard patterns and in order to acquire and evaluate topographical data such as heights, widths or angles of inclination. Conventional SEM, however, only achieves the required spatial resolution of fractions of micrometer down to a few nanometers for small working distance, and high accelerating voltages above approximately 20 kV are used which cause resistant structures and integrated circuits to be destructed and non-conductive or high resistant specimens to be charged which is a disadvantage [1]. Therefore, new researches are interesting to obtain high resolution observation at low relativistic accelerating voltages (less than 20 kV), particularly in observing a semiconductor by the SEM [2].

Intensive studies have been conducted to improve the magnetic lens geometry, emphasizing that each parameter of the magnetic lens has its relative significance from both the practical and theoretical sides. The optimization of the polepiece shape is studied for the symmetrical double polepiece lens by Cleaver [3] and for the asymmetrical double polepiece lens by Wenxiong [4]. The influence of the shape and position of the coil on the projector lens properties of the symmetrical double polepiece lens and the single polepiece was studied by Al-Khashab [5]. The asymmetrical lens is largely used as an objective lens in the imaging system of various types of electron microscope [6]. It was found that the symmetrical magnetic lens usually provides a higher magnetic flux density peak and lower aberration coefficients in comparison with the asymmetrical lens, due to the fact that the asymmetrical lens is purposefully designed to provide a large volume of free space for the specimen holder in the region of the polepieces,

and this requirement is found to be difficult to achieve when the symmetrical objective lens is used under the limited space available around the specimen [7].

It is difficult to develop a general optimal lens design for all applications [8]. The optimum design of the magnetic electron lens with low aberration coefficients is generally considered significant [9]. However, low aberration electron magnetic lens has been found to require a high flux density with low half-width [10]. The aim of the present work is to design five new asymmetrical magnetic objective lenses with different geometries and different energized coil shapes and positions to study their magnetic and optical properties in order to select the best resolution and lowest aberration coefficients lens the focal length (f_o) of which, sometimes called working distance, lies outside the lens region, where all of the lenses are analyzed at constant excitation ($NI=10$ kA.t). Then, the adequate one of the investigated lenses will be chosen as an objective lens for low voltage SEM.

Analysis Methods

Recently, the existence of computer eases the design and the analysis of electron microscope lenses in which this task was difficult to solve the mathematical functions numerically. The magnetic and electric flux density distribution function can now easily and accurately be generated by the aid of the computer calculation before we start the practical design [11]. The progress in computer simulations helps to solve a lot of complicated design problems which was impossible to implement previously. Munro [11]

has used the finite element method (FEM) to write packages used to calculate the magnetic and electric fields for electromagnetic lenses [12]. The design of electromagnetic lenses depends on the hypothetical mathematical models for the field distribution like the bell shaped model and on the experimental fields. The steps needed to design the electromagnetic lenses numerically are [13]:

- The finite element method (FEM) used to calculate the axial flux density distribution (B_z) for the proposed design.
- Calculation of the axial ray tracing (trajectory) by solving the ray tracing equation numerically using Runge-Kutta method.
- Calculation of the chromatic factors for the proposed model by using Simpson method for each value of the axial magnetic field distribution and axial ray tracing.

The Objective Lens Design

Five new models of asymmetrical electron magnetic objective lens have been designed. These are denoted as L1, L2, L3, L4 and L5, respectively. Fig. 1 clarifies the comparison between all of the designed lenses. It is seen that each one differs from the others in geometric structure of the iron circuit, coil shape, coil position, coil sectional area of (1615 mm², 1330 mm², 1300 mm², 1365 mm² and 1895 mm², respectively), axial bore diameter and other geometrical diameters. However, all of them have the same length of polepiece snout faces of (4mm).

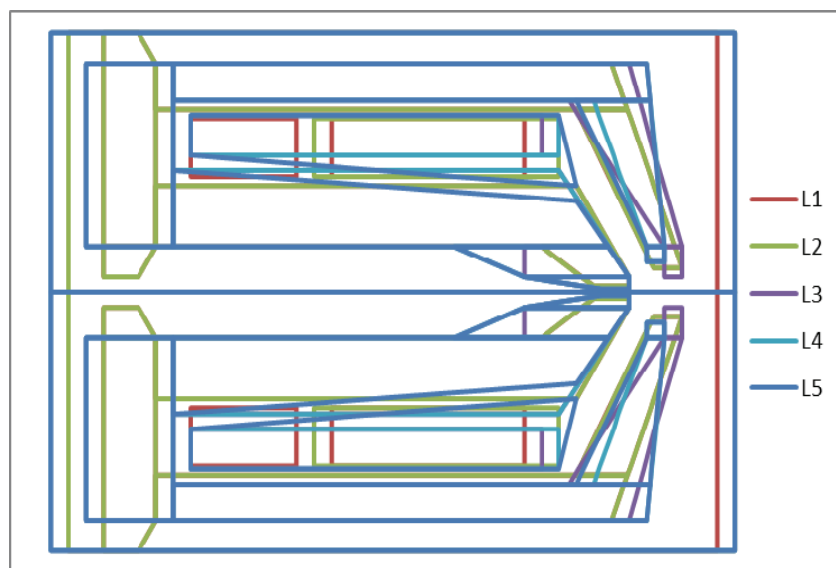


FIG. 1. Comparison between the schematic diagrams of the objective lens design.

The polepiece angles were taken equal to 62° (for L1 & L2), 60° (for L3 & L4) and 58° (for L5), according to the optimization of Al-Khashab and Ahmad [14], who found that the preferred angles for the double and single polepiece lenses is in the range from 55° to 63° . The recent designed lenses have the same radial diameter (150 mm), while their axial length is 170 mm (for L1, L2 and L3) and 165 mm (for L4 & L5). The distance between the polepiece face and the outer edge of the iron shroud bore, which is denoted as (d_{out}), is equal to 15 mm (for L1, L2 and L3) and 10 mm (for L4 & L5) as listed in Table (1) in the present paper. A cylindrical gap of 30 mm diameter and about 80 mm length has been designed in each lens to be used as a place of scan coil deflector preparatory for next future work. All the suggested lenses have been tested at a low relativistic corrected accelerating voltage ($V_r = 10$ kV) and an excitation ($NI = 10$ kA.t) as mentioned before.

The Axial Magnetic Flux Density Distributon

The axial magnetic flux density distribution (B_z) of the designed lenses has been studied with the aid of computer program (M11) for the asymmetrical polepiece lenses [13] using the finite element method. Fig. 2 illustrates the axial magnetic flux distribution for the designed lenses. It is noticed that, as we make headway from L1 up to L5, the peaks of B_z increased and the half-widths alternated ensuring that there is a noticed progress in the lenses design. This behavior is useful for focusing the electron beam passing through the optical axis of the lens. The change in half-width is due to the difference between spaces separating the polepiece snout and the axial bore of the iron shroud, which is the effective region of the magnetic field distribution. The increase in this region reduces the strength of the magnetic field and increases the half-width [15] and vice versa.

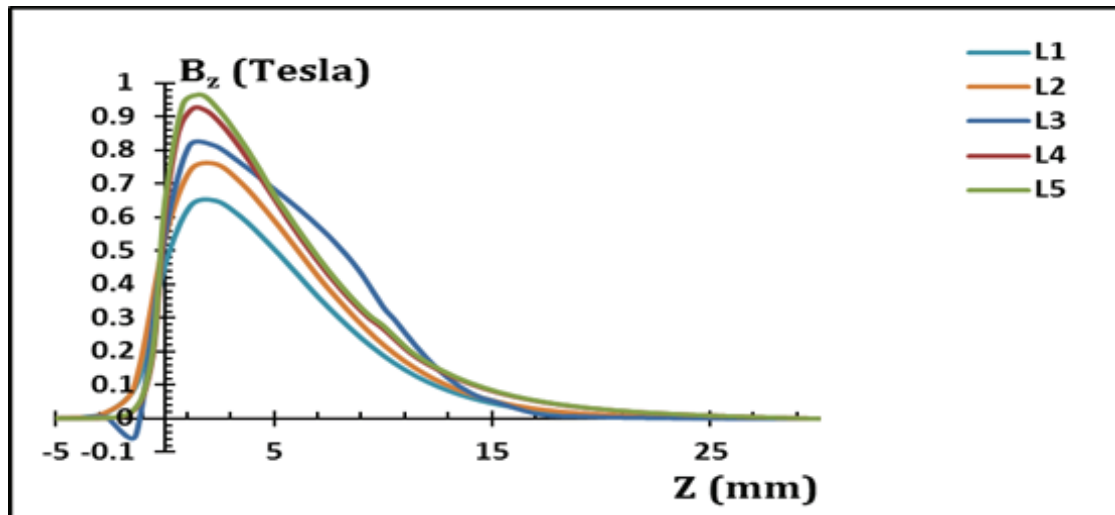


FIG. 2. The axial magnetic flux density distribution (B_z) for the designed lenses at a constant excitation ($NI = 10$ kA.t).

In spite of obtaining this clear difference in B_z , the outcome is still poor. This is because there are other characteristics carrying exaggerate importance needed to decide which lens is the best, such as the magnetic flux lines trajectory and the optical properties, which will be explained in the next sections. It can be said that this consequence is regarded as a primary indicator, but not as a definitive ruling, especially if it is well known that higher peaks of B_z can occur by increasing the sectional area of the excitation coil and decreasing the space between the coil and the yoke.

The Magnetic Flux Lines of the Designed Lenses

In order to demonstrate the effect of the lens geometrical shape on the magnetic flux lines, an inspection has been carried out using flux program (M13) for computing the flux density distribution throughout the magnetic circuits of unsaturated magnetic lenses [13] at ($V_r = 10$ kV) and ($NI = 10$ kA.t).

Fig. 3 illustrates the flux line trajectories of the designed lenses. It is clear that lens L4 seems to be the best one, according to the regular and

little leakage of its flux lines. In addition, its flux lines propagate in preferred way and path as it is needed to make the required effect on the charged particles passing throughout the lens.

This outcome gives a good indicator to distinguish the best liked lens. Nevertheless, this needs more investigation.

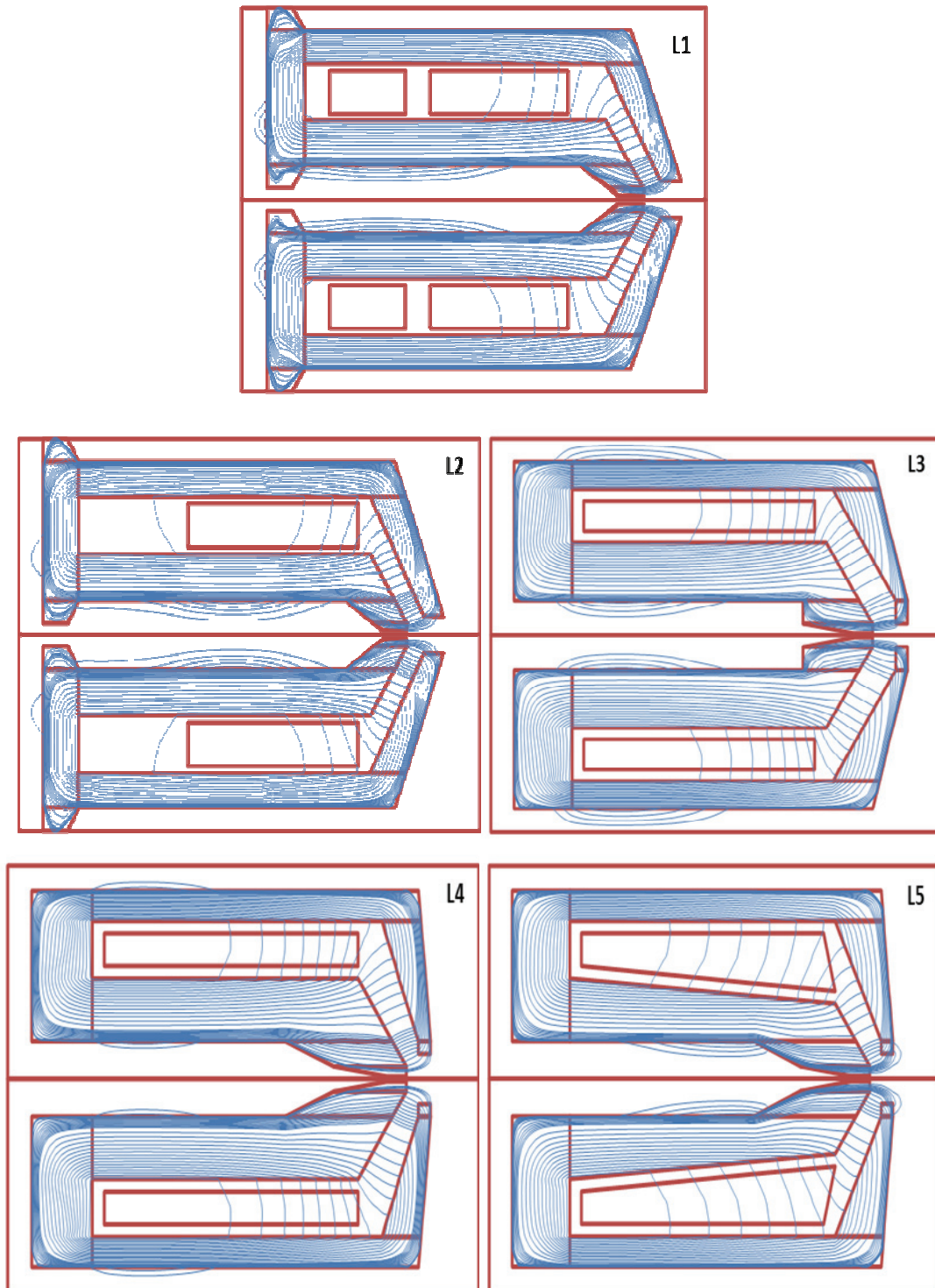


FIG. 3. The cross - section of the designed objective lenses and their flux line trajectories at a constant excitation (NI = 10 kA.t).

Objective Optical Properties

For the sake of selecting the preferred lens among the tested lenses, some aspects of the optical properties have been investigated using computer program (M21) for computing the objective properties of the magnetic lenses [13] in the low range of relativistic corrected accelerating voltage ($V_r = 10\text{V} - 100\text{ kV}$) at a constant excitation ($NI = 10\text{ kA.t}$). The values of V_r are auto-calculated by the aforesaid program according to the well-known relation [$V_r = V_a (1 + e/2mc^2) V_a$], where V_a is the accelerating

voltage. The effect of V_r on the optical properties of the introduced lenses has been investigated at zero image plane ($Z_i = 0$) within vast range of V_r (10 V–1000 kV). This investigation generates the relation cleared in Fig. 4. It is found that each design has its own V_r to constitute the image at zero plane on the axial axis. In addition, it is seen that lenses L4 & L5 possess the lower proportions of V_r , which means that these two lenses need lower potential values than the other lenses to show best liked optical properties.

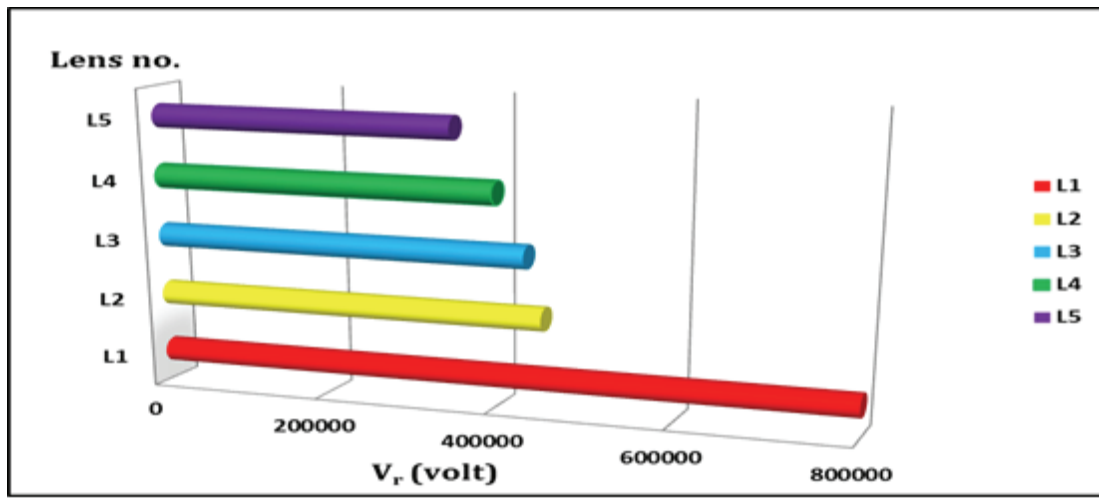


FIG. 4. The applied relativistic corrected accelerating voltages for the tested lenses needed to form a zero image plane ($Z_i = 0$).

The values of spherical aberration coefficient (C_s), chromatic aberration coefficient (C_c), resolving power (δ) and objective focal length (f_o) have been calculated and studied carefully. The resolving power δ (equal to $0.61C_s^{1/4}\lambda^{3/4}$, where λ is the electron wavelength) of the designed objective lenses here is drawn as a function of V_r . Fig. 5 demonstrates this relation. At first sight, it is shown that lenses L1, L2 and L5 emerge the lower in magnitudes compared with lenses L3 and L4, but they are overlapped to be the worse ones at a working voltage ($V_r = 10\text{ kV}$). Lenses L3 and L4 seem to be the best at this working point, and they are nearly conforming to each other. The preference between them is difficult and is a scarce task. It

is necessary to go to other optical properties to accomplish this.

Figs. 6 and 7 illustrate the relationship between the relative spherical and chromatic aberration coefficients to the focal length (C_s / f_o) and (C_c / f_o) respectively for the designed lenses as a function of an accelerating voltage (V_r). It seems clearly that the best regular behaviors obtained from lenses L3 and L4. For further clarification, Fig. 6 is maximized to show the specified operating point, where lenses L3 and L4 gave the lowest values, and that is consistent with the desired goal. They appear to be completely identical and it is difficult to distinguish the better one. Again, we need to look for other optical properties to discriminate between them.

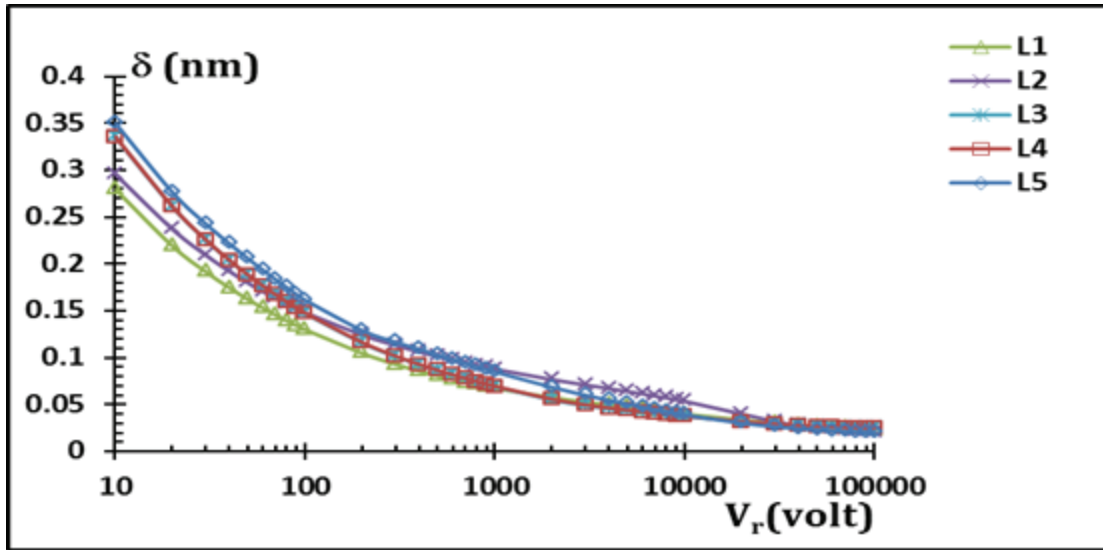


FIG. 5. Comparison between the resolving power (δ) of the designed lenses with the relativistic corrected accelerating voltage at a constant excitation ($NI = 10 \text{ kA.t}$).

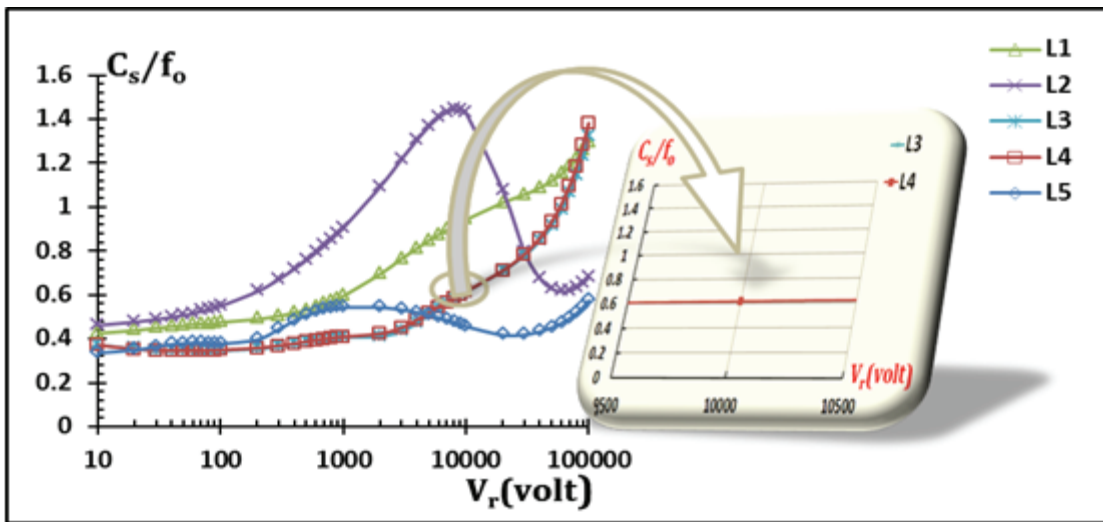


FIG. 6. Variation of the values (C_s / f_0) for the designed lenses as a function of (V_r) at a constant excitation ($NI = 10 \text{ kA.t}$).

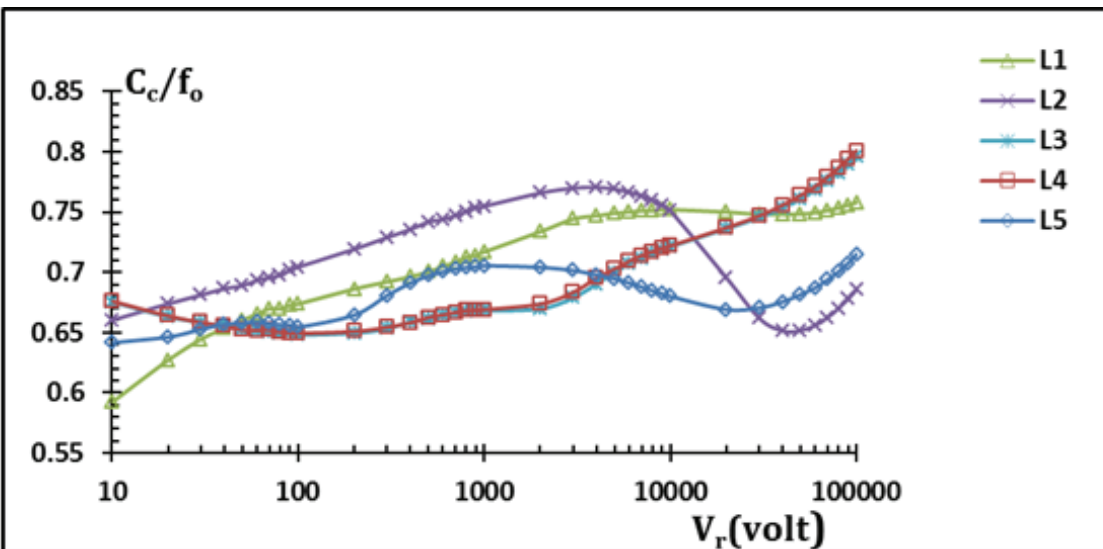


FIG. 7. Variation of the values (C_c / f_0) for the designed lenses as a function of (V_r) at a constant excitation ($NI = 10 \text{ kA.t}$).

Fig. 8 demonstrates the comparison between the objective focal lengths for the standing lenses as a function of (V_r). It is clear that lens L4 possesses the least value among all other lenses. Lenses L3 and L4 seem equal to each other in values, the magnified section in Fig. 8 clearly shows that the objective focal length of lens L4 is larger than those of lenses L1 and L2. At the first glance, one would think that lenses L1 and

L3 are the best depending on their low values of the focal length (f_o), but the truth is that lens L4 is the best for a very important reason, which is that the main purpose of this research is to design a strong objective lens with a short focal length to get a short working distance and to be located outside the region structure of the lens to facilitate the process of the specimen installation.

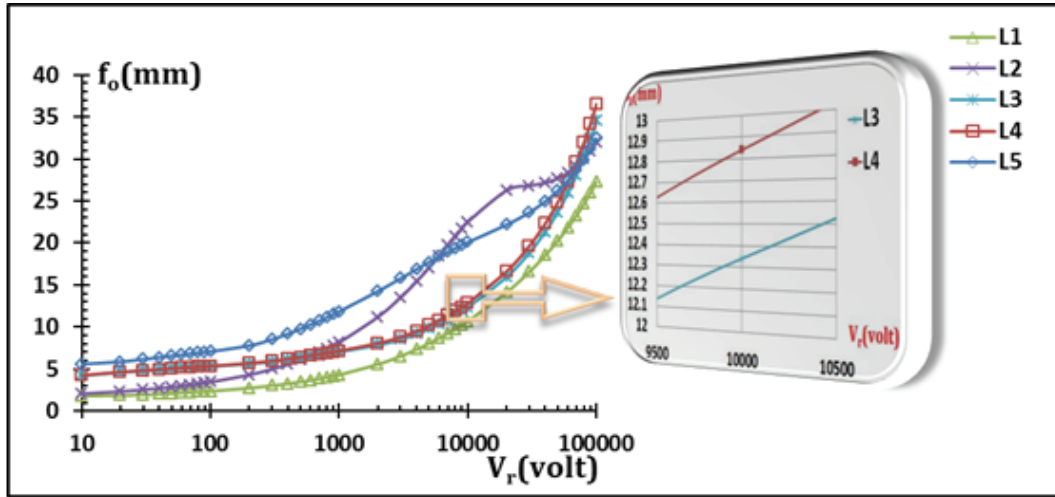


FIG. 8. Variation of objective focal lengths (f_o) for the designed lenses as a function of (V_r) at a constant excitation ($NI = 10 \text{ kA.t}$).

Table (1) records some aspects of the optical and geometrical values for the proposed lenses at working point ($V_r = 10 \text{ kV}$) and specified excitation ($NI = 10 \text{ kA.t}$). The distance between the face of the pole and the end of the outer edge of the iron shroud (d_{out}) varies from one lens to the other depending on the different designs. It is obvious that lens L3 has the value ($d_{out} = 15 \text{ mm}$), while its focal length is ($f_o = 12.34 \text{ mm}$), which means that the working distance has to be

inside the lens which is considered an undesirable property to achieve the goal of the research. However lens L4 has the magnitude ($d_{out} = 15 \text{ mm}$) and its focal length is ($f_o = 12.84 \text{ mm}$). In other words, its working distance is outside the lens structure and that complies with the requirements of the aim of the research work. Details of the comparison are shown and denoted in Table (1) below.

TABLE 1. The optical properties for the designed lenses at a working point of ($V_r = 10 \text{ kV}$) and a constant excitation ($NI = 10 \text{ kA.t}$)

Lens no.	$Z_i(\text{mm})$	$Z_p(\text{mm})$	$f_o(\text{mm})$	$d_{out}(\text{mm})$	$C_s(\text{mm})$	$C_c(\text{mm})$
L1	-119.9	-130.6	10.69	15	10.07	8.04
L2	-99.76	-122.3	22.53	15	32.2	16.92
L3	-114.1	-126.4	12.34	15	7.57	8.9
L4	-113.2	-126	12.84	10	7.9	9.27
L5	-86.42	-106.5	20.09	10	9.16	13.66

The above result has been considered as a crucial point for the selection of lens L4 as the best lens among the examined lenses, because it meets all the requirements necessary to achieve the goal of the research. It should be remembered that this lens showed the best

properties of the magnetic flux lines as mentioned previously. It should be pointed out here that although the working distance of lens L1 is outside the lens structure, it has been excluded during the search for its bad most general characteristics.

Conclusions

In this work, it is found that to make preference between many electron magnetic lens designs, both magnetic and optical analyses should be applied, and the optimization will depend on the aim of the research to facilitate the optimal choice. It is noticed practically that the optical properties of the electron lenses are improved when the excitation coil localizes

nearby the air gap between the polepiece and the iron shroud at the bottom of the objective lens. The selection of lens L4 in this work is based on its verification of the research goal. Lens L4 will be investigated later to improve its magnetic and optical properties, to fabricate it in a next research in order to use it practically as an objective lens in a low voltage SEM.

References

- [1] Forsien, J., U. S. Patent, No. 4, 926, 054, (1990).
- [2] Yonezawa, A., Sato, M. and Takaoka, O., U. S. Patent, No. 6, 037, 589, (2000).
- [3] Cleaver, J.R.A., *Scanning Microscope*, 2(3) (1980) 1283.
- [4] Wenxiong, C., *Scanning Microscope*, 2(3) (1988) 1283.
- [5] Al-Khashab, M.A., *Eng. Technology*, 20(10) (2001) 591.
- [6] Al-Khashab, M.A. and Abdullah, A.E., *Dirasat, Pure Sciences*, 33(1) (2006) 28.
- [7] Lenz, F., "Magnetic Electron Lenses", Ed. P. W. Hawks (Berlin, Springer, 1982) 119.
- [8] Al-Khashab, M.A. and Ahmad, A.A., *Jordan Journal of Physics*, 5(2) (2012) 67.
- [9] Al-Khashab, M.A. and Ahmad, A.A. *Dirasat, Pure Sciences*, 38(2) (2011) 161.
- [10] Mulvey, T., "Magnetic Electron Lens Properties", Ed. P. W. Hawks (Berlin, Springer, 1982) Ch. 5.
- [11] Munro, E., Ph.D. Thesis, University of Cambridge, (1971), U. K.
- [12] Hussain, S.H., Ph.D. Thesis, University of Al- Mustansiriyah, (2012), Baghdad, Iraq.
- [13] Munro, E., "A Set of Computer Programs for Calculating the Properties of Electron Lenses", University of Cambridge, Department of Engineering Report CUED/B-Elect TR45, (1975).
- [14] Al-Khashab, M.A. and Ahmad A.A., *Dirasat, Pure Sciences*, 31(1) (2004) 22.
- [15] Abbass, T.M. and Nasser, B.A., *British Journal of Science*, 6(2) (2012) 43.

Jordan Journal of Physics

ARTICLE

IBM-1 Calculations of Energy Levels and Electric Transition Probabilities B(E2) in “¹⁵⁸⁻¹⁶⁰Gd Isotopes”

K. A. Al-Maqtary

Physics Department, Faculty of Applied Sciences, Taiz University, Taiz, Yemen.

Received on: 9/2/2012; Accepted on: 25/11/2013

Abstract: In this paper, the interacting boson model (IBM-1) is described and employed for calculating the energy levels and electric transition probabilities B(E2) for “¹⁵⁸⁻¹⁶⁰Gd isotopes”. The values of the parameters have been determined using the IBM-1 Hamiltonian which yield the best fit to the available experimental energy levels. Particular attention has been paid to the B(E2) transition probabilities. In general, a good agreement has been achieved between the IBM-1 calculations and the available experimental results of energy levels and B(E2) values. The results showed that the “¹⁵⁸⁻¹⁶⁰Gd isotopes” are rotational (deformed) nuclei and that they have dynamical symmetry SU(3) in the interacting boson model IBM-1.

Keywords: Isotope; Energy levels; Interacting boson model; Transition probabilities.

Introduction

The interacting boson model (IBM) is a nuclear model proposed by Iachello and Arima in (1974) [1]. The basic idea of the IBM [1-5] is used to describe the low-lying collective states in even-even nuclei employing a system of interacting s- and d-bosons carrying angular momentums 0 and 2, respectively. (It is reasonable to view the boson states as being constructed from the valence space only and to identify the bosons as correlated pairs of like nucleons). The bosons number $N = n_s + n_d$ is finite and conserved in a given nucleus and simply given as half of the total number of valence nucleons. There are four versions of this model (IBM-1, IBM-2, IBM-3 and IBM-4). In the IBM-1 version, no distinction is made between protons and neutrons. Moreover, the valence number counting is always done relative to the nearest closed shells. Since the bosons could be pairs of holes or particles, the s (L=0) and d (L=2) bosons of the IBM-1 have six sub - states and therefore define six-dimensional space. This leads to a description in terms of the unitary group in six dimensions, U(6). Thus, many of the

characteristic properties of the IBM-1 can be derived by group- theoretical methods and analytically expressed. The different reductions of U(6) lead to three dynamical symmetries known as SU(5), SU(3) and O(6), which are related to the spherical vibrator, deformed rotor and asymmetric (γ -soft), respectively. The three corresponding dynamical symmetries, group chains of U(6) can be written as [5]:

$$U(6) \supset SU(5) \supset O(5) \supset O(3) \supset O(2) \quad (I)$$

$$U(6) \supset SU(3) \supset O(3) \supset O(2) \quad (II)$$

$$U(6) \supset O(6) \supset O(5) \supset O(3) \supset O(2) \quad (III)$$

The energy levels of “¹⁵⁸⁻¹⁶⁰Gd isotopes” have been extensively experimentally investigated using a wide variety of reactions. From these studies, the excited states in the “¹⁵⁸⁻¹⁶⁰Gd isotopes” have been investigated from (γ , γ'), (d, p), (α , $2n\gamma$), (α , $4n\gamma$), (n, γ), (n, $n'\gamma$) and coulomb excitation reactions which gave information about the experimental energy levels and the B(E2) values in these isotopes [6-28].

The aim of the present work is to investigate the dynamical symmetry of $^{158-160}\text{Gd}$ isotopes" and study the energy levels and the B(E2) values of these isotopes within the framework of the (IBM-1) model.

Theoretical Basics of IBM-1 Model

The most general Hamiltonian of IBM-1 is [5]:

$$\hat{H} = \left[\begin{array}{l} \varepsilon(\hat{n}_s + \hat{n}_d) + a_o \hat{P}^+ \hat{P} + a_1 \hat{L} \cdot \hat{L} \\ + a_2 \hat{Q} \cdot \hat{Q} + a_3 \hat{T}_3 \hat{T}_3 + a_4 \hat{T}_4 \hat{T}_4 \end{array} \right] \quad (1)$$

where ε is the bosons energy and the operators are [5]:

$$\left. \begin{array}{l} \hat{n}_s = \hat{s}^+ \cdot \hat{s} \quad , \quad \hat{n}_d = \hat{d}^+ \cdot \hat{d} \\ \hat{P} = \frac{1}{2}(\hat{d} \hat{d}^+ + \hat{d}^+ \hat{d}) - \frac{1}{2}(\hat{s} \hat{s}^+ + \hat{s}^+ \hat{s}) \\ \hat{L} = \sqrt{10} \left[\hat{d}^+ \times \hat{d} \right]^{(1)} \\ \hat{Q} = \sqrt{5} \left[(\hat{d}^+ \times \hat{s}^+) + (\hat{s}^+ \times \hat{d}^+) \right]^{(2)} + \chi \left[\hat{d}^+ \times \hat{d} \right]^{(2)} \\ \hat{T}_3 = \left[\hat{d}^+ \times \hat{d} \right]^{(3)} \\ \hat{T}_4 = \left[\hat{d}^+ \times \hat{d} \right]^{(4)} \end{array} \right\} \quad (2)$$

The phenomenological parameters $a_0, a_1, (a_2, a_3), a_4$, represent the strengths of the pairing, angular momentum, quadrupole, octupole, hexadecupole interactions between bosons, respectively.

The three chains of the dynamical symmetries of IBM-1 are:

Group Chain I: The Vibrational SU(5) Limit

This limit of dynamical symmetry group describes the vibrational nuclei which have a spherical shape. The Hamiltonian of this chain can be written as [3, 5]:

$$\hat{H}^{(I)} = \left[\begin{array}{l} \varepsilon(\hat{n}_s + \hat{n}_d) + a_1 \hat{L} \cdot \hat{L} \\ + a_3 \hat{T}_3 \hat{T}_3 + a_4 \hat{T}_4 \hat{T}_4 \end{array} \right] \quad (3)$$

Group Chain II: The Rotational SU(3) Limit

This limit is used to describe the rotational spectra of nuclei that possess axial symmetrical rotor. The Hamiltonian of this limit is given by [3, 5, 29]:

$$\hat{H}^{(II)} = a_1 \hat{L} \cdot \hat{L} + a_2 \hat{Q} \cdot \hat{Q} \quad (4)$$

Group Chain III: The γ -Unstable O(6) Limit

This limit is used to describe the asymmetric (γ -soft) deformed rotor of nuclei, the Hamiltonian of this limit is [3, 5, 30, 31]:

$$\hat{H}^{(III)} = a_0 \hat{P}^+ \hat{P} + a_1 \hat{L} \cdot \hat{L} + a_3 \hat{T}_3 \hat{T}_3 \quad (5)$$

Table 1 shows the behavior of these limits.

TABLE 1. Energy ratios and the basic conditions of the B(E2) values of the corresponding limits [3, 5].

Limit	$E \left(\frac{4_1^+}{2_1^+} \right)$	$E \left(\frac{6_1^+}{2_1^+} \right)$	$\frac{B(E2; 4_1^+ \rightarrow 2_1^+)}{B(E2; 2_1^+ \rightarrow 0_1^+)}$	$\frac{B(E2; 0_2^+ \rightarrow 2_1^+)}{B(E2; 2_1^+ \rightarrow 0_1^+)}$	$\frac{B(E2; 2_2^+ \rightarrow 2_1^+)}{B(E2; 2_1^+ \rightarrow 0_1^+)}$
SU(5)	2	3	< 2	< 2	< 2
SU(3)	3.33	7	< (10/7)	≈ 0	≈ 0
O(6)	2.5	4.5	< (10/7)	≈ 0	< (10/7)

The Electromagnetic Transitions Operator

The general form of the electromagnetic transitions operator in IBM-1 is [3, 5, 32]:

$$\left. \begin{aligned} \hat{T}^{(L)} = & \gamma_0 \left[\hat{S}^+ \times \hat{S} \right]^{(0)} \\ & + \alpha_2 \left[\hat{d}^+ \times \hat{S} + \hat{S}^+ \times \hat{d} \right]^{(2)} \\ & + \beta_L \left[\hat{d}^+ \times \hat{d} \right]^{(L)} \end{aligned} \right\} \quad (6)$$

where γ_0 , α_2 and β_L ($L = 0, 1, 2, 3, 4$) are parameters specifying the various terms in the corresponding operators. Eq. 6 yields transition operators for E0, M1, E2, M3 and E4 transitions with appropriate values of the corresponding parameters.

The electric quadrupole operator E2 has a widespread application in the analysis of γ -ray transitions and it is deduced from Eq. 6 as [3, 5, 31]:

$$\left. \begin{aligned} \hat{T}^{(E2)} = & \alpha_2 \left[\hat{d}^+ \times \hat{S} + \hat{S}^+ \times \hat{d} \right]^{(2)} \\ & + \beta_2 \left[\hat{d}^+ \times \hat{d} \right]^{(2)} \end{aligned} \right\} \quad (7)$$

It is clear that, for the E2 polarity, two parameters α_2 and β_2 are needed in addition to the wave functions of initial and final states.

The B(E2) values are defined in terms of reduced matrix elements by Iachello and Arima (1987) as [5, 31, 33]:

$$\left. \begin{aligned} B(E2; L_i \rightarrow L_f) = & \\ & \frac{1}{2L_i + 1} \left| \left\langle L_f \left\| \hat{T}^{(E2)} \right\| L_i \right\rangle \right|^2 \quad (eb)^2 \end{aligned} \right\} \quad (8)$$

Results and Discussion

Energy Levels

The IBM-1 model has been used in the calculation of the energy levels of the $^{158-160}\text{Gd}$ isotopes, using the experimental energy ratios $E\left(\frac{4_1^+}{2_1^+}\right) = 3.29, 3.3$ and $E\left(\frac{6_1^+}{2_1^+}\right) = 6.78, 6.84$,

respectively. It has been found that the $^{158-160}\text{Gd}$ isotopes are rotational (deformed) nuclei and that they have a dynamical symmetry SU(3) respecting to the IBM-1.

According to the Hamiltonian of the dynamical symmetry SU(3) limit (Eqs. 1 and 4), the energy levels of the $^{158-160}\text{Gd}$ isotopes (total number of bosons are 13, 14, respectively) have been calculated using the angular momentum and quadrupole parameters $[a_1, (a_2, \chi)]$. The best fit values of these parameters are given in Table 2, which shows the values of the relevant parameters, these values are obtained by fitting to get results of the energy levels that match with the experimentally reported data [12-27], whereas, the first two and the last term in equation (1) have not been included because they are irrelevant to the case of fully and weakly deformed nuclei (rotational nuclei).

TABLE 2. The best fit values of the Hamiltonian parameters for $^{158-160}\text{Gd}$ isotopes".

Isotopes	a_1 MeV	a_2 MeV	X MeV
^{158}Gd	0.0065	-0.0167	-1.16
^{160}Gd	0.00425	-0.0213	-0.61

Comparison between the experimentally determined energy levels and the IBM-1 calculations is shown in Fig. 1. Fig. 1 shows the experimental [12, 27] and the IBM-1 calculations of ground state, γ and β bands of $^{158-160}\text{Gd}$ isotopes. It shows that there is a good agreement between experimental and the IBM-1 calculations.

Root mean square deviation [34]

$$RMSD = \left[\frac{1}{N} \sum (E_{cal} - E_{Exp})^2 \right]^{\frac{1}{2}} \quad \text{is used to}$$

compare between experimental results and calculations of energy levels (N is the number of levels). The (RMSD) for ^{158}Gd is found to be 0.044 in ground state band for seven levels and it is 0.0165 for five levels in γ -band. However, it is 0.0466 in β -band for four levels, and the (RMSD) for ^{160}Gd is found to be 0.0724 in ground state band for nine levels and for seven levels it is 0.05 in γ -band. However, it is 0.028 in β -band for two levels (there is no available experimental data).

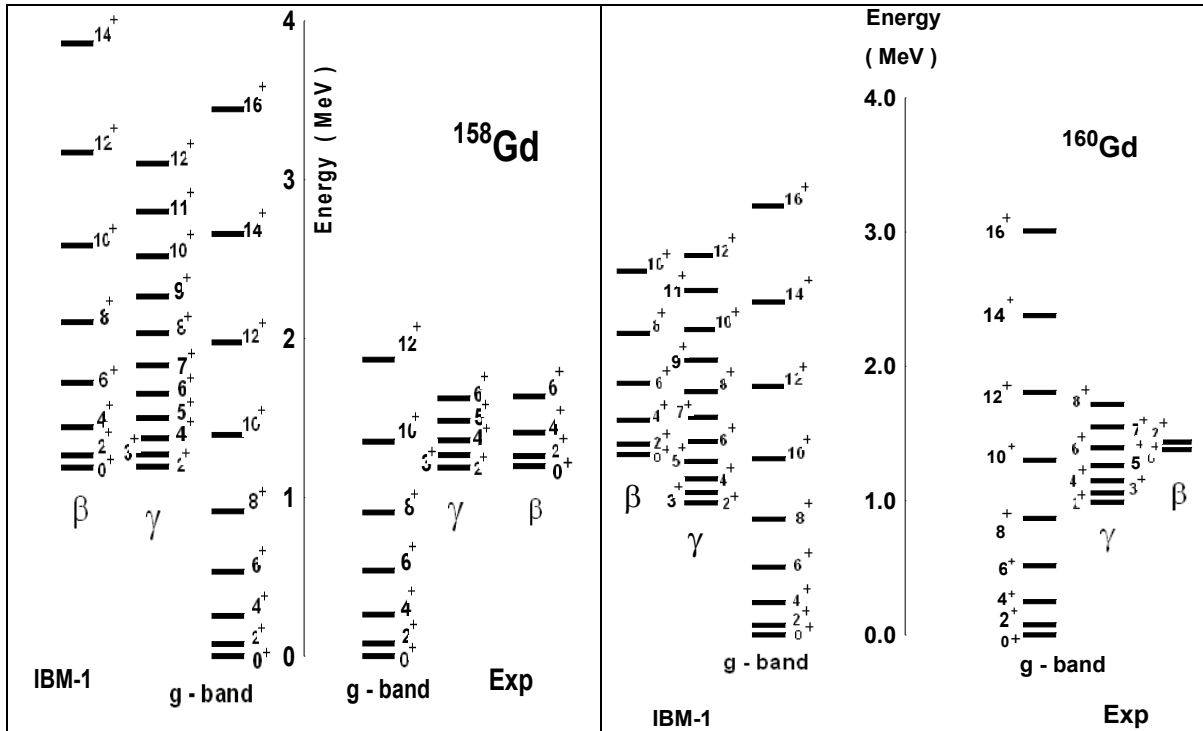


FIG. 1. The experimental [12,27] and calculated energy levels of " $^{158-160}\text{Gd}$ isotopes".

A very good agreement has been obtained between the experimental and the calculated energy level variations with the angular momentum as depicted in Fig.2. This figure shows that the experimental and the theoretical energy levels of the ground state, β and γ bands in " $^{158-160}\text{Gd}$ isotopes" increase with increasing angular momentum. A very good agreement was also found between the experimental and the theoretical energy levels of the ground state band

and a good agreement was achieved in energy levels of β and γ bands. In general, the experimental and the IBM-1 calculations of energy levels in " $^{158-160}\text{Gd}$ isotopes" increase with angular momentum as $l(l+1)$ because these isotopes are rotational (deformed) nuclei. Comparison between the ground state, β and γ bands of the experimentally determined energy levels and the IBM-1 calculations is shown in Fig. 2.

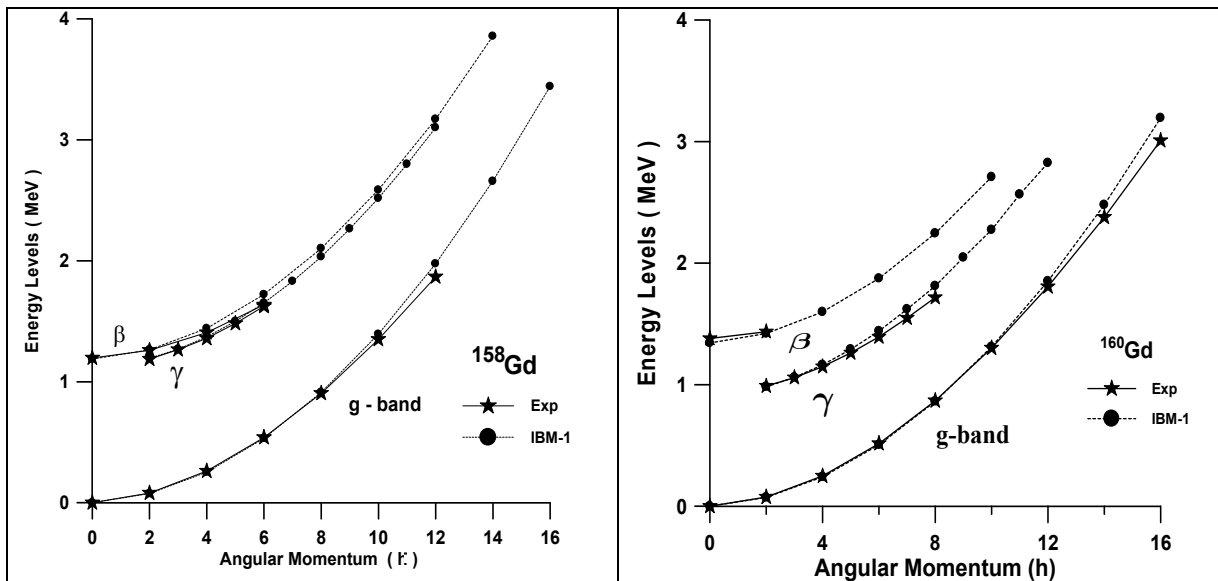


FIG. 2. Variation of energy levels with the angular momentum for " $^{158-160}\text{Gd}$ isotopes".

The condition of energy ratios of the corresponding limits is shown in Table 1. It has been found from calculations of energy levels from IBM-1, for $^{158-160}\text{Gd}$ isotopes" that $E(\frac{4_1^+}{2_1^+}) = 3.33, 3.326$ and $E(\frac{6_1^+}{2_1^+}) = 6.99, 6.964$; therefore the $^{158-160}\text{Gd}$ isotopes" are considered as rotational (deformed) nuclei and the dynamical symmetry of these isotopes is SU(3) in the IBM-1.

Electric Transition Probabilities B(E2)

Once the wave functions have been fixed by fitting the energy levels, one could determine the B(E2) values between these levels. The calculated B(E2) values for transitions in $^{158-160}\text{Gd}$ isotopes" were obtained by employing Eq. 8. The used $T^{(E2)}$ parameters of $^{158-160}\text{Gd}$ isotopes" are given in Table 3.

TABLE 3. The used $T^{(E2)}$ parameters α_2 and β_2 for $^{158-160}\text{Gd}$ isotopes".

Isotopes	α_2 (eb)	β_2 (eb)
^{158}Gd	0.148	-0.0317
^{160}Gd	0.132	-0.033

A comparison between the experimentally determined values of B(E2) [12,16,27,28] and those calculated by the IBM-1 model is given in Table 4, this table show that the B(E2)

transitions between γ -band to g-band and β -band to g-band are smaller than the B(E2) transitions between g-band to g-band. This table also shows that, in general, there is a good agreement between the experimentally reported and calculated B(E2) values in ground state bands in $^{158-160}\text{Gd}$ isotopes" except the transition 10_1^+ to 8_1^+ in ^{158}Gd isotope", where the experimental and calculated B(E2) values of this transition have weak agreement. The experimental and calculated B(E2) transitions between β -band to g-band and γ -band to g-band in general are in a very good agreement except the transitions 4_2^+ to 2_1^+ , 2_3^+ to 2_1^+ and 0_2^+ to 2_1^+ in ^{158}Gd isotope" which have weak agreement. The weak agreement between the experimental and calculated values in some B(E2) in those isotopes can be explained by the fact that many small components of the initial and final wave functions contribute coherently to the value of this reduced E2 transition probability, since these small components are not stable enough against small changes in the model parameters [35]. There is no available experimental transition data to many transitions in Table 4, therefore, these data have been predicted by using IBM-1. Experimental and calculated B(E2) values are also compared with available theoretical values.

TABLE 4. Experimental and calculated B(E2) values of g-band to g-band, γ -band to g-band, β -band to g-band and β -band to γ -band in $^{158-160}\text{Gd}$ isotopes".

^{158}Gd isotope								
(g-band to g-band)		B(E2)(e^2b^2)		(γ-band to g-band)		B(E2)(e^2b^2)		
initial state	final state	Exp.	IBM-1	initial state	final state	Exp.	IBM-1	IBA[36]
2_1^+	0_1^+	1.005	1.063	2_2^+	0_1^+	0.0178	0.018	0.0170
4_1^+	2_1^+	1.467	1.499	2_2^+	2_1^+	0.03	0.029	0.0266
6_1^+	4_1^+	-	1.611	2_2^+	4_1^+	0.0014	0.0019	0.0018
8_1^+	6_1^+	1.65	1.626	4_2^+	2_1^+	0.0057	0.0091	-
10_1^+	8_1^+	1.69	1.589	4_2^+	4_1^+	0.037	0.034	-
12_1^+	10_1^+	1.55	1.516					
(β-band to g-band)		B(E2)(e^2b^2)			(β-band to γ-band)		B(E2)(e^2b^2)	
initial state	final state	Exp.	IBM-1	IBA[36]	initial state	final state	Exp.	BM-1
0_2^+	2_1^+	0.006	0.0097	-	0_2^+	2_2^+	-	0.051
2_3^+	0_1^+	0.0016	0.0015	0.002	2_3^+	2_2^+	-	0.0099
2_3^+	2_1^+	0.001	0.0025	0.0033	2_3^+	4_2^+	-	0.0165
2_3^+	4_1^+	0.007	0.006	0.0076	4_3^+	4_2^+	-	0.0118

¹⁶⁰ Gd isotope							
(g-band to g-band)		B(E2)(e ² b ²)		(γ-band to g-band)		B(E2)(e ² b ²)	
initial state	final state	Exp.	IBM-1	initial state	final state	Exp.	IBM-1 IBA[36]
2 ₁ ⁺	0 ₁ ⁺	1.041	1.0417	2 ₂ ⁺	0 ₁ ⁺	0.0202	0.02027 0.0176
4 ₁ ⁺	2 ₁ ⁺	-	1.473	2 ₂ ⁺	2 ₁ ⁺	0.0366	0.0365 0.0275
6 ₁ ⁺	4 ₁ ⁺	-	1.593	2 ₂ ⁺	4 ₁ ⁺	0.0037	0.003 0.0018
8 ₁ ⁺	6 ₁ ⁺	-	1.622	4 ₂ ⁺	2 ₁ ⁺	-	0.0081 -
10 ₁ ⁺	8 ₁ ⁺	-	1.603	4 ₂ ⁺	4 ₁ ⁺	-	0.0433 -
12 ₁ ⁺	10 ₁ ⁺	-	1.5503				
(β-band to g-band)		B(E2)(e ² b ²)		(β-band to γ-band)		B(E2)(e ² b ²)	
initial state	final state	Exp.	IBM-1	initial state	final state	Exp.	IBM-1
0 ₂ ⁺	2 ₁ ⁺	-	0.00022	0 ₂ ⁺	2 ₂ ⁺	-	0.0988
2 ₃ ⁺	0 ₁ ⁺	-	0.00004	2 ₃ ⁺	2 ₂ ⁺	-	0.0165
2 ₃ ⁺	2 ₁ ⁺	-	0.00003	2 ₃ ⁺	4 ₂ ⁺	-	0.0321
2 ₃ ⁺	4 ₁ ⁺	-	0.00013	4 ₃ ⁺	4 ₂ ⁺	-	0.0189

Note: The relation between Weisskopf unit and electron barn unit is $B(E2) (W.U) = 5.9435 \times 10^{-6} A^{4/3} (e^2 b^2)$ [37].

In general, there is a good agreement between the experimentally reported B(E2) values and the theoretically calculated ones.

Comparison between the ground state bands of the experimentally determined B(E2) values and the IBM-1 calculations in ¹⁵⁸Gd isotope is shown in Fig.3.

According to the basic conditions of B(E2) ratios of corresponding limits in Table 1, the experimental and the calculated values of B(E2) ratios are given in Table 5.

A comparison between Table 5 and the basic conditions of B(E2) ratios in Table 1 shows that "¹⁵⁸⁻¹⁶⁰Gd isotopes" are considered as rotational (deformed) nuclei possessing dynamical symmetry SU(3) according to the IBM-1.

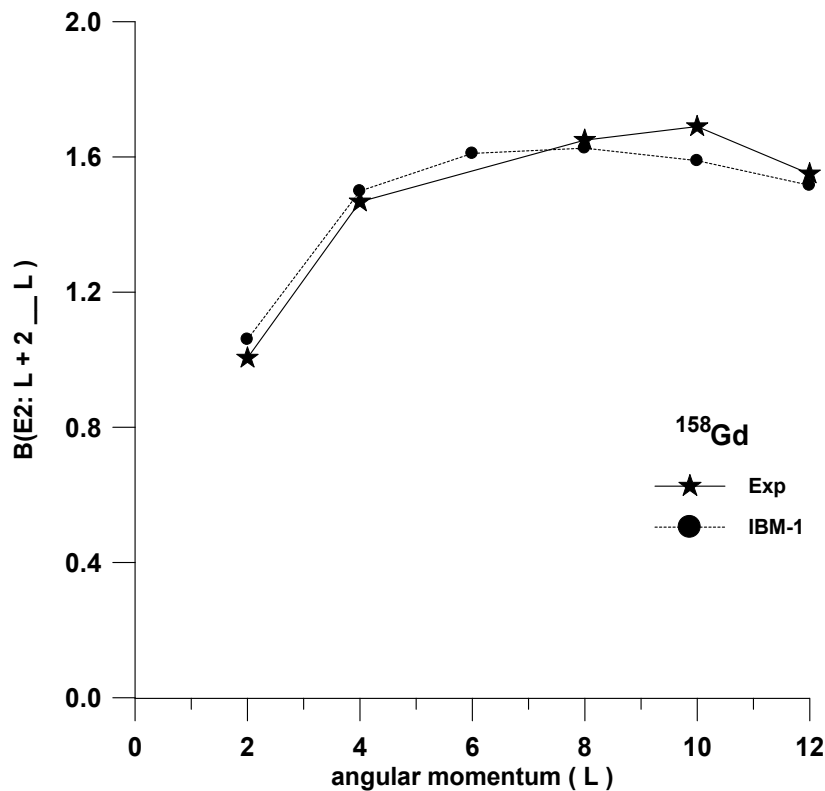


FIG. 3. Variation of B(E2) values with the angular momentum in g-band for ¹⁵⁸Gd.

TABLE 5. Experimental and calculated values of B(E2) ratios in $^{158-160}\text{Gd}$ isotopes.

Isotope	$\frac{B(E2; 4_1^+ \rightarrow 2_1^+)}{B(E2; 2_1^+ \rightarrow 0_1^+)}$		$\frac{B(E2; 0_2^+ \rightarrow 2_1^+)}{B(E2; 2_1^+ \rightarrow 0_1^+)}$		$\frac{B(E2; 2_2^+ \rightarrow 2_1^+)}{B(E2; 2_1^+ \rightarrow 0_1^+)}$	
	Exp	IBM-1	Exp	IBM-1	Exp	IBM-1
	^{158}Gd	1.459	1.41	0.0058	0.0091	0.03
^{160}Gd	-	1.414	-	0.0002	0.035	0.035

Conclusions

Theoretical calculations using IBM-1 model were performed for $^{158-160}\text{Gd}$ isotopes with proton number 64. These isotopes have a total number of bosons of 13 and 14, respectively and considered as fully rotational (fully deformed) nuclei, and the dynamical symmetry of these isotopes is SU(3). The low-lying positive parity states (energy levels) and the theoretically obtained B(E2) values for these isotopes using IBM-1 model are compared with the

experimentally reported values. A very good agreement was obvious. Therefore, it is possible to describe the energy levels of $^{158-160}\text{Gd}$ isotopes by using IBM-1 model. Moreover, it is worth to mention that more experimental investigation on $^{158-160}\text{Gd}$ isotopes B(E2) values is required in order to identify the strength of E2 transitions within the ground state band, from β -band to ground band and from γ -band to ground band and from β -band to γ -band.

References

- [1] Iachello, F. and Arima, A., Phys. Lett. B, 53 (1974) 309.
- [2] Lipes, P.O., Toivonen, P. and Hammaren, E., Nucl. Phys. A, 469 (1987) 348.
- [3] Casten, R.F. and Warner, D.D., Rev. Mod. Phys., 60 (1988) 389.
- [4] Arima, A. and Iachello, F., Ann. Phys., 123 (1979) 468.
- [5] Iachello, F. and Arima, A., "The Interacting Boson Model", (Cambridge University Press, Cambridge, England, 1987).
- [6] Kluk, A.F., Johnson, N.R. and Hamilton, J.H., Phys. Rev. C, 10(5) (1974) 1966.
- [7] Greenwood, R.C., Putnam, M.H. and Watts, K.D., Nucl. Instrum. Methods. Phys. Res. A, 378 (1996) 312.
- [8] Greenwood, R.C., Helmer, R.G., Putnam, M.H. and Watts, K.D., Nucl. Instrum. Methods. Phys. Res. A, 390 (1997) 95.
- [9] Soloviev, V.G., Sushkov, A.V., Shirikova, N.Yu. and Kollewe, N.Lo., Nucl. Phys. A, 600(2) (1996) 155.
- [10] Nojarov, R. and Dingfelder, M., Nucl. Phys. A, 613 (1997) 25.
- [11] Bonitz, M. and Hansen, N.J.S., Nucl. Phys. A, 111 (1968) 551.
- [12] Helmer, R.G., Nucl. Data Sheets, 77(3) (1996) 471.
- [13] Sugawara, M., Kusakari, H., Morikawa, T., Inoue, H., Yoshizawa, Y., Virtanen, A., Piiparinen, M. and Horiguchi, T., Nucl. Phys. A, 557 (1993) 653.
- [14] Baktash, C., Saladin, J.X., Brien, J.O., Lee, I.Y. and Holden, J.E., Phys. Rev. C, 10 (1974) 2265.
- [15] Ronningen, R.M., Hamilton, J.H., Ramayya, A.V., Varnell, L., Garcia-Bermudez, G., Lange, J., Lourens, W., Riedinger, L.L., Robinson, R.L., Stelson, P.H. and Ford, J.L., Phys. Rev. C, 15 (1977) 1671.
- [16] Raman, S., Nestor, C.W. and Tikkanen, P., At. Data, Nucl. Data, Tables, 78(1) (2001) 1.
- [17] Morcos, N.A., James, W.D., Adams, D.E. and Kuroda, P.K., Nucl. Chem., 35 (1973) 3659.
- [18] Berg, U.E.P., Blasing, C., Drexler, J., Heil, R.D., Kneissl, U., Naatz, W., Ratzek, R., Chennach, S.S., Stock, R., Weber, T., Wickert, H., Fischer, B., Hollick, H. and Kollewe, D., Phys. Lett., 149 B (1984) 59.
- [19] Pitz, H.H., Berg, U.E.P., Heil, R.D., Kneissl, U., Stock, R., Wesselborg, C. and Brentano, P.von., Nucl. Phys. A, 492 (1989) 411.

- [20] Elbek, B., Kregar, M. and Vedelsby, P., Nucl. Phys., 86 (1966) 385.
- [21] Bloch, R., Elbek, B. and Tjom, P.O., Nucl. Phys. A, 91 (1967) 576592.
- [22] De Coster, C. and Heyde, K., Phys. Rev. Lett., 63 (1989) 2797.
- [23] Sugawara, M., Kusakari, H., Morikawa, T., Inoue, H., Yoshizawa, Y., Virtanen, A., Piiparinen, M. and Horiguchi, T., Nucl. Phys. A, 459 (1993) 653.
- [24] Ronningen, R.M., Hamilton, J.H., Varnell, L., Lange, J., Ramayya, A.V., Garcia-Bermudez, G., Lourens, W., Riedinger, L.L., McGowan, F.K., Stelson, P.H., Robinson, R.L. and Ford, J.L., Phys. Rev. C, 16 (1977) 2208.
- [25] Baktash, C., Saladin, J.X., Brien, J.O., Lee, I.Y. and Holden, J.E., Phys. Rev. C, 10 (6) (1974) 2265.
- [26] Ronningen, R.M., Hamilton, J.H., Ramayya, A.V., Varnell, L., Garcia-Bermudez, G., Lange, J., Lourens, W., Riedinger, L.L., Robinson, R.L., Stelson, P.H. and Ford, J.L., Phys. Rev. C, 15 (1977) 1671.
- [27] Reich, C.W., Nucl. Data Sheets, 105(3) (2005) 557.
- [28] Venkova, T. and Andrejtscheff, W., At. Data, Nucl. Data, Tables, 26(2) (1981) 93.
- [29] Maino, G., Ventura, A., Van Isacker, P. and Zuffi, L., Phys. Rev. C, 33 (1986) 1089.
- [30] Arima, A. and Iachello, F., Ann. Phys., 111(1) (1978) 201.
- [31] Al-Maqtary, K.A., Al-Zuhairy, M.H., Al-Sharaby, M.N. and Shamlan, N.A., Jordan Journal of Physics (JJP), 4(1) (2011) 51.
- [32] Arima, A. and Iachello, F., Ann. Phys., 281(1-2) (1978) 2.
- [33] Yazar, H.R. and Erdem, U., Chi. J. Phys., 46(3) (2008) 270.
- [34] Xu, F.X., Wu, C.S. and Zeng, J.Y., Phys. Rev. C, 40(5) (1989) 2337.
- [35] Kucukbursa, A. and Manisa, K., Math. Comp. App., 10(1) (2005) 9.
- [36] McGowan, F.K. and Milner W.T., Phys. Rev. C, 23(5) (1981) 1926.
- [37] Bohr, A. and Mottelson, B., "Nuclear Structure", Vol. I (World Scientific, New Jersey, 1998).

Authors Index

Al-Ajaleen A. A.	79
Al-Bataina B. A.	47
Al-Khasawneh B.	65
Al-Khashab M. A.	87
Al-Maqtary K. A.	95
Almomani R. R.	47
Al-Rayashi W. S.	47
Al-Salih R. Y.	87
Altaie M.B.	65
Ershaidat N. M.	47
Isam A.	73
Jaradat E. K.	55
Nawafleh K. I.	79

Subject Index

Active detector	47
Dark matter	65
Discrete space	73
Diurnal variation	47
Electron magnetic properties	87
Electron optical properties	87
Energy levels.....	95
Fractional Canonical Quantization	55
Fractional Caputo's Definition	55
Fractional Schrödinger Lagrangian density	55
Fractional time dependent Schrödinger equation.....	55
Gravitational mass	65
Heat equation	47
Inertial mass	65
Interacting boson model.....	95
Irbid.....	47
Isotope.....	95
Low voltage SEM	87
Nonholonomic constraints	79
Objective lens geometry design	87
Phosphatic formation	47
Quantization concept	73
Quantization.....	79
Quantum gravity	73
RAD7®.....	47
Relativistic corrected accelerating voltage	87
Soil radon.....	47
Transition probabilities	95
Virial theorem.....	65
WKB approximation.....	79

طرائق البحث (التجريبية / النظرية): يجب أن تكون هذه الطرائق موضحة بتفصيل كاف لإتاحة إعادة إجرائها بكفاءة، ولكن باختصار مناسب، حتى لا تكون تكرارا للطرائق المنشورة سابقا.

النتائج: يستحسن عرض النتائج على صورة جداول وأشكال حيثما أمكن، مع شرح قليل في النص ومن دون مناقشة تفصيلية.

المناقشة: يجب أن تكون موجزة وتركز على تفسير النتائج.

الاستنتاج: يجب أن يكون وصفا موجزا لأهم ما توصلت إليه الدراسة ولا يزيد عن صفحة مطبوعة واحدة.

الشكر والعرفان: الشكر والإشارة إلى مصدر المنح والدعم المالي يكتبان في فقرة واحدة تسبق المراجع مباشرة.

المراجع: يجب طباعة المراجع بأسطر مزدوجة ومرقمة حسب تسلسلها في النص. وتكتب المراجع في النص بين قوسين مربعين. ويتم اعتماد اختصارات الدوريات حسب نظام Wordlist of Scientific Reviewers.

الجدول: تعطى الجداول أرقاما متسلسلة يشار إليها في النص. ويجب طباعة كل جدول على صفحة منفصلة مع عنوان فوق الجدول. أما الحواشي التفسيرية، التي يشار إليها بحرف فوقي، فتكتب أسفل الجدول.

الرسوم التوضيحية: يتم ترقيم الأشكال والرسومات والرسومات البيانية (المخططات) والصور، بصورة متسلسلة كما وردت في النص.

تقبل الرسوم التوضيحية المستخرجة من الحاسوب والصور الرقمية ذات النوعية الجيدة بالأبيض والأسود، على أن تكون أصيلة وليست نسخة عنها، وكل منها على ورقة منفصلة ومعرفة برقمها بالمقابل. ويجب تزويد المجلة بالرسومات بحجمها الأصلي بحيث لا تحتاج إلى معالجة لاحقة، وألا تقل الحروف عن الحجم 8 من نوع Times New Roman، وألا تقل سماكة الخطوط عن 0.5 وبكثافة متجانسة. ويجب إزالة جميع الألوان من الرسومات ما عدا تلك التي ستنتشر ملونة. وفي حالة إرسال الرسومات بصورة رقمية، يجب أن تتوافق مع متطلبات الحد الأدنى من التمايز (1200 dpi Resolution) لرسومات الأبيض والأسود الخطية، و 600 dpi للرسومات باللون الرمادي، و 300 dpi للرسومات الملونة. ويجب تخزين جميع ملفات الرسومات على شكل (jpg)، وأن ترسل الرسوم التوضيحية بالحجم الفعلي الذي سيظهر في المجلة. وسواء أرسل المخطوط بالبريد أو عن طريق الشبكة (Online)، يجب إرسال نسخة ورقية أصلية ذات نوعية جيدة للرسومات التوضيحية.

مواد إضافية: تشجع المجلة الباحثين على إرفاق جميع المواد الإضافية التي يمكن أن تسهل عملية التحكيم. وتشمل المواد الإضافية أي اشتقاقات رياضية مفصلة لا تظهر في المخطوط.

المخطوط المنقح (المعدل) والأقراص المدمجة: بعد قبول البحث للنشر وإجراء جميع التعديلات المطلوبة، فعلى الباحثين تقديم نسخة أصلية ونسخة أخرى مطابقة للأصلية مطبوعة بأسطر مزدوجة، وكذلك تقديم نسخة إلكترونية تحتوي على المخطوط كاملا مكتوبا على Microsoft Word for Windows 2000 أو ما هو استجد منه. ويجب إرفاق الأشكال الأصلية مع المخطوط النهائي المعدل حتى لو تم تقديم الأشكال إلكترونيا. وتخزن جميع ملفات الرسومات على شكل (jpg)، وتقدم جميع الرسومات التوضيحية بالحجم الحقيقي الذي ستظهر به في المجلة. ويجب إرفاق قائمة ببرامج الحاسوب التي استعملت في كتابة النص، وأسماء الملفات على قرص مدمج، حيث يعلم القرص بالاسم الأخير للباحث، وبالرقم المرجعي للمخطوط للمراسلة، وعنوان المقالة، والتاريخ. ويحفظ في مغلف واقٍ.

الفهرسة: تقوم المجلة الأردنية للفيزياء بالإجراءات اللازمة لفهرستها وتلخيصها في جميع الخدمات الدولية المعنية.

حقوق الطبع

يُشكّل تقديم مخطوط البحث للمجلة اعترافاً صريحاً من الباحثين بأن مخطوط البحث لم يُنشر ولم يُقدّم للنشر لدى أي جهة أخرى كانت وبأي صيغة ورقية أو إلكترونية أو غيرها. ويشتترط على الباحثين ملء نموذج يُنصّ على نقل حقوق الطبع لتصبح ملكاً لجامعة اليرموك قبل الموافقة على نشر المخطوط. ويقوم رئيس التحرير بتزويد الباحثين بإنموذج نقل حقوق الطبع مع النسخة المُرسلة للتنقيح. كما ويُمنع إعادة إنتاج أي جزء من الأعمال المنشورة في المجلة من دون إذن خطّي مُسبق من رئيس التحرير.

إخلاء المسؤولية

إن ما ورد في هذه المجلة يعبر عن آراء المؤلفين، ولا يعكس بالضرورة آراء هيئة التحرير أو الجامعة أو سياسة اللجنة العليا للبحث العلمي أو وزارة التعليم العالي والبحث العلمي. ولا يتحمل ناشر المجلة أي تبعات مادية أو معنوية أو مسؤوليات عن استعمال المعلومات المنشورة في المجلة أو سوء استعمالها.

معلومات عامة

المجلة الأردنية للفيزياء هي مجلة بحوث علمية عالمية متخصصة مُحكمة تصدر بدعم من صندوق دعم البحث العلمي، وزارة التعليم العالي والبحث العلمي، عمان، الأردن. وتقوم بنشر المجلة عمادة البحث العلمي والدراسات العليا في جامعة اليرموك، إربد، الأردن. وتُنشر البحوث العلمية الأصيلة، إضافة إلى المراسلات القصيرة Short Communications، والملاحظات الفنية Technical Notes، والمقالات الخاصة Feature Articles. ومقالات المراجعة Review Articles، في مجالات الفيزياء النظرية والتجريبية، باللغتين العربية والإنجليزية.

تقديم مخطوط البحث

تُرسل نسخة أصلية وثلاث نسخ من المخطوط، مُرفقة برسالة تغطية من جانب الباحث المسؤول عن المراسلات، إلى رئيس التحرير:

أ.د. نهاد عبدالرؤف يوسف،

رئيس التحرير، المجلة الأردنية للفيزياء،

عمادة البحث العلمي والدراسات العليا،

جامعة اليرموك، إربد، الأردن.

هاتف : 00 962 2 72 11 111 / فرعي: 2075

فاكس : 00 962 2 72 11 121

بريد إلكتروني : jjp@yu.edu.jo

تقديم المخطوطات إلكترونياً: اتبع التعليمات في موقع المجلة على الشبكة العنكبوتية.

ويجري تحكيم البحوث الأصيلة والمراسلات القصيرة والملاحظات الفنية من جانب مُحكمين اثنين في الأقل من ذوي الاختصاص والخبرة. وتُشجّع المجلة الباحثين على اقتراح أسماء المحكمين. أما نشر المقالات الخاصة في المجالات الفيزيائية النشطة، فيتم بدعوة من هيئة التحرير، ويُشار إليها كذلك عند النشر. ويُطلب من كاتب المقال الخاص تقديم تقرير واضح يتسم بالدقة والإيجاز عن مجال البحث تمهيداً للمقال. وتُنشر المجلة أيضاً مقالات المراجعة في الحقول الفيزيائية النشطة سريعة التغير، وتُشجّع كاتبي مقالات المراجعة أو مُسندتها على إرسال مقترح من صفتين إلى رئيس التحرير. ويُرفق مع البحث المكتوب باللغة العربية ملخص (Abstract) وكلمات دالة (Keywords) باللغة الإنجليزية.

ترتيب مخطوط البحث

يجب أن تتم طباعة مخطوط البحث بينط 12 نوعه Times New Roman، وبسطر مزدوج، على وجه واحد من ورق A4 (21.6 × 27.9 سم) مع حواشي 3.71 سم، باستخدام معالج كلمات ميكروسوفت وورد 2000 أو ما استُجد منه. ويجري تنظيم أجزاء المخطوط وفق الترتيب التالي: صفحة العنوان، الملخص، رموز التصنيف (PACS)، المقدمة، طرق البحث، النتائج، المناقشة، الخلاصة، الشكر والعرفان، المراجع، الجداول، قائمة بدليل الأشكال والصور والإيضاحات، ثم الأشكال والصور والإيضاحات. وتُكتب العناوين الرئيسية بخط غامق، بينما تُكتب العناوين الفرعية بخط مائل.

صفحة العنوان: وتشمل عنوان المقالة، أسماء الباحثين الكاملة وعناوين العمل كاملة. ويكتب الباحث المسؤول عن المراسلات اسمه مشاراً إليه بنجمة، والبريد الإلكتروني الخاص به. ويجب أن يكون عنوان المقالة موجزاً وواضحاً ومعبراً عن فحوى (محتوى) المخطوط، وذلك لأهمية هذا العنوان لأغراض استرجاع المعلومات.

الملخص: المطلوب كتابة فقرة واحدة لا تزيد على مائتي كلمة، موضحة هدف البحث، والمنهج المتبع فيه والنتائج وأهم ما توصل إليه الباحثون.

الكلمات الدالة: يجب أن يلي الملخص قائمة من 4-6 كلمات دالة تعبر عن المحتوى الدقيق للمخطوط لأغراض الفهرسة.

PACS: يجب إرفاق الرموز التصنيفية، وهي متوافرة في الموقع <http://www.aip.org/pacs/pacs06/pacs06-toc.html>.

المقدمة: يجب أن توضّح الهدف من الدراسة وعلاقتها بالأعمال السابقة في المجال، لا أن تكون مراجعة مكثفة لما نُشر (لا تزيد المقدمة عن صفحة ونصف الصفحة مطبوعة).

Jordan Journal of

PHYSICSAn International Peer-Reviewed Research Journal issued by the
Support of the Scientific Research Support Fund

Published by the Deanship of Research & Graduate Studies, Yarmouk University, Irbid, Jordan

Name: الأسم:
 Specialty: التخصص:
 Address: العنوان:
 P.O. Box: صندوق البريد:
 City & Postal Code: المدينة/الرمز البريدي:
 Country: الدولة:
 Phone: رقم الهاتف:
 Fax No: رقم الفاكس:
 E-mail: البريد الإلكتروني:
 No. of Subscription: عدد الاشتراكات:
 Method of Payment: طريقة الدفع:
 Amount Enclosed: المبلغ المرفق:
 Signature: التوقيع:

Cheques should be paid to Deanship of Research and Graduate Studies - Yarmouk University.

I would like to subscribe to the Journal
For

- One Year
 Two Years
 Three Years

One Year Subscription Rates

	Inside Jordan	Outside Jordan
Individuals	JD 8	€ 40
Students	JD 4	€ 20
Institutions	JD 12	€ 60

Correspondence**Subscriptions and Sales:**

Prof. Ibrahim O. Abu-AlJarayesh
 Deanship of Research and Graduate Studies
 Yarmouk University
 Irbid – Jordan
Telephone: 00 962 2 711111 Ext. 2075
Fax No.: 00 962 2 7211121



جامعة اليرموك



المملكة الأردنية الهاشمية

المجلة الأردنية

للفيزياء

مجلة بحوث علمية عالية متخصصة محكمة
تصدر بدعم من صندوق دعم البحث العلمي

المجلد (6)، العدد (2)، 2013م / 1435هـ

المجلة الأردنية
للفيزياء
مجلة بحوث علمية عالمية محكمة

المجلد (6)، العدد (2)، 2013م / 1435هـ

المجلة الأردنية للفيزياء: مجلة علمية عالمية متخصصة محكمة تصدر بدعم من صندوق دعم البحث العلمي، وزارة التعليم العالي والبحث العلمي، الأردن، وتصدر عن عمادة البحث العلمي والدراسات العليا، جامعة اليرموك، إربد، الأردن.

رئيس التحرير:

نهاد عبد الرؤوف يوسف

قسم الفيزياء، جامعة اليرموك، إربد، الأردن.

nihadyusuf@yu.edu.jo

هيئة التحرير:

ضياء الدين محمود عرفة

قسم الفيزياء، الجامعة الأردنية، عمان، الأردن.

darafah@ju.edu.jo

نبيل يوسف أيوب

قسم الفيزياء، جامعة اليرموك، إربد، الأردن.

nayoub@yu.edu.jo

جميل محمود خليفة

قسم الفيزياء، الجامعة الأردنية، عمان، الأردن.

jkalifa@ju.edu.jo

سامي حسين محمود

قسم الفيزياء، الجامعة الأردنية، عمان، الأردن.

s.mahmood@ju.edu.jo

مروان سليمان موسى

قسم الفيزياء، جامعة مؤتة، الكرك، الأردن.

mmousa@mutah.edu.jo

ابراهيم عثمان أبو الجرايش

قسم الفيزياء، جامعة اليرموك، إربد، الأردن.

ijaraysh@yu.edu.jo

أكرم عبد المجيد الروسان

قسم الفيزياء التطبيقية، جامعة العلوم والتكنولوجيا الأردنية، إربد، الأردن.

akram@just.edu.jo

سعدي محمود عبد الجواد

قسم الفيزياء الجامعة الهاشمية، الزرقاء، الأردن.

ssadi@hu.edu.jo

سكرتير التحرير: مجدي الشناق

ترسل البحوث إلى العنوان التالي:

الأستاذ الدكتور نهاد عبد الرؤوف يوسف

رئيس تحرير المجلة الأردنية للفيزياء

عمادة البحث العلمي والدراسات العليا، جامعة اليرموك

إربد، الأردن

هاتف 00 962 2 7211111 فرعي 2075

E-mail: jjp@yu.edu.jo

Website: <http://Journals.yu.edu.jo/jjp>

